Politecnico di Milano

Industrial Engineering

Space Engineering Graduate Course

"ESMO Spacecraft Attitude Dynamics: Propellant Sloshing and Mass Expulsion Torques Model"

Thesis advisors: Prof. Franco BERNELLI
                   Dr.   Massimiliano VASILE

Stefania SOLDINI   Matr. 740414

Academic Year 2010/2011

In memoria del mio nonno Sergio
(In loving memory of my grandfather Sergio)

Abstract

This dissertation deals with the Newton and Euler dynamics equations of ESMO, where a mathematical formulation has been developed. The purpose is to design the internal (non-environmental) disturbances of the spacecraft, by focusing attention on the mass expulsion disturbance torques and the propellant sloshing effect. Moreover the dynamics of the reaction wheels has been taken into account. A review of the propellant sloshing models has been investigated and has been described in brief throughout the dissertation. Particular attention has been given to the propellant sloshing model that has been embraced and to the sate of the art of the mass expulsion torques. Additionally, the propellant consumption that affects some terms of the equation of motions has been considered. This dissertation intends to be an interface between the orbit dynamics and the attitude dynamics disciplines. The two dynamics equations are uncoupled because the environmental torques, that are the coupling terms, are not considered. The outcome of the thesis is the developing of the software that implements the spacecraft attitude dynamics of ESMO and the internal dynamics of the satellite. Therefore this software is going to be used by the ESMO Mission Analysis (MIAS) Team of the University of Strathclyde, Glasgow to give information on the thrust vector orientation (attitude of ESMO) and for passing the control law for contingency analysis (a.g. delay in the actuation). Moreover this software can be used by the ESMO Attitude and Orbit Control (AOCS1) System Team of Politecnico di Milano to integrate the internal dynamics of ESMO with the simulator that the AOCS1 Team has developed.

Sommario

L'oggetto di studio di questa tesi é la formulazione matematica delle equazioni della dinamica di ESMO, nella forma di Eulero-Newton. Lo scopo e il motivo di questo lavoro sono di implementare un modello dei disturbi interni al satellite. É stata rivolta particolare attenzione nei confronti dei disturbi associati all'espulsione di massa e alla dinamica di sloshing dei serbatoi. Inoltre per ragioni di completezza, la dinamica delle ruote di reazione é stata inclusa alle equazioni del moto. In questa tesi sará presentato lo stato dell'arte dei modelli di sloshing e delle coppie di disturbo causate dall'espulsione di massa. Il modello delle equazioni é completato con il modello di consumo del carburante che influenza alcuni termini nell'equazioni del moto. Questa tesi ha l'intento di costituire un'interfaccia fra due importanti discipline: la meccanica orbitale e la dinamica d'assetto. Le equazioni della dinamica d'assetto e della meccanica orbitale rimangono comunque disaccoppiate, poiché le coppie di disturbo esterne o d'ambiente, (che sono quelle che garantiscono l'accoppiamento) non sono state incluse alle equazione del moto. L'intento di questa tesi si configura nello sviluppo di un software che implementi la dinamica d'assetto di ESMO e le dinamiche di disturbo interne al satellite. Tale software attualmente é stato utilizzato, e continuerá ad esserlo, dal team di analisi di missione della University of Strathclyde, Glasgow per ottenere informazioni sull'orientazione del vettore di spinta e per le eventuali analisi di imprevisti malfunzionamenti degli attuatori. Infine questo software potrá essere utilizzato e integrato, dal team di controllo d'assetto del Politecnico di Milano, per inserire all'interno del simulatore giá sviluppato dal AOCS1 team, il modello delle dinamiche interne di ESMO.

Acknowledgments

I would like to thank Dr. Massimilano Vasile, advisor of my thesis, of The University of Strathclyde who gave me the chance to spend the last six months in Glasgow and to work with the Advanced Space Concepts Laboratory Team. I am thankful to my advisor of Politecnico di Milan, prof. Franco Bernelli-Zazzera for encourage me to write my thesis. Many thanks to all the PhD students/students and Dr. of the University of Strathclyde: Eirini, Luca, Willem, Federico, Massimo, Steven, Craig, Alison, Daniele, Fabrizio, Marta, Thomas and Marcel; Johannes and Iain; Camilla and Christie; that for six months have been not only a "*colleagues*" but also a friends. I am also indebted to Craig for giving me useful suggestions for the improvement of this dissertation and to Eirini for being a very good friend. Thank you to my teacher of middle school Gabriella Meli that always believe in me. I am grateful to my teachers of high school, Maria Rita Bianchi and Maria Rosaria Guerra for their fundamental support. A special thank you to Emanuela Beneventano, my English teacher and friend. I am grateful to all the colleagues of Politecnico di Milano, in particular to Laura, Debora and Edoardo. Thank you to my "*old*" friends: Federica, Silvia and Camilla that always support me. My gratitude to my stepfather Pietro and to my father Donato that gave to me the opportunity to study and that support me everyday of my life. Thank you to my grandmother Marisa that encouraged me. A special thank you to my mother Daniela that is always proud of me. A thought to my brother Riccardo for encouraging him to follow his dreams. Last but not least, a very special thank you to my boyfriend Francesco for supporting me in every difficult moments (thank you to have been patient with me!).

Stefania

Ringraziamenti

Contents

List of Figures

List of Tables

Chapter 1

Introduction

1.1   The European Student Moon Orbiter (ESMO)
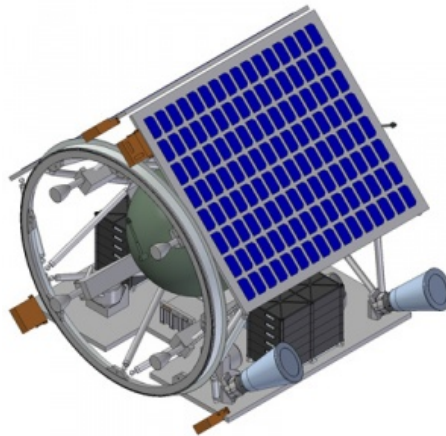
Figure 1.1: ESMO view.

The European Student Moon Orbiter Fig. (1.1) is the first European Student Mission to the Moon and the fourth mission within ESA [1] Education Satellite Programme after SSETI Express, YES2 and ESEO [2]. ESMO has currently completed a Phase A Feasibility Study and is proceeding with preliminary design activities in Phase B. The purpose of the mission is to place the spacecraft on a polar orbit around the Moon, return new data by acquiring surface images of the Moon South Pole and test new technology. The Moon South Pole Fig. (1.2) is of special interest to scientists because of the assumption of the occurrence

---

[1] European Space Agency.

[2] The European Student Earth Orbiter planned to be launched in LEO in 2013.

of ice in permanently shadowed areas. Thinking about the future human space missions, the Moon is still an interesting target not only for scientific reasons but also for testing technology and methodology for the support of the human life in a hostile environment such as the lunar surface. We could consider the future human mission to the Moon as training for future interplanetary missions. Mars is definitely a planet of major scientific interest and ESA hopes to one day plan a future human mission to Mars [3]. In addition, ESMO has a powerful education outreach aspect by giving the opportunity to students across the ESA Member States to work on a real project and contribute to the scientific knowledge.
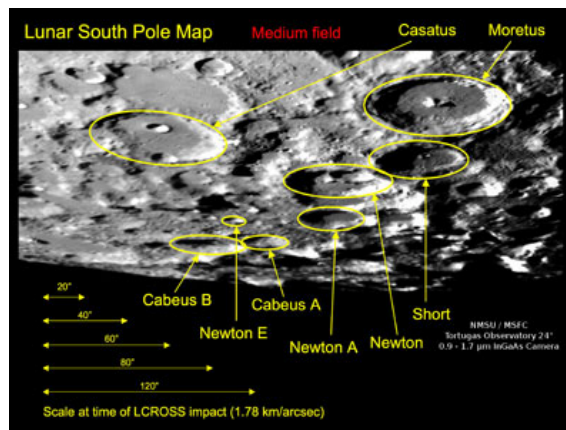
Figure 1.2: Lunar South Pole Map.

1.2   Spacecraft Attitude dynamics

The subject of this dissertation is the study of ESMO Spacecraft Attitude Dynamics with a particular interest in modeling internal disturbance effects. *Spacecraft Attitude Dynamics* is the discipline that predicts how spacecraft orientation evolves. As the reader could easily imagine, Attitude Dynamics interacts with other disciplines that we will mention in brief in this section:

Orbital dynamics. Attitude and orbital dynamics are in general mutually coupled. They respectively study the rotational and translational dynamics. A "classical" dynamical problem is to consider the gravity force field effect. The translational and rotational motion are coupled by their gravitational interaction. As an example in which the orbit affects the attitude, the disturbance torques acting on a spacecraft often depend on altitude (e.g. air drag and solar radiation

---

[3]AURORA Programme.

torques.) On the contrary the attitude affects the orbit in the case of interplanetary solar sailing. The purpose is to use the solar radiation pressure by adjusting the attitude to produce the desired trajectory. Usually these two disciplines are treated separately. Indeed, the coupling effect occurs only when there are environmental torques that depend on orbital variables that it is possible to treat as external disturbances.

Structures Interaction. It is common in the field of astrodynamics to model the spacecraft as a rigid-body. However real spacecraft are not rigid bodies. The advantage is in the simplicity of the rigid-body attitude model but unfortunately it is a geometrical abstraction. Rigid-body assumptions entirely ignore the Second Law of Thermodynamics. On the other hand, accurate structural analysis implies an enormous increase in math model complexity.

Fluids Interaction. The dynamics of fluids affect the attitude dynamics. The propellant sloshing effect is not easily incorporated into attitude dynamics modeling. Writing the spacecraft attitude dynamics of ESMO with the propellant sloshing dynamics is one of the major purpose of this thesis. We will diffusely treat this subject within the dissertation.

1.3 State of the Art

Different sources of disturbances affect the spacecraft attitude dynamics by appearing as applied torques. Usually they are categorized as External and Internal Torques. External torques are caused by environmental sources and Internal torques are self-generated inside the spacecraft and considered as non-environmental torques. As it is well known the absence of external or environmental torques imply the conservation of angular momentum about the mass center. However, the internal torques can redistribute the angular momentum in a body reference frame and can alter the system's kinetic energy. The internal, or non-environmental torques, operating on a satellite, are the outcome of internal moving parts. These internal dynamics, that no longer allow us to assume the spacecraft as rigid, are caused by: reaction wheels dynamics, ejected mass , flexible antenna, solar array, liquid inside partially filled tanks, the motion of internal hardware and crew motion [4]. In general there are two different ways to treat the non-environmental torques, depending on the nature of the disturbances. If the non-environmental torques are of a passive nature, we prefer to regard them as dynamical terms in the attitude dynamic equations. On the other hand when we write the non-environmental torques in the "right hand" of the motion equation, these terms can appear as external torques. This point of view is appropriate

---

[4]The crew motion is not predictable, except statistically. They are best treated stochastically.

when these terms are the outcome of active control. In this dissertation two internal disturbances, which alter the ESMO attitude dynamics, are investigated: *Mass Expulsion Torques* and *Propellant Sloshing Effect*. In this section, we will finally show in brief a classical fuel problem: the *Fuel Rigid-Slug Model*. This model was numerically implemented as a reference test case.

1.3.1   Mass Expulsion Torques

Mass Expulsion Torques are the torques that may result when mass is expelled from a spacecraft. Determination of these torques requires knowledge of the mass flow nature. Indeed, the mass can be ejected from the spacecraft in solid, liquid or gaseous state. These kind of torques are treated and categorized in NASA [1] and they can occur in several different ways due to anomalous design or operational conditions. In the NASA [1] report only the effects during space flight are investigated, therefore launch and de-orbiting effects are excluded. NASA has classified the different nature of the mass expulsion torques by learning those experienced in previous missions. The previous missions outlined how these disturbances can affect the prediction of a spacecraft's attitude. The first category is representative of all "sources intended to produce a force or torque that is necessary for the proper operation of spacecraft", (NASA [1]). Most of the mass expulsion torques that have been identified belong to this category. NASA examples include:

- Leakage of fuel or pressurizing agent;

- Thrust vector misalignment;

- Reaction forces resulting from plume impingement on the vehicle;

- Anomalous firing time.

The second category contains all the "sources intended to expel mass but that place on the spacecraft forces or torques which must be controlled or minimized", (NASA [1]). These disturbances occur infrequently, perhaps only once during the flight. When these disturbances occur, they manifest general problems. NASA examples include:

- Dumping of residual propellants;

- Venting of compartments, subsystems, and spacecraft;

- Subliming mechanisms;

- Payload separation and ejection;

- Equipment jettison.

The third category includes all the "unintentional sources where neither the force nor the expulsion of mass are permitted in spacecraft design", (NASA [1]). This category includes outgassing, sublimation, and leakage from spacecraft equipment.

However analytical methods and test facilities that study the magnitude of these torques, and design techniques that minimize these disturbance effects, are widely diffused. As explained in Chapter 3, we investigated the most significant disturbances within the mass expulsion torques: *Thrust Vector Misalignment.*

1.3.2 Propellant Sloshing Model

"Our everyday experience in carrying a cup of coffee or a bowl of soup may be frustrating unless we are very careful as to how we move, but may still deceive us into believing that the "sloshing" of the liquid is simple". (*H. Norman Abramson* [2])

Liquid sloshing in storage tanks has long been of interest to researchers and engineers. The dynamic loads from the fuel have both inertial and dissipative components, and both can affect the attitude stability of a spacecraft and the integrity of the tank structure. Sloshing describes the free-surface oscillations of a fluid in a partially filled tank. These oscillations result from lateral and longitudinal displacements or angular motions. Several methods have been employed to reduce the sloshing effect, such as adding baffles inside the tank. This technique is helpful but does not always succeed in canceling the sloshing load. The liquid sloshing problem can be faced with two different approaches: *Fluid Mechanics Approach* and *Equivalent Mechanical Model.* Fluid mechanics is the discipline that studies fluids motion. The basic equations governing the motion are the well known Navier-Stokes equations. These equations are nonlinear partial differential equations with boundary conditions at the free surfaces and at the tank "walls". Fluid mechanics can be mathematically complex. A closed-form solution is available only for very simple problems, and usually it is necessary to adopt a numerical approach in order to obtain a solution. A modern discipline, called computational fluid dynamics (CFD [3]) Fig. (1.3), is devoted to this approach to solving fluid mechanics problems. Alternatively one can adopt the equivalent mechanical model in which the sloshing effect is represented by an equivalent mechanical object. As one could easily understand the mechanical model is an approximation of the problem, therefore it is less precise than the exact solution (of the Navier-Stokes equations). The mechanical approach is a very helpful model as it allows the dynamical model of the propellant sloshing to be integrated into the equations of motion of the satellite. Furthermore the simplicity of a mechanical model means that less numerical power in the solution of the problem in comparison with the fluid mechanics approach. For these reasons, the equivalent mechanical sloshing model has been embraced and coupled with

the equations of motion of ESMO. Two different mechanical models have been investigated: *Mass-Spring-Damper Model* and *3D Spherical Pendulum*[5].
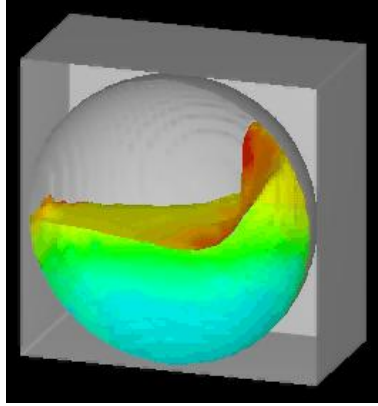
Figure 1.3: Computational fluid dynamics solution in a spherical tank.

Mass-Spring-Damper Model. The basic assumptions in modeling the propellant sloshing, by assuming the previous outline approach, have been formulated in the models of sloshing presented in Abramson (1961), [4]. These assumptions include:

- Small displacements, velocities, and slope of the liquid-free surfaces;

- A rigid tank;

- Nonviscous liquid;

- Incompressible and homogeneous fluid.
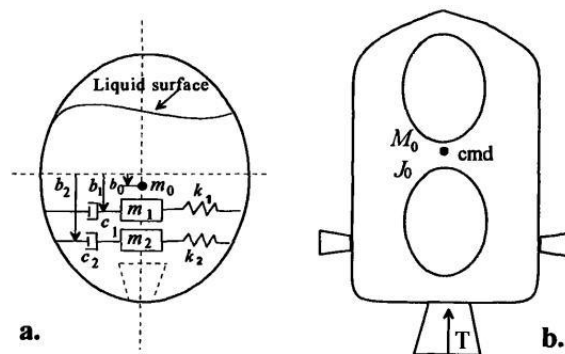
Figure 1.4: Mass-Spring-Damper Model reproduced from Abramson (1966).

---

[5]A very good reference is [2]

After these assumptions, one can write the sloshing dynamics model using an infinite number of small masses. The results obtained with such a model must be checked with experimental measurements, (see [4]). In Fig. (1.4), m_0 is the mass of the nonsloshing part of the fuel inside the tank and m_1, m_2 are two assumed masses contributing to the sloshing load [6]. These three masses are distanced b_0, b_1 and b_2 from the center of the tank. The terms k_1, k_2 and c_1, c_2 are the spring coefficients and damping parameters. In Fig. (1.4.b), "cmd" is the center of *dry* mass; M_0 is the nonsloshing mass of the satellite, and J_0 is the moment of inertia of the satellite without the contribution of the sloshing masses. This mechanical model under Abramson's assumptions is analogous to a pendulum model, (see Fig. (1.5)). The difficult part in modeling the sloshing effect is to define (analytically or experimentally) the equivalent arm length l_j $(j = 0, ..., n)$, the equivalent masses m_j $(j = 0, ..., n)$, the equivalent spring constants k_j $(j = 0, ..., n)$ and the damping constants c_j $(j = 0, ..., n)$. These parameters depend on the geometrical parameters of the container, the characteristics of the fluid and the fill ratio of the container. The force produces a linear acceleration that one can calculate as:

$$a = \frac{|\vec{T}|}{M_0 + \sum_{j=0}^{n} m_j} \qquad (1.3.1)$$

The spring constants Eq. (1.3.2) and the angular velocity Eq. (1.3.3) are defined as follows:

$$k_j = \frac{m_j \, a}{l_j} \qquad (1.3.2)$$

$$\omega_j = \sqrt{\frac{k_j}{m_j}} \qquad (1.3.3)$$

The mass-spring-damper model has the advantage of being a very simple model to implement. We have numerically implemented this model by adding the equations of motion of ESMO. In developing the first version of the software with the mass-spring-damper model we encountered a series of problem. First of all the equivalent masses and spring constants are dependent on the shape of the tank (only for the cylinder and rectangular tanks does there exist the empirical expressions to obtain these parameters), the fuel property and the surface level. Secondly, this model makes sense only under the hypothesis of one-dimensional linear motion, which is a limitation for our model. It has also been encountered problems of boundary condition, in which the sloshing masses have crossed the "wall" of the tank and this does not make sense physically speaking. We desired to have a non linear model that respects the boundary conditions. This lead to

---

[6]The distinction of nonsloshing and sloshing fuel masses is usually adopted in missile applications where the great acceleration constrains part of the fuel to stay fixed on the bottom of the tank. For a spacecraft this distinction is not necessary yet.
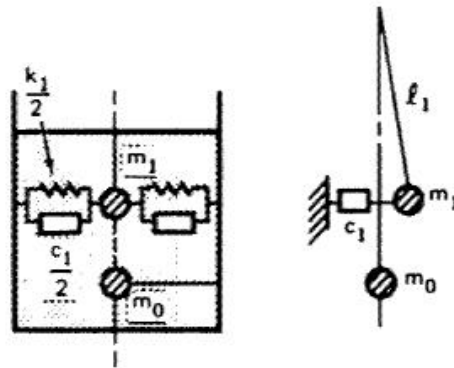
Figure 1.5: Pendulum analogy reproduced from Abramson (1966).

the consideration of another mechanical model in the *3D Spherical pendulum.*

3D Spherical Pendulum. The 3D spherical pendulum model Fig. (1.6) is a pendulum with three degrees of freedom. The length of the pendulum is the distance that connect the center of mass of the fuel and the center of the spherical tank. The fuel is supposed to be rigid and covered by a viscous layer. For a spherical tank this model is very useful because it naturally respects the boundary conditions. This model can treat not only nonlinearity but also a 3D sloshing load. We developed a second version of the software in which we solved all the problems that we had in the first version by implementing the 3D spherical pendulum model instead of the mass-spring-damper model.
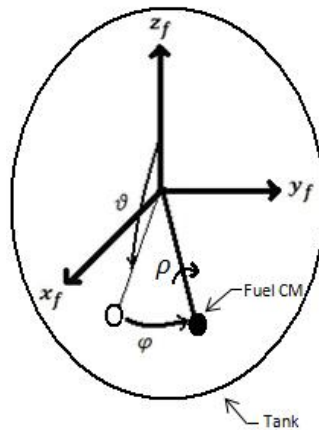
Figure 1.6: 3D Spherical Pendulum.

In Fig. (1.6), θ, ϕ and ρ are the degrees of freedom of the pendulum.

1.3.3 Fuel Rigid-Slug Model

In the literature it is possible to find an interesting "classical" dynamical problem: the fuel rigid-slug model. It is also known as flat-spin maneuvers. This model is based on a tank centered in the mass center of the spacecraft. The tank is supposed to be full of propellant, therefore the propellant is assumed to be a rigid sphere covered by a viscous layer. As it is well known, for free-rigid body dynamics without dissipation the rotation is stable about the axes of maximum and minimum moments of inertia. In this case both the angular momentum and the kinetic energy are conserved. In case of dissipation for free-rigid body dynamics only the angular momentum is still conserved and the kinetic energy decreases. In this configuration the rotation is now unstable about the axes of minimum moment of inertia. The reader can find the equations of motion and two numerical examples of this dynamical model in the appendix, (see Appendix (A.1)). The fuel rigid-slug model is a particular case of the 3D spherical pendulum in which the pendulum length collapses to zero and the fuel inside the tank is represented by a complete sphere instead of the hemisphere. Therefore we use that model as a test case.

1.4 The Purpose of the Dissertation

The purpose of this dissertation was to develop a software that implements the ESMO attitude dynamic equations, with special interest paid to modeling the internal disturbances such as the thrust vector misalignment and the propellant sloshing model. The equations are formulated in such a way as to allow the orbit and attitude dynamics to work together. Nevertheless the equations are still uncoupled due to the fact that we don't take into account the environmental torques that, as we said before, are responsible for coupling the orbit with the attitude equations. I was a visiting student at the University of Strathclyde in Glasgow [7] and I had the opportunity to work with the Mission Analysis (MIAS) Team of ESMO. This software is used by the MIAS team to give information about the attitude of the ESMO spacecraft and verify if the internal disturbances will create problems for orbit determination and navigation. On the other hand Politecnico di Milano is in charge of the development of Attitude and Orbital Control System (AOCS1 Team), therefore this work can be used by the AOCS1 Team to have an internal description of the ESMO spacecraft (as the propellant sloshing dynamics.). The software is written in a MATLAB environment without the support of the SIMULINK tool of MATLAB. The development of this software allows, for the first time, an interface with the MIAS and AOCS1 Team in which the orbital mechanic and attitude dynamic equations are solved at the same moment. This was

---

[7]Scotland.

possible because the MIAS team provided a MATLAB function that implements
the orbit determination model. As a result of a confidentiality agreement with
the MIAS Team, the orbital determination model function is not visible by users
working with the software developed in this work. However a brief knowledge of
the orbit determination and navigation strategy is necessary. The Earth-Moon
transfer strategy is based on the weak stability boundary (WSB) transfer approach
in the restricted four-body [8] problem. This transfer is used in order to obtain the
in-plane lunar transfer and have a low cost inclination change.

1.5   Arrangement of the work

The dissertation is organized in three chapters:

Chapter 2. This chapter is mainly based on the theory behind the ESMO equa-
tions of motion and the sloshing model equations. An introduction to the reference
frames and rotational kinematic is required to understand how the equations are
written. Finally a description is included of how the consumption of the masses
has been taken into account.
Chapter 3. An entire chapter is dedicated to have a deep understanding of all the
torques acting on ESMO. Particular attention is given to the non-environmental
torques. Finally it is shown how it is possible to pass a control law to the software.
Chapter 4. This chapter is dedicated to showing the results that one can obtain
using the software and the validation of the software to ensure the system equa-
tions were correctly implemented.

Throughout the dissertation, we will use the following mathematical conventions:

$\rightarrow$	vector
Bold letter	matrix
Capital letter	vector defined in the $\mathcal{F}_i$ frame
$\times$	cross product
$\cdot$	dot product

Table 1.1: List of Symbols.

---

[8]Four-Body: Earth, Moon, Sun and Spacecraft.

Chapter 2

Attitude Dynamics of ESMO: Multi-Rigid-Body System

2.1 Rotational Kinematics

Before developing the equation of motion that describe the orientation of the ESMO spacecraft, it is important to focus our attention on certain basic concepts. The orientation of a vector can be defined only with respect to other reference vectors. The minimum noncoplanar reference vectors are three. The orientation of a generic vector $\vec{v}$ is uniquely determinate by the direction cosines between $\vec{v}$ and these reference vectors. The reference vectors form a *Reference Frame*. Under the important assumption of rigid-body, the orientation of a spacecraft can be given by knowing the orientation of a body-fixed reference frame with respect to other. Therefore in case of a multi-body dynamic system, it is necessary to declare the single body-fixed frames for all the objects inside the satellite that one desires to describe, (see Fig. (2.1)). This is the procedure adopted to construct the attitude dynamic equations of ESMO. In Fig. (2.1) is sketched a concept of the ESMO spacecraft and all the reference frames that we have been taken into account to develop the system of equations. We refer to the multi-rigid-body dynamics of ESMO meaning that we consider an internal degrees of freedom due to moving objects inside the satellite. It is not really suitable to talk about multi-rigid-body system when there are internal degrees of freedom. Therefore, it is definitely more correct to use the term *quasi*-rigid instead of simply rigid body. The objects inside ESMO, treating within this dissertation, are: the four reaction wheels[1] and the oxidizer and fuel tanks[2]. In Fig. (2.1) we called with $\mathcal{F}_i$, $\mathcal{F}_o$, $\mathcal{F}_b$, $\mathcal{F}_w$ and $\mathcal{F}_s$ respectively: the inertial frame, the orbital frame, the body-fixed frame, the wheel-fixed frame and the sloshing-fixed frame.

---

[1]The reaction wheels are in a tetrahedral configuration.
[2]To describe the sloshing loads.
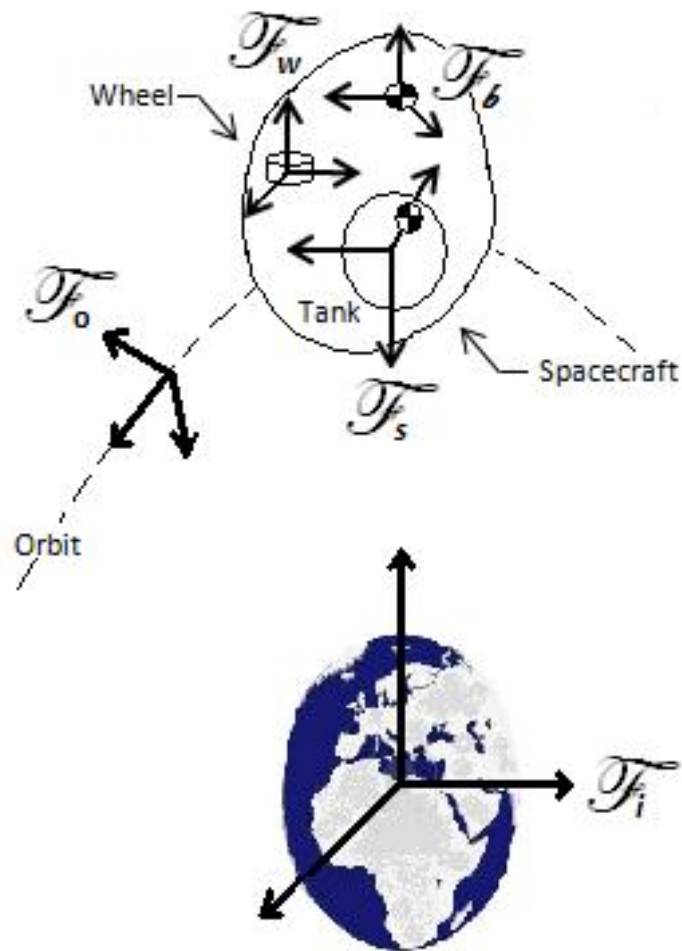
Figure 2.1: Reference Frames.

2.1.1   Reference Frames and Rotations

The origin of the body-fixed frame $\mathcal{F}_b$ is not coincident with the center of ESMO dry mass. The strategy is to choose a geometrical reference frame *embedded* within ESMO that give the orientation of the satellite with respect to other reference frames. We anticipate that it would be more convenient to choose a principal axis frame where the center of mass is coincident with the origin of the reference system. Therefore the motion equations would be simplified. The reason in which we do not follow this strategy is because we would like to consider the propellant mass consumption. It is evident that a reference frame fixed with the mass center will change during the time simulation. On the other hand the geometrical frame is always fixed with the satellite and does not depend on the masses configuration. In the case of the reaction wheel, we choose a reference frame in which the origin is centered with the four wheels mass center. The axises of the wheel-fixed frame $\mathcal{F}_w$ are parallel to those of the $\mathcal{F}_b$ frame, (see Fig. (2.2)). This mean that the direction cosine matrix, describing the orientation of the $\mathcal{F}_w$ frame with respect to the $\mathcal{F}_b$ frame, is an identity. Regarding the propellant-fixed frame $\mathcal{F}_p$ only one axis is *embedded* within the length of the pendulum[3] (see Fig. (2.2)). This is the strategy adopted for both the fuel and the oxidizer tanks. Finally the origin of the inertial frame $\mathcal{F}_i$ has been centered in the center of the celestial-body of interest (see Fig. (2.2)). In Figure (2.2) the $\vec{\omega}$, $\vec{\omega}_w$ and $\vec{\omega}_p$ are the absolute angular velocity of the satellite, the reaction wheels and the 3D spherical pendulum with respect to $\mathcal{F}_i$ frame[4]. CM_d, CM_p and CM_w are the center of mass: dry, of the propellant and of the four reaction wheels.

Direction Cosine Matrix. As we said before, the direction cosine matrix describes the orientation of a reference frame with respect to another. On the viewpoint of the spacecraft, the internal dynamics are in relative motion with the satellite. Therefore for writing the translational and angular equilibrium equations with respect to the $\mathcal{F}_b$ frame, we need to know the relative rotation (rotational matrix) between one frame to another. This rotational matrix is the direction cosine matrix. We define the direction cosine matrixes as follow:

$$\vec{v}_b \triangleq \boldsymbol{C}_{bi}(t)\ \vec{v}_i \tag{2.1.1}$$

$$\vec{v}_f \triangleq \boldsymbol{C}_{fb}(t)\ \vec{v}_b \tag{2.1.2}$$

$$\vec{v}_o \triangleq \boldsymbol{C}_{ob}(t)\ \vec{v}_b \tag{2.1.3}$$

---

[3]The length of the pendulum is assumed to be rigid.

[4]The components of vectors: $\vec{\omega}$ are in the $\mathcal{F}_b$ frame, $\vec{\omega}_w$ are in the $\mathcal{F}_w$ frame and $\vec{\omega}_p$ are in the $\mathcal{F}_p$ frame.

Where $\vec{v}_i$, $\vec{v}_b$, $\vec{v}_f$ and $\vec{v}_o$ are generic vectors in which their components are respectively defined in $\mathcal{F}_i$, $\mathcal{F}_b$, $\mathcal{F}_{p_f}$ and $\mathcal{F}_{p_o}$ [5]. $\boldsymbol{C}_{bi}(t)$ is the rotation between $\mathcal{F}_b$ and $\mathcal{F}_i$ frames. $\boldsymbol{C}_{fb}(t)$ or $\boldsymbol{C}_{ob}(t)$ are the rotation between $\mathcal{F}_{p_f}$ or $\mathcal{F}_{p_o}$ and $\mathcal{F}_b$ frames. By using the rule of sequence rotations, we can write:

$$\boldsymbol{C}_{fi}(t) \triangleq \boldsymbol{C}_{fb}(t) \, \boldsymbol{C}_{bi}(t) \tag{2.1.4}$$

$$\boldsymbol{C}_{oi}(t) \triangleq \boldsymbol{C}_{ob}(t) \, \boldsymbol{C}_{bi}(t) \tag{2.1.5}$$

The rotation matrixes are time depending, therefore the direction cosine derivatives are:

$$\dot{\boldsymbol{C}}_{bi}(t) = -\vec{\omega} \times \boldsymbol{C}_{bi}(t) \tag{2.1.6}$$

$$\dot{\boldsymbol{C}}_{fb}(t) = -\vec{\Omega}_f \times \boldsymbol{C}_{fb}(t) \tag{2.1.7}$$

$$\dot{\boldsymbol{C}}_{ob}(t) = -\vec{\Omega}_o \times \boldsymbol{C}_{ob}(t) \tag{2.1.8}$$

Where $\vec{\Omega}_f$ and $\vec{\Omega}_o$ are the relative angular velocity of the fuel and the oxidizer pendulum with respect to $\mathcal{F}_b$ frame.

Angular Velocity. The decomposition of the angular velocity shows the relation between the absolute and the relative angular velocity, therefore:

$$\vec{\omega}_f = \boldsymbol{C}_{fb} \, \vec{\omega} + \vec{\Omega}_f \tag{2.1.9}$$

$$\vec{\omega}_o = \boldsymbol{C}_{ob} \, \vec{\omega} + \vec{\Omega}_o \tag{2.1.10}$$

Since every term in the vectorial equation must be expressed in the same frame, the Eq. (2.1.9 and 2.1.10) are depending on the cosine direction matrixes: $\boldsymbol{C}_{fb}$ and $\boldsymbol{C}_{ob}$. The orientation of a spacecraft can be expressed with the Euler axis $\vec{a}$ and angle ϕ (Euler's Theorem). It is possible to compute the direction cosine matrix form $\vec{a}$ and ϕ and vice versa. Starting from $\vec{a}$ and ϕ, another kinematic formulation can be given such as: Euler angles, quaternions, direction cosine and Gibbs vector.

---

[5] $\mathcal{F}_{p_f}$ and $\mathcal{F}_{p_o}$ are the fuel and the oxidizer pendulum fixed frame.
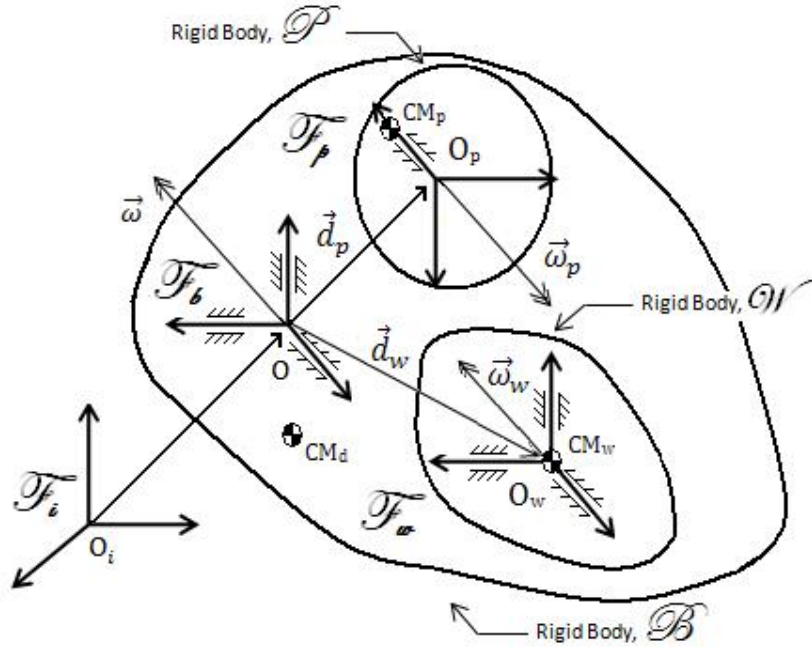
Figure 2.2: ESMO Reference Frames.

2.1.2   Kinematic Formulation

It has been anticipated that several kinematic formulations exist. This section is focused only on the kinematic formulations used for computing the equation of motions. Only two formulations have been used: the quatenions and the Euler angles kinematics. As is well known, it is possible to switch from one formulation to another.

Quaternions. The quaternions are a function of the Euler axis and angle:

$$q = \left\{ \begin{array}{c} \vec{q} \\ q_4 \end{array} \right\} \tag{2.1.11}$$

Where $\vec{q} \equiv \vec{\varepsilon} \triangleq \vec{a} \, \sin\frac{\phi}{2}$ and $q_4 \equiv \eta \triangleq \cos\frac{\phi}{2}$ are a function of the Euler's parameter $\vec{\varepsilon}$ and η. The quaternions kinematic is very useful and it has been used during the integration of the motion equations. Indeed this formulation does not show singularity problems. One can write the differential equation for q which is time depending:

$$\dot{q} = \frac{1}{2} \, \mathcal{Q}(\vec{\omega}) \, q \tag{2.1.12}$$

$$\mathcal{Q}(\vec{\omega}) = \left[\begin{array}{cc} \vec{\omega}\times & \vec{\omega} \\ -\vec{\omega}^T & 0 \end{array} \right] \tag{2.1.13}$$

The Eq. (2.1.12) describes the kinematic of the satellite with respect to the $\mathcal{F}_i$ frame. Therefore the direction cosine matrix $\boldsymbol{C}_{bi}(\boldsymbol{q}, t)$ can be found starting from the quaternions kinematic and vice versa. We also need to define the relative orientation of the fuel and the oxidizer pendulum with respect to the $\mathcal{F}_b$ frame. This means that other two quaternions kinematic formulations need to be defined. Fuel-pendulum quaternions kinematic:

$$\dot{\boldsymbol{q}}_f = \frac{1}{2} \, \boldsymbol{\mathcal{P}}(\vec{\Omega}_f) \, \boldsymbol{q}_f \tag{2.1.14}$$

$$\boldsymbol{\mathcal{P}}(\vec{\Omega}_f) = \begin{bmatrix} \vec{\Omega}_f \times & \vec{\Omega}_f \\ -\vec{\Omega}_f^T & 0 \end{bmatrix} \tag{2.1.15}$$

Oxidizer-pendulum quaternions kinematic:

$$\dot{\boldsymbol{q}}_o = \frac{1}{2} \, \boldsymbol{\mathcal{W}}(\vec{\Omega}_o) \, \boldsymbol{q}_o \tag{2.1.16}$$

$$\boldsymbol{\mathcal{W}}(\vec{\Omega}_o) = \begin{bmatrix} \vec{\Omega}_o \times & \vec{\Omega}_o \\ -\vec{\Omega}_o^T & 0 \end{bmatrix} \tag{2.1.17}$$

The Eq. (2.1.14 and 2.1.16) describes the kinematics of the fuel and the oxidizer pendulum with respect to the $\mathcal{F}_b$ frame. Therefore the direction cosine matrixes $\boldsymbol{C}_{fb}(\boldsymbol{q_f}, t)$ and $\boldsymbol{C}_{ob}(\boldsymbol{q_o}, t)$ can be found starting from the quaternions kinematic and vice versa.

Euler angles. The Euler angles formulation consists of a sequence of three rotations. This kinematic formulation definitely has singularity problems, therefore it is not useful to use Euler angles for integrating the kinematic. On the other hand, working with the angles is more intuitive. It is convenient to express the orientation of the spacecraft with respect to $\mathcal{F}_i$ frame by using the classical azimuth and elevation angles. Throughout the MATLAB code this formulation has been used as an interface with: the user that needs to define the initial ESMO orientation and the orbit navigation function that requires the angles as an input. The Euler angles formulation is closely depending on the sequence of rotations and on the order of the three rotations. If we call with θ_1, θ_2 and θ_3 the rotating angles arounds respectively the first, the second and the third axis, the sequence, that it has been used, is:

$$\boldsymbol{C}(\vec{\theta}) \triangleq \boldsymbol{C}_1(\theta_1) \, \boldsymbol{C}_2(\theta_2) \, \boldsymbol{C}_3(\theta_3) \tag{2.1.18}$$

$$C(\vec{\theta}) = \begin{bmatrix} c_2c_3 & c_2s_3 & -s_2 \\ s_1s_2c_3 - c_1s_3 & s_1s_2s_3 + c_1c_3 & s_1c_2 \\ c_1s_2c_3 + s_1s_3 & c_1s_2s_3 - s_1c_3 & c_1c_2 \end{bmatrix} \tag{2.1.19}$$

In the Equation (2.1.19) c_1, c_2 and c_3 are a brief expression of $\cos\theta_1$, $\cos\theta_2$ and $\cos\theta_3$ and same goes for s_1, s_2 and s_3 that are a brief expression of $\sin\theta_1$, $\sin\theta_2$ and $\sin\theta_3$.

2.2 Newton and Euler's Approach
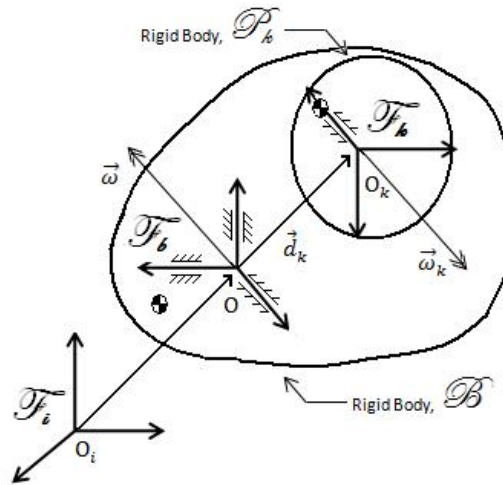
Figure 2.3: Reference Frames.

The formulation adopted to describe the motion equations is vectorial and the basic equations are:

$$\dot{\vec{P}} = \vec{F} \tag{2.2.20}$$

$$\dot{\vec{H}} = \vec{M} \tag{2.2.21}$$

These motion equations are associated with Newton Eq. (2.2.20) and Euler Eq. (2.2.21), so the approach is called "Newton and Euler". In this formulation, one can consider separately the dynamical and kinematical differential equations. We will deeply explain how to write the Equations (2.2.20 and 2.2.21) in the following sections. The Newton and Euler's approach consists in writing the

translational and rotational equilibrium equations of the entire system. In case of additional internal degrees of freedom, inside the spacecraft, it is necessary to add the dynamic equations that describe the movement of the single objects . As we said during the introduction, we have been used the MIAS team function that integrate the translational dynamics. Nevertheless, we treat both the translational and rotational dynamics only to have a complete theoretical formulation. In Fig. (2.3) that it is representative of the reference system, the variable "k" is depending on the number of the tanks.

2.2.1   Linear Momentum

For writing the translational equation of equilibrium, it is necessary to define the linear momentum of the spacecraft and of all the rigid body inside the satellite. The linear momentum of the ESMO satellite $\mathcal{B}$ is:

$$\vec{p} \triangleq \int_{\mathcal{B}} \vec{v} \ dm \qquad (2.2.22)$$

In the Eq.(2.2.22), $\vec{v}$ is the absolute velocity of a generic point P with infinitesimal mass dm within the body $\mathcal{B}$. The absolute velocity must be measured with respect to $\mathcal{O}_i$. If $\vec{\rho}$ is the distance from P to $\mathcal{O}$ and $\vec{v} \triangleq \vec{v}_{\mathcal{O}} + \dot{\vec{\rho}} + \vec{\omega} \times \vec{\rho}$. For a rigid body, $\dot{\vec{\rho}}$ is equal to zero and we can rewrite the angular momentum in the following way:

$$\vec{p} = m_d \ \vec{v}_{\mathcal{O}} + \vec{\omega} \times \vec{c} \qquad (2.2.23)$$

The linear momentum of the reaction wheel system $\mathcal{W}$ is:

$$\vec{p}_w \triangleq \int_{\mathcal{W}} \vec{v}_w \ dm_w \qquad (2.2.24)$$

In the Eq.(2.2.24), $\vec{v}_w$ is the absolute velocity of a generic point P with infinitesimal mass dm_w within the reaction wheels system $\mathcal{W}$. $\vec{\rho}_w$ is the distance from P to $\mathcal{O}_w$ and $\vec{v}_w \triangleq \vec{v}_{\mathcal{O}} + \vec{\omega} \times \vec{d}_w + \vec{\omega}_w \times \vec{\rho}_w$. The reaction wheel system is considered as a rigid body so $\dot{\vec{\rho}}_w$, is equal to zero and we can rewrite the angular momentum as follow:

$$\vec{p}_w = m_w \ \vec{v}_{\mathcal{O}} + m_w \ \vec{\omega} \times \vec{d}_w + \vec{\omega}_w \times \vec{c}_w \qquad (2.2.25)$$

We have been considered the case in which the reaction wheels mass center is coincident with $\mathcal{O}$. Under this hypothesis, $\vec{c}_w$ is equal to zero. The linear momentum of the fuel $\mathcal{P}_f$ and oxidizer $\mathcal{P}_o$ 3D spherical pendulum are:

$$\vec{p}_f \triangleq \int_{\mathcal{P}_f} \vec{v}_f \ dm_f \qquad (2.2.26)$$

$$\vec{p}_o \triangleq \int_{\mathcal{P}_o} \vec{v}_o \ dm_o \qquad (2.2.27)$$

In the Equations (2.2.26 and 2.2.27), $\vec{v}_f$ and $\vec{v}_o$ are the absolute velocity of a generic point P with infinitesimal mass dm_f and dm_o within the 3D spherical pendulum $\mathcal{P}_f$ and $\mathcal{P}_o$. $\vec{\rho}_f$ and $\vec{\rho}_o$ are the distance from P to respectively $\mathcal{O}_f$ and $\mathcal{O}_o$ (see Fig. 2.3). The absolute velocities are: $\vec{v}_f \triangleq \vec{v}_{\mathcal{O}} + \vec{\omega} \times \vec{d}_f + \vec{\omega}_f \times \vec{\rho}_f$ and $\vec{v}_o \triangleq \vec{v}_{\mathcal{O}} + \vec{\omega} \times \vec{d}_o + \vec{\omega}_o \times \vec{\rho}_o$. Under the hypothesis of rigid pendulum $\dot{\vec{\rho}}_f$ and $\dot{\vec{\rho}}_f$ must be zero. One can rewrite:

$$\vec{p}_f = m_f \ \vec{v}_{\mathcal{O}} + m_f \ \vec{\omega} \times \vec{d}_f + \vec{\omega}_f \times \vec{c}_f \qquad (2.2.28)$$

$$\vec{p}_o = m_o \ \vec{v}_{\mathcal{O}} + m_o \ \vec{\omega} \times \vec{d}_o + \vec{\omega}_o \times \vec{c}_o \qquad (2.2.29)$$

In the Equations (2.2.22, 2.2.24, 2.2.26 and 2.2.27), m_d, m_w, m_f and m_o are respectively the dry mass of $\mathcal{B}$, the reaction wheels mass, the fuel mass and the oxidizer mass. Other new terms comparing in those equations are the static momentum of: the satellite $\vec{c}$, the reaction wheels $\vec{c}_w$, the fuel and the oxidizer pendulum $\vec{c}_f$ and $\vec{c}_o$. The generic definition of the Static Momentum is:

$$\vec{c} \triangleq \int_{\mathcal{B}} dm \qquad (2.2.30)$$

We anticipate that in case of propellant consumption, $\vec{c}$ becomes time depending. Therefore we have to compute the differential equation for $\vec{c}$.

2.2.2 Angular Momentum

For writing the rotational equation of equilibrium, it is necessary to define the angular momentum of the spacecraft and of all the rigid bodies inside the satellite. The angular momentum of the ESMO satellite $\mathcal{B}$ is:

$$\vec{h} \triangleq \int_{\mathcal{B}} \rho \times \vec{v} \ dm \qquad (2.2.31)$$

As for the linear momentum of $\mathcal{B}$ the velocity $\vec{v}$ is $\vec{v}_{\mathcal{O}} + \vec{\omega} \times \vec{\rho}$ and the Eq. (2.2.31) becomes:

$$\vec{h} = \vec{c} \times \vec{v}_{\mathcal{O}} + \boldsymbol{I}_d \ \vec{\omega} \qquad (2.2.32)$$

The angular momentum of the reaction wheel system $\mathcal{W}$ is:

$$\vec{h}_w \triangleq \int_{\mathcal{W}} \vec{\rho}_w \times \vec{v}_w \; dm_w \tag{2.2.33}$$

In the Eq.(2.2.33), the absolute velocity $\vec{v}_w$ is $\vec{v}_{\mathcal{O}} + \vec{\omega} \times \vec{d}_w + \vec{\omega}_w \times \vec{\rho}_w$. Therefore rewriting the Eq. (2.2.33) we have:

$$\vec{h}_w = \boldsymbol{I}_w \; \vec{\omega}_w \tag{2.2.34}$$

We have four reaction wheels in a tetrahedral configuration, therefore the Eq. (2.2.34) has not been written properly. It is better to express the angular momentum in the following way:

$$\vec{h}_w = \boldsymbol{A}_w \; \boldsymbol{I}_w \; \vec{\omega}_w \tag{2.2.35}$$

In the equation (2.2.35), $\boldsymbol{A}_w$ is a (3 X 4) matrix dimension. The columns of this matrix represent the direction cosine of the rotational axis of each wheel:

$$\boldsymbol{A}_w = \begin{bmatrix} -a & a & a & -a \\ -a & -a & a & a \\ a & a & a & a \end{bmatrix} \tag{2.2.36}$$

The project parameter "a", in the equation (2.2.36), is equal to $\frac{1}{\sqrt{3}}$ [6]. The angular momentum of the fuel $\mathcal{P}_f$ and oxidizer $\mathcal{P}_o$ 3D spherical pendulum are:

$$\vec{h}_f \triangleq \int_{\mathcal{P}_f} \rho_f \times \vec{v}_f \; dm_f \tag{2.2.37}$$

$$\vec{h}_o \triangleq \int_{\mathcal{P}_o} \rho_o \times \vec{v}_o \; dm_o \tag{2.2.38}$$

The absolute angular velocity $\vec{v}_f$ and $\vec{v}_o$ of the equations (2.2.37 and 2.2.38) are respectively $\vec{v}_f \triangleq \vec{v}_{\mathcal{O}} + \vec{\omega} \times \vec{d}_f + \vec{\omega}_f \times \vec{\rho}_f$ and $\vec{v}_o \triangleq \vec{v}_{\mathcal{O}} + \vec{\omega} \times \vec{d}_o + \vec{\omega}_o \times \vec{\rho}_o$. The equations (2.2.37 and 2.2.38) become:

$$\vec{h}_f = \vec{c}_f \times \vec{v}_{\mathcal{O}} + \boldsymbol{J}_{fb} \; \vec{\omega} + \boldsymbol{I}_f \; \vec{\omega}_f \tag{2.2.39}$$

$$\vec{h}_o = \vec{c}_o \times \vec{v}_{\mathcal{O}} + \boldsymbol{J}_{fo} \; \vec{\omega} + \boldsymbol{I}_o \; \vec{\omega}_o \tag{2.2.40}$$

---

[6]Tetrahedral configuration.

In the Equations (2.2.32, 2.2.34, 2.2.39 and 2.2.40), $\boldsymbol{I}_d$, $\boldsymbol{I}_w$, $\boldsymbol{I}_f$ and $\boldsymbol{I}_o$ are respectively the moment of inertia of: the satellite $\mathcal{B}$, the reaction wheels, the fuel and the oxidizer pendulum. The satellite moment of inertia in the dry mass case is:

$$\boldsymbol{I}_d{}^7 \triangleq \int_{\mathcal{B}} (|\vec{\rho}|^2 - \vec{\rho}\vec{\rho}^T)\,dm \tag{2.2.41}$$

The moment of inertia of the reaction wheels system is:

$$\boldsymbol{I}_w \triangleq \int_{\mathcal{W}} (|\vec{\rho}_w|^2 \mathbf{1} - \vec{\rho}_w \vec{\rho}_w^T)\,dm_w \tag{2.2.42}$$

For the fuel and oxidizer 3D spherical pendulum the moments of inertia are:

$$\boldsymbol{I}_f \triangleq \int_{\mathcal{P}_f} (|\vec{\rho}_f|^2 \mathbf{1} - \vec{\rho}_f \vec{\rho}_f^T)\,dm_f \tag{2.2.43}$$

$$\boldsymbol{I}_o \triangleq \int_{\mathcal{P}_o} (|\vec{\rho}_o|^2 \mathbf{1} - \vec{\rho}_o \vec{\rho}_o^T)\,dm_o \tag{2.2.44}$$

In the equations (2.2.39 and 2.2.40), there are other two moments of inertia terms: $\boldsymbol{J}_{fb}$ and $\boldsymbol{J}_{fb}$. They are mixed moment of inertia between the spacecraft and the fuel or oxidizer pendulum. These moments of inertia are defined as follow:

$$\boldsymbol{J}_{fb} \triangleq \vec{c}_f^T \vec{d}_f - \vec{c}_f \vec{d}_f^T \tag{2.2.45}$$

$$\boldsymbol{J}_{ob} \triangleq \vec{c}_o^T \vec{d}_o - \vec{c}_o \vec{d}_o^T \tag{2.2.46}$$

We anticipate that in case of propellant consumption the moments of inertia become time depending. Therefore we have to compute the differential equation for the static momentum and the moments of inertia that are a function of the propellant mass.

---

[7]Dyadic of inertia.

2.2.3   The Equation of Motion: propellant sloshing dynamics

The translational equilibrium or Newton equation of the multi-*quasi*-rigid body system is:

$$\dot{\vec{P}} = \vec{F}^{ext} + \boldsymbol{C}_{fb}^T \vec{F}_f + \boldsymbol{C}_{ob}^T \vec{F}_o \qquad (2.2.47)$$

Where $\dot{\vec{P}}$ is the derivative of the total linear momentum with respect to the inertial frame $\mathcal{F}_i$, see the following equation:

$$\dot{\vec{P}} = \dot{\vec{p}} + \vec{\omega} \times \vec{p} \qquad (2.2.48)$$

In the Eq. (2.2.48), $\vec{p}$ is the total linear momentum of the multi-*quasi*-rigid body system and one can write:

$$\vec{p} = \vec{p}_b + \vec{p}_w + \boldsymbol{C}_{fb}^T \, \vec{p}_f + \boldsymbol{C}_{ob}^T \, \vec{p}_o \qquad (2.2.49)$$

If we substitute the Eq. (2.2.49) in the Eq. (2.2.48), therefore the Eq. (2.2.48) changes into:

$$\begin{aligned}
&\dot{\vec{p}}_b + \dot{\vec{p}}_w + \dot{\boldsymbol{C}}_{fb}^T \, \vec{p}_f + \boldsymbol{C}_{fb}^T \, \dot{\vec{p}}_f + \dot{\boldsymbol{C}}_{ob}^T \, \vec{p}_o + \boldsymbol{C}_{ob}^T \, \dot{\vec{p}}_o + \\
&\vec{\omega} \times (\vec{p}_b + \vec{p}_w + \boldsymbol{C}_{fb}^T \, \vec{p}_f + \boldsymbol{C}_{ob}^T \, \vec{p}_o) = \vec{F}^{ext} + \boldsymbol{C}_{fb}^T \vec{F}_f + \boldsymbol{C}_{ob}^T \vec{F}_o
\end{aligned} \qquad (2.2.50)$$

The rotational equilibrium or the Euler equation of the entire system is:

$$\dot{\vec{H}} = \vec{M}^{ext} + \boldsymbol{C}_{fb}^T \vec{M}_f + \boldsymbol{C}_{ob}^T \vec{M}_o \qquad (2.2.51)$$

$\dot{\vec{H}}$ is the derivative of the total angular momentum with respect to the inertial frame $\mathcal{F}_i$, therefore one can write:

$$\dot{\vec{H}} = \dot{\vec{h}} + \vec{\omega} \times \vec{h} + \vec{v}_{\mathcal{O}} \times \vec{p} \qquad (2.2.52)$$

In the Eq. (2.2.52), $\vec{h}$ is the total angular momentum of the system, see the following equation:

$$\vec{h} = \vec{h}_b + \vec{h}_w + \boldsymbol{C}_{fb}^T \, \vec{h}_f + \boldsymbol{C}_{ob}^T \, \vec{h}_o \qquad (2.2.53)$$

If we substitute the Eq.(2.2.53) in the Eq. (2.2.52), therefore the Eq. (2.2.52) changes into:

$$\dot{\vec{h}}_b + \dot{\vec{h}}_w + \dot{\boldsymbol{C}}_{fb}^T \, \vec{h}_f + \boldsymbol{C}_{fb}^T \, \dot{\vec{h}}_f + \dot{\boldsymbol{C}}_{ob}^T \, \vec{h}_o + \boldsymbol{C}_{ob}^T \, \dot{\vec{h}}_o + \vec{\omega} \times (\vec{h}_b +$$
$$\vec{h}_w + \boldsymbol{C}_{fb}^T \, \vec{h}_f + \boldsymbol{C}_{ob}^T \, \vec{h}_o) + \vec{v}_{\mathcal{O}} \times \vec{p} = \vec{M}^{ext} + \boldsymbol{C}_{fb}^T \vec{M}_f + \boldsymbol{C}_{ob}^T \vec{M}_o \tag{2.2.54}$$

The dynamics of the reaction wheels is described by the following equation:

$$\dot{\vec{h}}_w = (A)_w \boldsymbol{I}_w \dot{\vec{\omega}}_w = \vec{M}_w \tag{2.2.55}$$

One can substitute the Eq. (2.2.55) into the Eq. (2.2.54) and write:

$$\dot{\vec{h}}_b + \dot{\boldsymbol{C}}_{fb}^T \, \vec{h}_f + \boldsymbol{C}_{fb}^T \, \dot{\vec{h}}_f + \dot{\boldsymbol{C}}_{ob}^T \, \vec{h}_o + \boldsymbol{C}_{ob}^T \, \dot{\vec{h}}_o + \vec{\omega} \times (\vec{h}_b +$$
$$\vec{h}_w + \boldsymbol{C}_{fb}^T \, \vec{h}_f + \boldsymbol{C}_{ob}^T \, \vec{h}_o) + \vec{v}_{\mathcal{O}} \times \vec{p} = \vec{M}^{ext} + \boldsymbol{C}_{fb}^T \vec{M}_f + \boldsymbol{C}_{ob}^T \vec{M}_o - \vec{M}_w \tag{2.2.56}$$

In the Eq. (2.2.56) the dynamics of the reaction wheel is viewed such as an external torques but its nature is non-environmental. Therefore $\vec{M}_w$ is the control torques of the reaction wheels. Looking at the right side of the equations (2.2.50 and 2.2.54), $\vec{F}^{ext}$ and $\vec{M}^{ext8}$ are the external forces and torques acting on the satellite. $\vec{F}_f, \vec{F}_o$, $\vec{M}_f$ and $\vec{M}_o$ are the forces and the torques acting on the fuel and oxidizer pendulum masses center. These forces and torques are depending on the linear acceleration induced by the engine thrust. The equations (2.2.50, 2.2.54 and 2.2.55) are not sufficient to close the problem. Other two rotational equations of equilibrium are needed, therefore we wrote the fuel and the oxidizer 3D spherical pendulum equations:

$$\dot{\vec{H}}_f = \dot{\vec{h}}_f + \vec{\omega}_f \times \vec{h}_f + \boldsymbol{D}_f \, \vec{\Omega}_f + \vec{v}_{\mathcal{O}} \times \vec{p}_f = \vec{M}_f \tag{2.2.57}$$

$$\dot{\vec{H}}_o = \dot{\vec{h}}_o + \vec{\omega}_o \times \vec{h}_o + \boldsymbol{D}_o \, \vec{\Omega}_o + \vec{v}_{\mathcal{O}} \times \vec{p}_o = \vec{M}_o \tag{2.2.58}$$

$\boldsymbol{D}_f$ and $\boldsymbol{D}_o$ are the damping coefficients matrixes. $\vec{\Omega}_f$ and $\vec{\Omega}_o$ are the relative angular velocities with respect to the $\mathcal{F}_b$ frame. These relative angular velocity have been written as:

$$\vec{\Omega}_f = \vec{\omega}_f - \boldsymbol{C}_{fb} \, \vec{\omega} \tag{2.2.59}$$

$$\vec{\Omega}_o = \vec{\omega}_o - \boldsymbol{C}_{ob} \, \vec{\omega} \tag{2.2.60}$$

---

[8] $\vec{M}^{ext}$ is calculated respect the origin $\mathcal{O}$.

Finally we can organize the equations above in the following system:

$$\begin{cases} \dot{\vec{P}} = \vec{F}^{ext} + \boldsymbol{C}_{fb}^T\vec{F}_f + \boldsymbol{C}_{ob}^T\vec{F}_o \\ \dot{\vec{H}} = \vec{M}^{ext} + \boldsymbol{C}_{fb}^T\vec{M}_f + \boldsymbol{C}_{ob}^T\vec{M}_o \\ \dot{\vec{H}}_f = \vec{M}_f \\ \dot{\vec{H}}_o = \vec{M}_o \\ \dot{\vec{h}}_w = \vec{M}_w \end{cases} \tag{2.2.61}$$

The Eq. (2.2.61) is the so called Newton and Euler equations. In that system of equations the $\vec{M}_f$ and $\vec{M}_o$ are the torques due to the induced acceleration by the engines and they are respectively defined in the $\mathcal{F}_{p_f}$ and $\mathcal{F}_{p_o}$ frame. The direction of the length of the fuel and oxidizer pendulum, $\vec{d}_f$ and $\vec{d}_o$ are constant in the $\mathcal{F}_{p_f}$ and $\mathcal{F}_{p_o}$ frame. The direction of the induced acceleration vectors $\vec{a}_f$ and $\vec{a}_o$ are constant in the $\mathcal{F}_b$ frame [9]. The length of the fuel and the oxidizer pendulum define in the $\mathcal{F}_{p_f}$ and $\mathcal{F}_{p_o}$ frame are:

$$\vec{l}_f = \begin{Bmatrix} l_f \\ 0 \\ 0 \end{Bmatrix} \tag{2.2.62}$$

$$\vec{l}_o = \begin{Bmatrix} l_o \\ 0 \\ 0 \end{Bmatrix} \tag{2.2.63}$$

The induced acceleration vectors define in the $\mathcal{F}_b$ frame are:

$$\vec{a}_f = \begin{Bmatrix} 0 \\ 0 \\ -a_f \end{Bmatrix} \tag{2.2.64}$$

$$\vec{a}_o = \begin{Bmatrix} 0 \\ 0 \\ -a_o \end{Bmatrix} \tag{2.2.65}$$

The torques due to these accelerations, that are defined in the $\mathcal{F}_f$ and $\mathcal{F}_o$ frame, can be written as $\vec{M}_f = m_f\, \vec{l}_f \times \boldsymbol{C}_{fb}^T\, \vec{a}_f$ and $\vec{M}_o = m_o\, \vec{l}_o \times \boldsymbol{C}_{ob}^T\, \vec{a}_o$.

---

[9]They depend on the ESMO configuration.

2.3 Kinetic and Potential Energy

The other dynamical quantity of interest is the kinetic energy. We studied the free-body dynamics to demonstrate that without external torques, the angular momentum is conserved, with respect to the $\mathcal{F}_i$, only along the direction of the induced acceleration. The energy is conserved if there are not dissipative sinks. The kinetic energy of the entire system is:

$$
\begin{aligned}
T \;=\; & \frac{1}{2} \int_{\mathcal{B}} (\vec{v}_{\mathcal{O}} + \vec{\omega} \times \vec{\rho}_b) \cdot (\vec{v}_{\mathcal{O}} + \vec{\omega} \times \vec{\rho}_b)\, dm_b \;+ \\
& \frac{1}{2} \int_{\mathcal{W}} (\vec{v}_{\mathcal{O}} + \vec{\omega} \times \vec{d}_w) \cdot (\vec{v}_{\mathcal{O}} + \vec{\omega} \times \vec{d}_w)\, dm_w \;+ \\
& \frac{1}{2} \int_{\mathcal{P}_f} (\vec{v}_{\mathcal{O}} + \vec{\omega} \times \vec{d}_f + \vec{\omega}_f \times \vec{\rho}_f) \cdot (\vec{v}_{\mathcal{O}} + \vec{\omega} \times \vec{d}_f + \vec{\omega}_f \times \vec{\rho}_f)\, dm_f \;+ \\
& \frac{1}{2} \int_{\mathcal{P}_o} (\vec{v}_{\mathcal{O}} + \vec{\omega} \times \vec{d}_o + \vec{\omega}_o \times \vec{\rho}_o) \cdot (\vec{v}_{\mathcal{O}} + \vec{\omega} \times \vec{d}_o + \vec{\omega}_o \times \vec{\rho}_o)\, dm_o \quad (2.3.66)
\end{aligned}
$$

The potential energy is $U = m_f\, \vec{l}_f \cdot \boldsymbol{C}_{fb}^T\, \vec{a}_f + m_o\, \vec{l}_o \cdot \boldsymbol{C}_{ob}^T\, \vec{a}_o$ and the total energy is $E = T - U$. In order to test the equation above, one can simplify the system by setting the $\vec{v}_{\mathcal{O}}$ equal to zero.
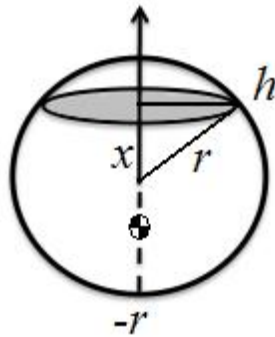
2.4 Propellant Consumption

Figure 2.4: Tank view.

Due to the propellant consumption, there are some terms in the Eq. (2.3.66) that become time depending, such as the static and angular momentum of the fuel an oxidizer pendulum. Before deriving these two quantities, we need to follow the

method that we are going to show in this section. As it is well known, the mass consumption is compute as follow:

$$\frac{dm_w}{dt} = -\frac{|\vec{T}|}{I_{sp}g_0} \tag{2.4.67}$$

In Eq. (2.4.67), m_w, $\vec{T}$, I_{sp} and g_0 are respectively the mass wet of the satellite, the thrust vector, the specific impulse and the gravity acceleration. Starting from the wet mass and knowing the fuel-oxidizer ratio, one can find m_f and m_o. Therefore we can compute the volume inside the fuel and oxidizer tank: V_f and V_o [10]. In the following equations we consider a generic tank, therefore all the expressions are valid for both the fuel and oxidizer tanks. The volume V of the tank is defined with its integral expression:

$$V(m_w) = \int_{-r}^{h} A_s \, dx = \int_{-r}^{h} \pi s^2 \, dx \tag{2.4.68}$$

In the Eq. (2.4.68), h is the unknown and it is the level distance from the center of the tank. The position of the centre of mass with respect to the center of the tank is:

$$x_{cm} = y_{cm} = 0; \; z_{cm}(m_w) = \frac{\int_{-r}^{h} \pi(r^2 - x^2)x \, dm}{V(m_w)} \tag{2.4.69}$$

The linear and the angular momentum are computed with respect to the origin of the tank in the following way:

$$\vec{c}(m_w) = m_{tk}\vec{l}_p \tag{2.4.70}$$

$$\boldsymbol{I}(m_w) = \int_{-r}^{h} \int_{-\sqrt{r^2-x^2}}^{\sqrt{r^2-x^2}} \int_{-\sqrt{r^2-x^2-y^2}}^{\sqrt{r^2-x^2-y^2}} \rho(x,y,x) \, \boldsymbol{\mathcal{I}}(x,y,z) \, dz \, dy \, dx \tag{2.4.71}$$

In the Eq. (2.4.71), $\boldsymbol{\mathcal{I}}(x,y,z)$ is defined as:

$$\boldsymbol{\mathcal{I}}(x,y,z) = \begin{bmatrix} y^2 + x^2 & -xy & -xz \\ -xy & z^2 + x^2 & -yz \\ -xz & -yz & x^2 + y^2 \end{bmatrix} \tag{2.4.72}$$

Now we can calculate the differential for $\vec{c}(m_w)$ and $\boldsymbol{I}(m_w)$:

---

[10]The fuel and oxidizer densities are consider as a constants: ρ_f and ρ_o.

$$\frac{d\vec{c}}{dt} = \frac{d\vec{c}}{dm_{tk}} \frac{dm_{tk}}{dt} \tag{2.4.73}$$

$$\frac{d\boldsymbol{I}}{dt} = \frac{d\boldsymbol{I}}{dm_{tk}} \frac{dm_{tk}}{dt} \tag{2.4.74}$$

The term m_{tk} is the expression of the mass inside the tank.

Chapter 3

Spacecraft Torques

3.1 Environmental Torques

In Chapter 2 we dealt with the mathematical formulation but we do not alight
on the "right hand" terms of the equation of motions, that is the aim of Chap-
ter 3. As said in the Introduction, the spacecraft torques can be classified into
two categories: external or internal torques. The external torques stem from the
interaction between the spacecraft and the environment. Calculation of external
torques requires knowledge of the satellite characteristics and of the space envi-
ronment. The principal external torques are: the gravitational, the aerodynamic,
the radiation and the magnetic torques. In this dissertation we deal only with the
internal torques, therefore the AOCS1 Team is in charge of developing the space
environment model. For this reason, we limit ourself to considering the nature of
the external torques instead of showing their analytical formulations.

3.2 Non-Environmental Torques

As we have just mentioned, the internal torques are self generated. For a deeply
"state of the art" review of the internal torques, we refer to the Introduction. In
this section, only the thrust vector misalignment torques are treated because they
are more significant than the others in this case.

3.2.1 Thrust Vector Misalignment

"A standard procedure is to assume a fixed misalignment of from one to several
degrees and evaluate the torque or angular impulse", NASA [1]. Additionally, one
can estimate the location and the variation in the center of gravity from mass
properties data. The major cause of disturbance torques from thrust-generation
systems are: the misalignment of the thrust vector, the impingement of the ex-
ternal plume and the deviation between the geometric axis of the thruster and

the actual line of the thrust. For reaction control system, misalignment and impingement cause the disturbances torques. In this dissertation we only study the disturbance effects due to the misalignment. Thrust misalignment problems tend to increase as nozzle size decreases. For larger nozzles, it is possible to have thrust misalignment as small as 0.1° or 0.2°, otherwise small nozzles often have as mach as 1° or 2°. We can mechanically aline a nozzle to about 15 arcmin, but this alignment will be degraded by subsequent handling and environmental stresses. On new designs, it appears that the misalignment is about 1° or 2° due to the thermal distortions coupled with mechanical discontinuities; this misalignment can be reduced to about 0.2° to 0.3° by refinement of the design. Usually if engines has the thrust vector control, the misalignment disturbances became negligible. In the case of ESMO we fixed the thrust misalignment angle to 1°. In a three dimensional space the thrust vector belongs to a cone in which the cone angle is the misalignment angle (see Fig. 3.1). Obviously there exists an uncertainty in how the thrust vector is oriented with respect to this cone. The idea is to use the random function of MATLAB with a Gaussian distribution, where 3σ is half of the interval rotational degree of freedom around the axis of the cone. Therefore, if 3σ is equal to half of a complete rotation π, σ is equal to $\frac{\pi}{3}$. ESMO has four main engines so for each engine the thrust had an uncertainty in the orientation.
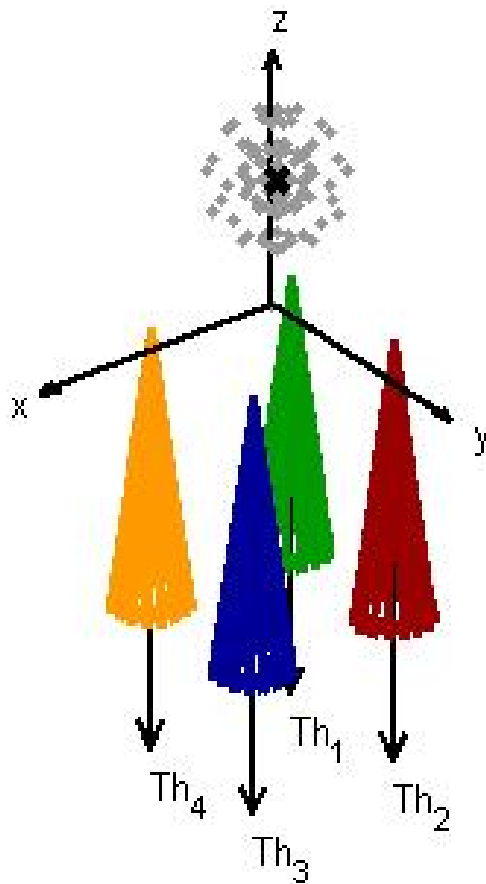
Figure 3.1: Thrust Vector Misalignment with the Uncertainly in the center of Mass[2].

3.3   Control Torques

Usually, the control torques act on the satellite throughout the actuators and their purpose is to counteract the disturbances torques. ESMO is equipped with four reaction wheels and four cold thrusters that are orientated in the same direction as the main engines. When the control torques are output from the control system, they are passed to the actuators system. In the development of the software, we did not write a control law as the AOCS2 team is in charge of designing it. Nevertheless this software is arranged in such a way that the user can easily pass the control law like an input. For our study, it was unnecessary to develop an actuator model. Therefore the control torques are directly acting on the "right hand" of the equations.

Chapter 4

Analysis and Results

4.1   Propellant Sloshing Disturbances

During the development of the software, intermediate analysis and tests have been done to validate the MATLAB code. First of all to validate the simple Euler equation, the conservation of the angular momentum and of the kinetic energy [1] have been investigated. Secondly to verify that the numerical solution [2], in terms of angular velocity and quaternions, are correct; a simple analytical solution have been compared with the numerical one. As it is well known, under simplify hypothesis it is possible to find an analytical close-form solution. A very interesting approximate close-form solution (Wertz [5]) has been used to verify the quaternions numerical one without restricted hypothesis on the angular velocity[3]. We are not going to show the analytical solutions because they are largely treated into the literature, but we find very interesting the approximate close-form solution for the quaternions that one can find into the Appendix (B.1).

3D Rigid Spherical Pendulum. The purpose of this dissertation is to model the propellant sloshing effect from an engineering viewpoint: the 3D rigid spherical pendulum model[4] has been embraced. In the early study we wrote the dynamics of the pendulum by using the Euler approach. As it is well known, without external torques (free-torques dynamics), the angular momentum with respect to the inertial frame $\mathcal{F}_i$ is conserved. In the case of the pendulum, we have a self generated disturbances due to the engines thrust. This disturbance has the form of an induced acceleration that on the viewpoint of the pendulum, is treated like an "external" disturbance. Obviously the nature of this disturbance is non-environment. This mean that for the conservation of the angular momentum, we

---

[1]Under the hypothesis of free-torques dynamics without sink source.

[2]ODE MATLAB function.

[3]The quaternions numerical solution in analytical close-form can be verify only under the hypothesis of constants angular velocity.

[4]The 3D rigid spherical pendulum is a generalization of the fuel slug model.

will expect that only the component direct as the acceleration vector is conserved, (see Fig. (4.1)).
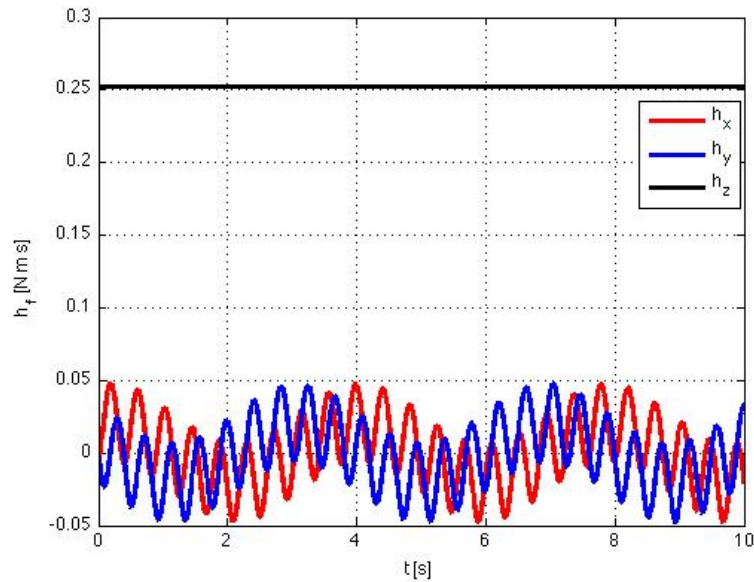

Figure 4.1: 3D Pendulum: Angular Momentum.

The other quantity of interest is the kinetic energy that, without dissipative sink, is conserved. In the following figures (4.2, 4.3,4.4 and 4.5), one can appreciate the effect of the damping element. In table (4.1), the initial conditions, used for obtaining the follows solutions, have been summarized.
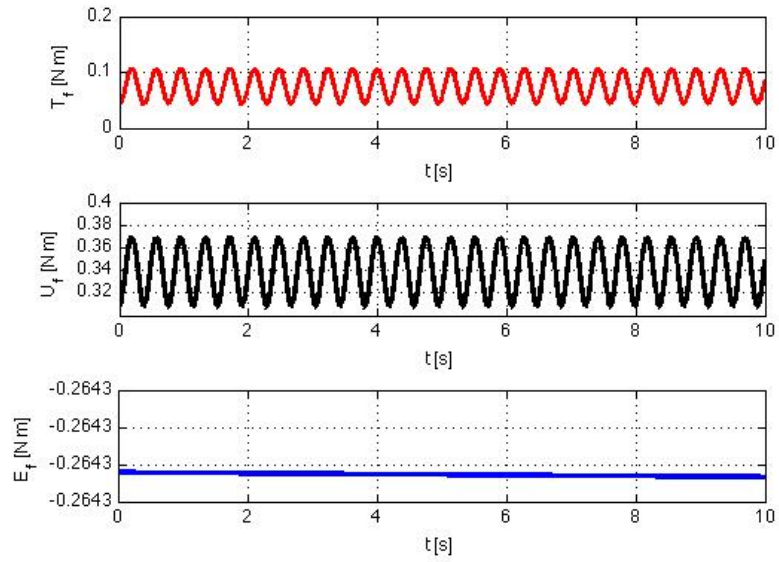
Figure 4.2: 3D Pendulum: Energy.
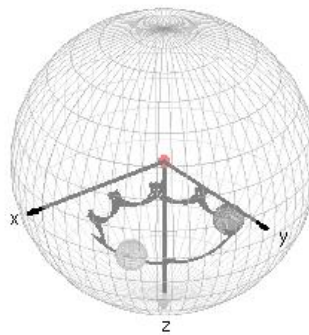
Figure 4.3: 3D Pendulum: Trajectory.
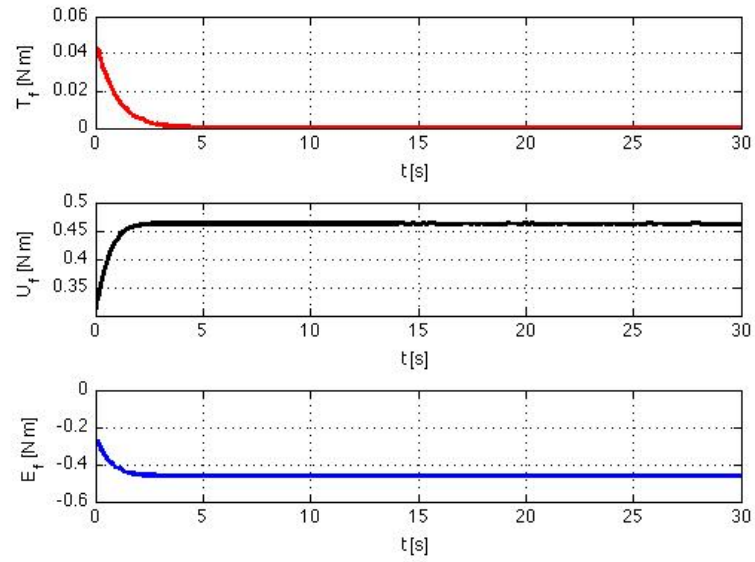
Figure 4.4: 3D Pendulum: Energy.
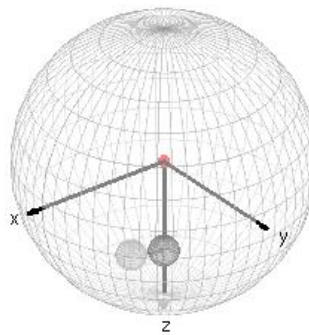
Figure 4.5: 3D Pendulum: Trajectory with damper effect.

Case	$\vec{\Omega}_0[rad/s]$	$c_f[Nms]$	$a_f[ms^{-1}]$	$a_o[ms^{-1}]$
1	[0,0,0.5]	0	0.1011	0.1011
2	[0,0,0.5]	0.4	0.1011	0.1011

Table 4.1: 3D Pendulum: initial condition.

Two-Rigid-Body Model. After the verification of the 3D pendulum solution, it has been developed an improved model: the two-rigid-body dynamics. This model is quite similar to the fuel rigid-slug model where the tank is centered at the origin of the $\mathcal{F}_b$ frame. The two rigid bodies are the satellite $\mathcal{B}$ and the 3D fuel pendulum $\mathcal{P}_f$. The two dynamics equations are coupled only throughout the damper coefficient, (see Appendix (B.2)), and then it has been verified that, without the damper effect, the pendulum dynamics do not affect the satellite motion.

ESMO Multi-Rigid-Body Model. Finally we have implemented the system of the equations applied to ESMO, (see the mathematical approach in Chapter 2). The multi-rigid-body model deals with the Newton and Euler equations in which the dynamics of the fuel and oxidizer sloshing and of the four reaction wheels, has been investigated. A brief overview of the ESMO configuration and data, has been given in section (4.3). In section (4.1.1), different solutions depending on the initial conditions, has been investigated. In this software, two different dynamics, has been implemented and studied, (see section (4.1.2)): one describes the two-rigid-body model, (see Appendix (B.2)) and the other one is the multi-rigid-body model, (see Chapter 2). Each of these dynamics have two different variants:

- In one case the equations have been solved without the orbit dynamics model;

- In the other case the attitude dynamics and the orbit dynamics equations have been interfaced.

The solutions are sensitive on the damper coefficient parameter [5], (see section (4.1.3)). For each dynamics equations that one can choose in this software, there is the possibility to consider or not the propellant consumption, (see section (4.1.4)). The effect of the mass expulsion torques, in the solutions, has been given in section (4.2). All the solutions and results that one can encounter throughout this dissertation, has been influenced by the initial condition of ESMO in its trajectory transfer, (see section (4.4)).

---

[5]This parameter depend on: the size of the tank, the characteristic of the fluid and the fill ratio of the container. They are depending on experimental data.

4.1.1   Initial Condition

The solution of the motion equations is sensitive to the initial conditions. In the Tab. (4.2 and 4.3), the initial conditions of the two cases analyzed has been given.

Case	$\omega_b[rad/s]$	$\Omega_f[rad/s]$	$\Omega_o[rad/s]$	$c_f[Nms]$	$c_o[Nms]$
1	[0,0,0]	[0,1.5, 0]	[0,1.5, 0]	0	0
2	[0,0,0]	[0,0,0.9]	[0,0,0.9]	0	0

Table 4.2: Initial Condition.

Case	$\vec{\alpha}_0[deg]$	$\vec{\alpha}_{f_0}[deg]$	$\vec{\alpha}_{o_0}[deg]$
1	[0,0,0]	[0,90, 0]	[0,90, 0]
2	[0,0,0]	[0,-10,0]	[0,-10,0]

Table 4.3: Kinematic Initial Condition.

The vectors $\vec{\alpha}$, $\vec{\alpha}_f$ and $\vec{\alpha}_o$ are the Euler angles and they describe respectively the orientation: of the satellite with respect to $\mathcal{F}_i$ frame and of the fuel and the oxidizer pendulum with respect to $\mathcal{F}_b$ frame.

Case 1
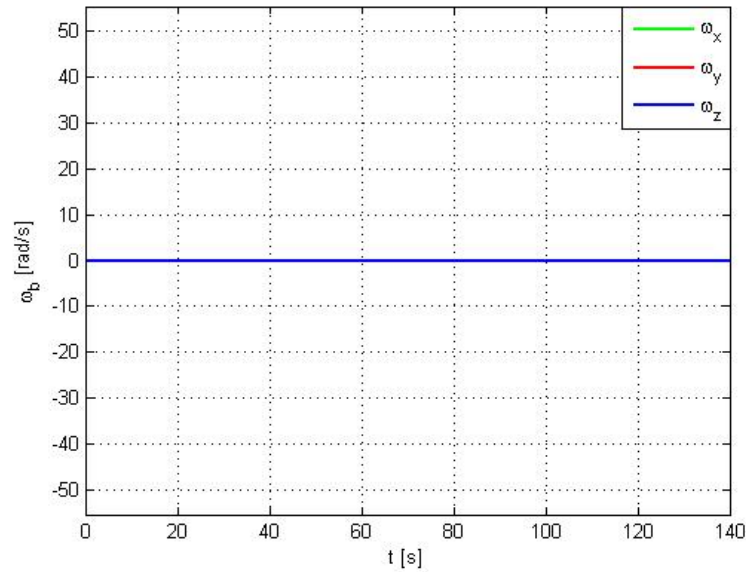
Figure 4.6: Case 1: Angular Velocity of ESMO.
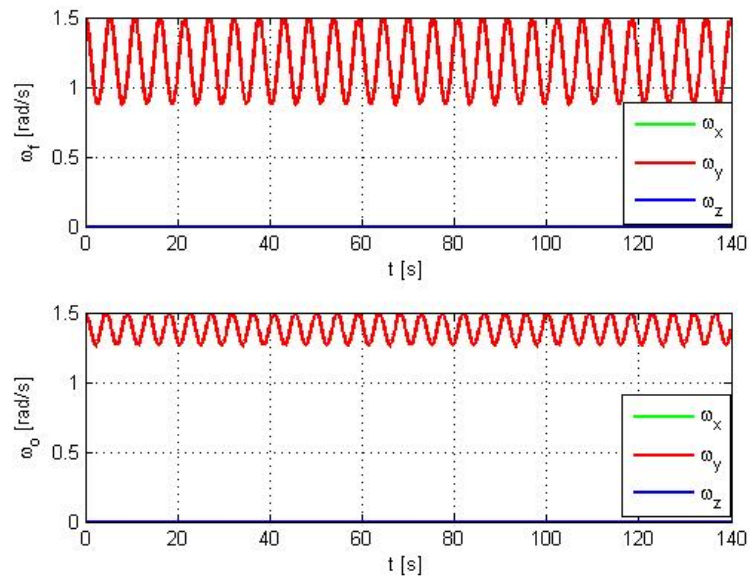
Figure 4.7: Case 1: Angular Velocity of the Fuel and Oxidizer Pendulum.
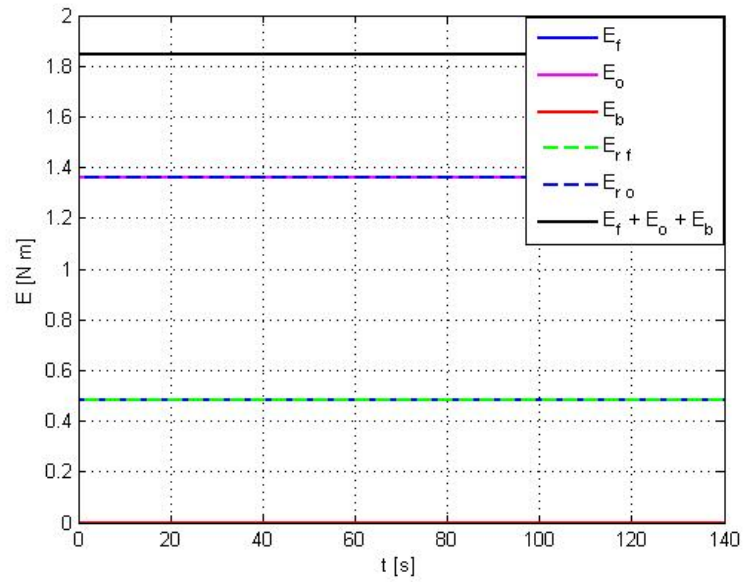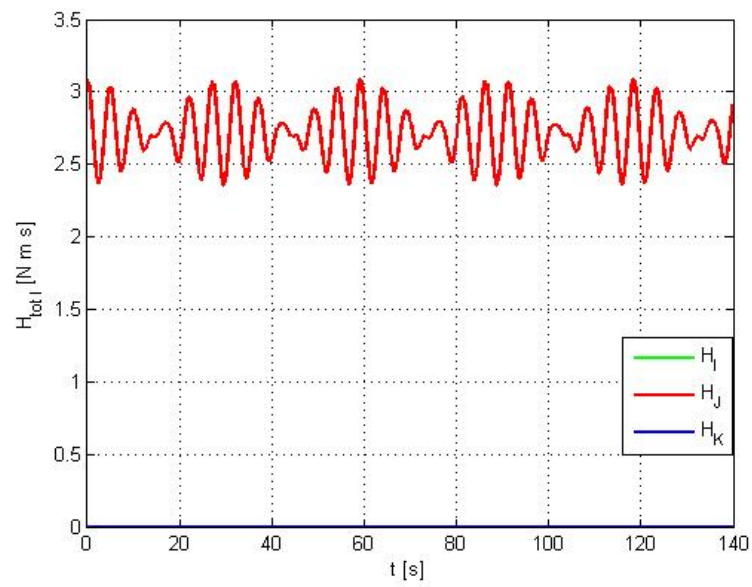

Figure 4.8: Case 1: Total Energy of the System [6].

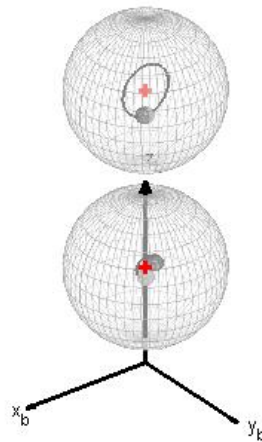Figure 4.9: Case 1: Total Angular Momentum of the System.

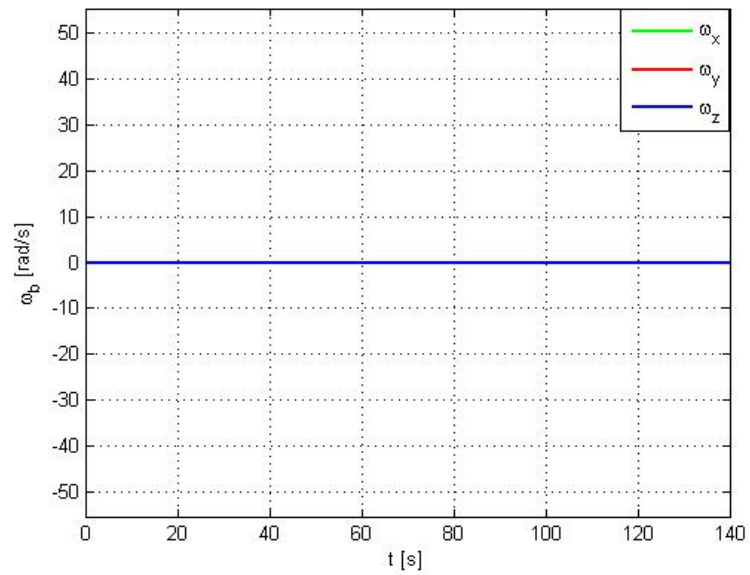Figure 4.10: Case 1: ESMO configuration.

Case 2
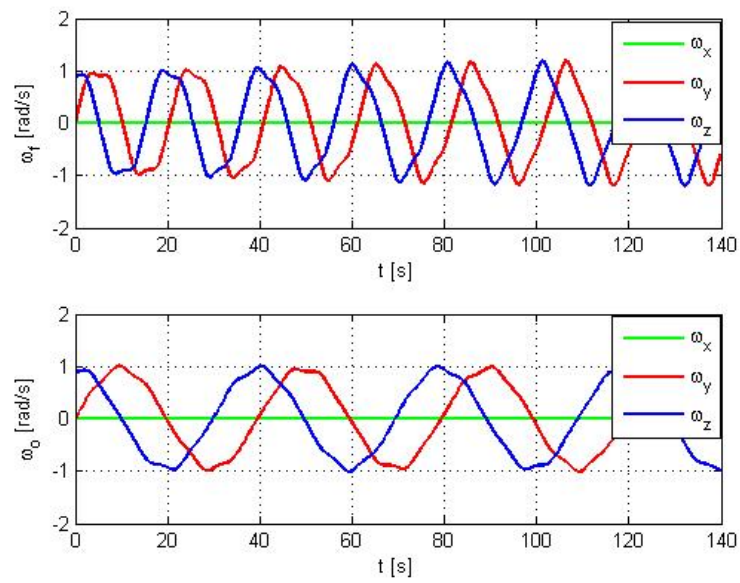

Figure 4.11: Case 2: Angular Velocity of ESMO.

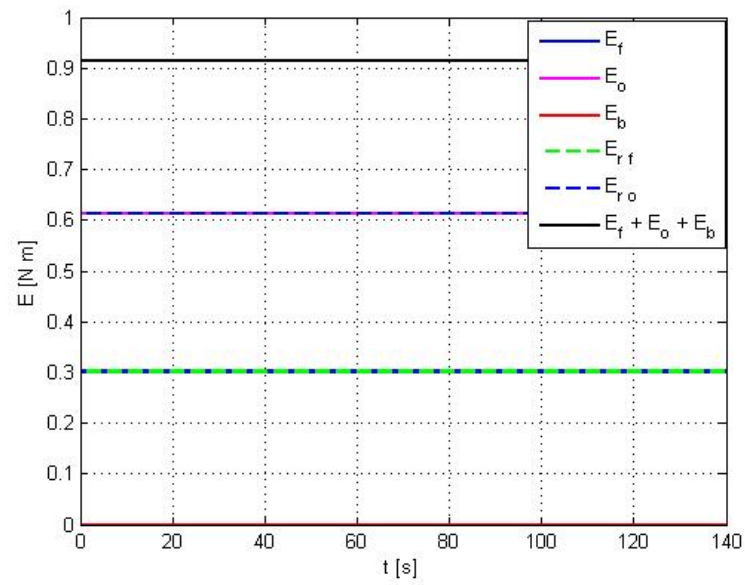Figure 4.12: Case 2: Angular Velocity of the Fuel and Oxidizer Pendulum.

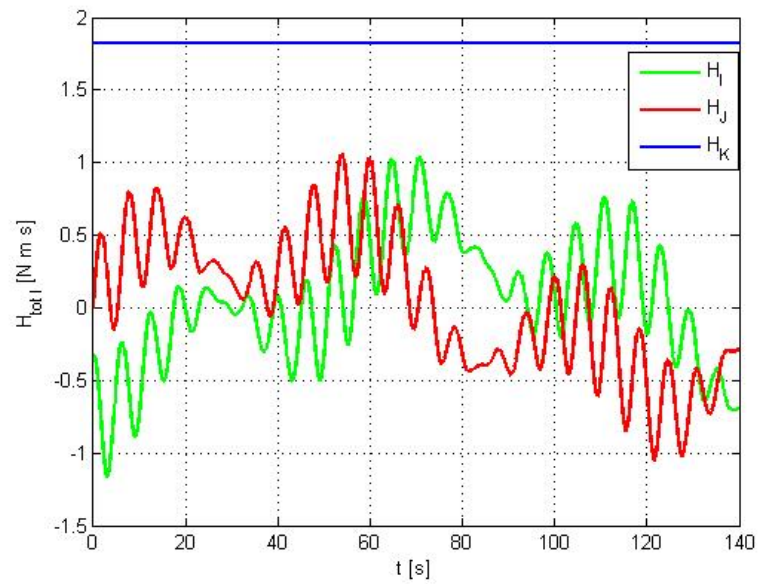Figure 4.13: Case 2: Total Energy of the System.

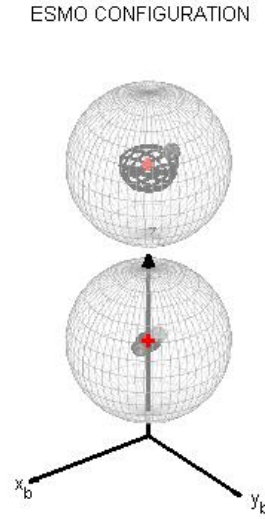Figure 4.14: Case 2: Total Angular Momentum of the System.

ESMO CONFIGURATION

Figure 4.15: Case 2: ESMO configuration.

As one can notice in both cases the energy and the angular momentum along the z-axes are conserved, see Fig. (4.8,4.9, 4.13 and 4.14). Without the damper effect the sloshing load does not affect the satellite dynamics, (see Fig. (4.6 and 4.11)). Two differentness relative velocities of the fuel and oxidizer pendulum, have been given Fig. (4.7 and 4.12), this means that the final solutions are different, see Fig. (4.10 and 4.15).

4.1.2 Dynamical Model

Case	$\omega_b[rad/s]$	$\Omega_f = [rad/s]$	$[rad/s]$	$c_f[Nms]$	$c_o[Nms]$
1	[0,0,0]	[0,0, 0]	[0,0, 0]	0	0
2	[0,0,0]	[0,0,0]	[0,0,0]	0	0

Table 4.4: Initial Condition.

In this section it has been showed how, starting form the same initial condition, the solution change by taking into account (Case 1) or not (Case 2) the orbit dynamics effect. In Tab. (4.4 and 4.5), the initial condition are summarized, as one can notice we suppose that the internal and the satellite dynamics are in a state of quiet. Obviously, these initial conditions are not really significant for the Case 1, in which the initial solution is not perturbed, (see Fig. (4.16, 4.17, 4.18, 4.19 and 4.16)). On the other hand, as one can notice for the Case 2, the orbital

motion affect the attitude; therefore the movement of the fuel and oxidizer masses
Fig. (4.20, 4.21, 4.22, 4.23 and 4.20).

Case	$\vec{\alpha}_0[deg]$	$\vec{\alpha}_{f_0}[deg]$	$\vec{\alpha}_{o_0}[deg]$	$a_f[ms^{-2}]$	$a_o[ms^{-2}]$
1	[0,0,0]	[0,90, 0]	[0,90, 0]	0.1011	0.1011
2	[0,0,0]	[0,90,0]	[0,90,0]	0.1011	0.1011

Table 4.5: Kinematic and Induced Acceleration.

Case 1
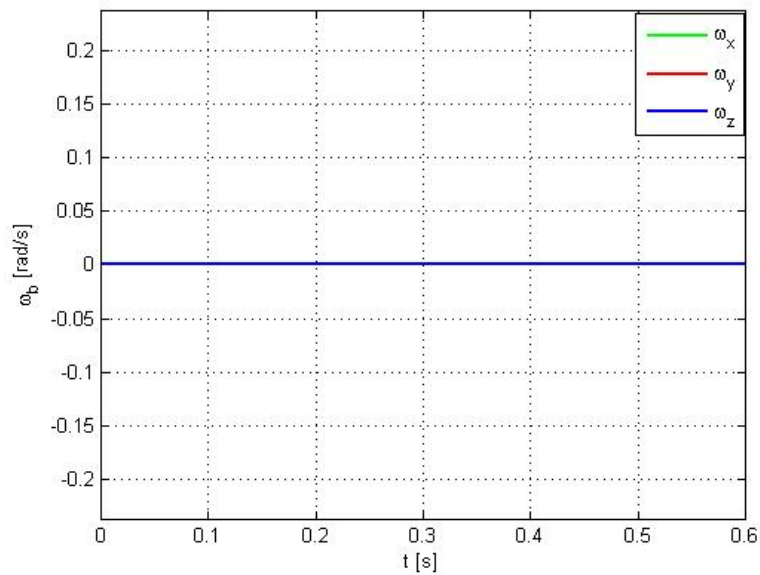
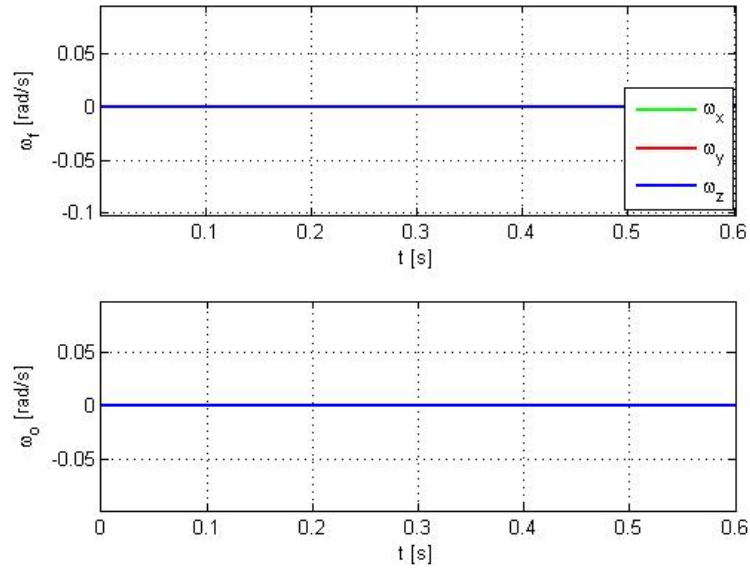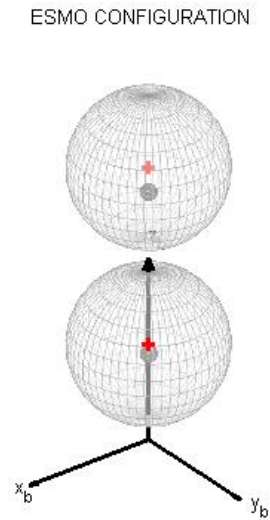Figure 4.16: Case 1: Angular Velocity of ESMO.

Figure 4.17: Case 1: Angular Velocity of the Fuel and Oxidizer Pendulum.

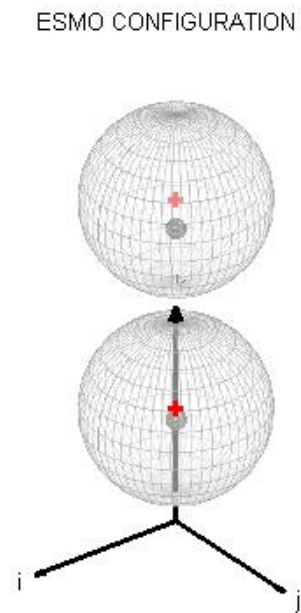Figure 4.18: Case 1: ESMO configuration respect with the $\mathcal{F}_b$ frame.

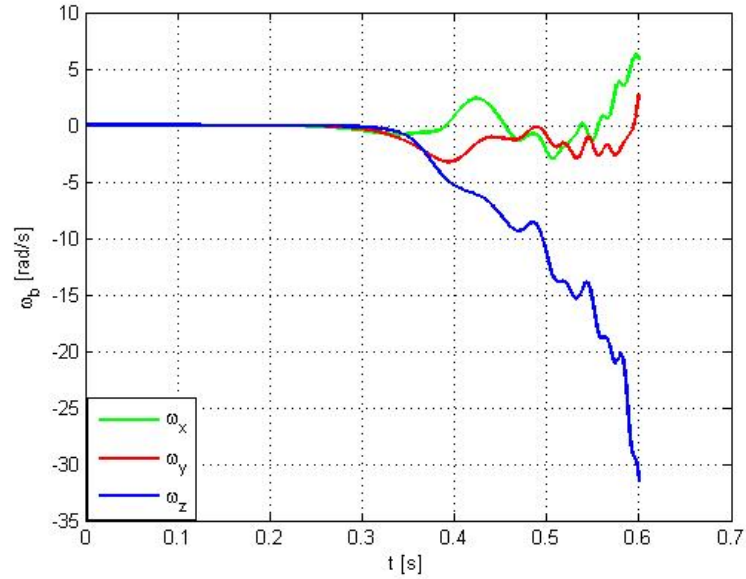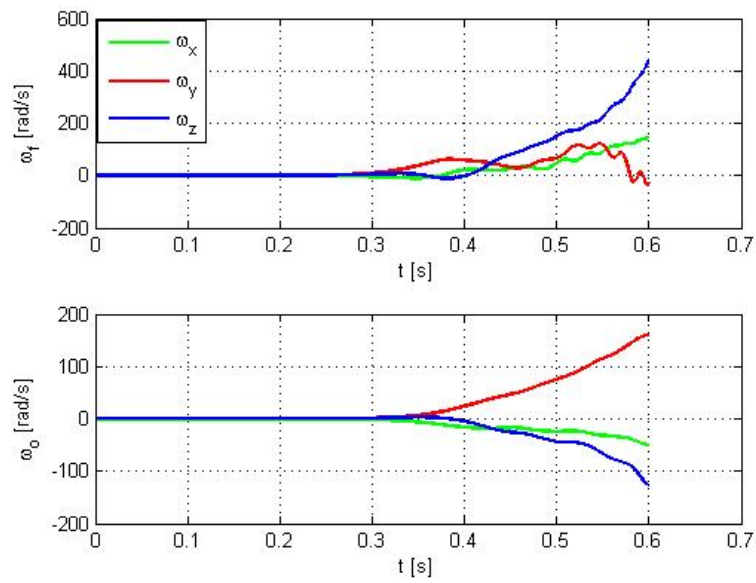Figure 4.19: Case 1: ESMO configuration respect with the $\mathcal{F}_i$ frame.

Case 2

Figure 4.20: Case 2: Angular Velocity of ESMO.

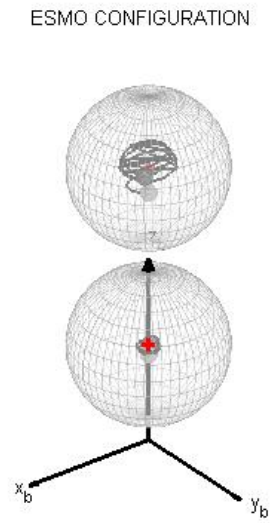Figure 4.21: Case 2: Angular Velocity of the Fuel and Oxidizer Pendulum.

ESMO CONFIGURATION

Figure 4.22: Case 2: ESMO configuration respect with the $\mathcal{F}_b$ frame.
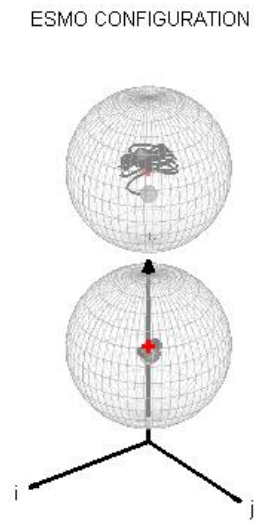
ESMO CONFIGURATION

Figure 4.23: Case 2: ESMO configuration respect with the $\mathcal{F}_i$ frame.

For both cases, the fuel and oxidizer mass center trajectories have been studied from the viewpoint of the body-fixed $\mathcal{F}_b$ frame and the inertial $\mathcal{F}_i$ frame.

4.1.3 Damper Effect

Case	$\omega_b[rad/s]$	$\Omega_f = [rad/s]$	$[rad/s]$	$c_f[Nms]$	$c_o[Nms]$
1	[0,0,0]	[0,0, 0]	[0,0, 0]	0.1	0.1
2	[0,0,0]	[0,0,0]	[0,0,0]	3	3

Table 4.6: Initial Condition.

Case	$\vec{\alpha}_0[deg]$	$\vec{\alpha}_{f_0}[deg]$	$\vec{\alpha}_{o_0}[deg]$	$a_f[ms^{-2}]$	$a_o[ms^{-2}]$
1	[0,0,0]	[0,-10, 0]	[0,-10, 0]	0.1011	0.1011
2	[0,0,0]	[0,-10,0]	[0,-10,0]	0.1011	0.1011

Table 4.7: Kinematic and Induced Acceleration.

In this section, the damper coefficient effect on the system of equations (under the same initial condition), has been investigated. Since the damper coefficient depend on the experimental data, it seems interesting to make a trade-off with this parameter. In both cases, as we have just previously mentioned, the damper coefficient is a coupling term in which, at the end of the simulation, the sloshing effect caused a residual spinning velocity to the satellite. What it is very interesting is that with a damper coefficient of 0.1 Nms, the energy of the entire system is growing down, this mean that the sloshing load has a dissipative effect such as the flat-spin maneuvers model, (see Fig. (4.24, 4.25, 4.26, 4.27 and 4.28)). On the contrary, a damper coefficient of 3 Nms shows that the energy of the satellite is growing up, (see Fig. (4.29, 4.30, 4.31, 4.32 and 4.33)). In the Appendix (B.4), another solution has been given with a higher damper coefficient. It is very easy to understand that the damper coefficient is a parameter that influenced a lot the dynamics equation.
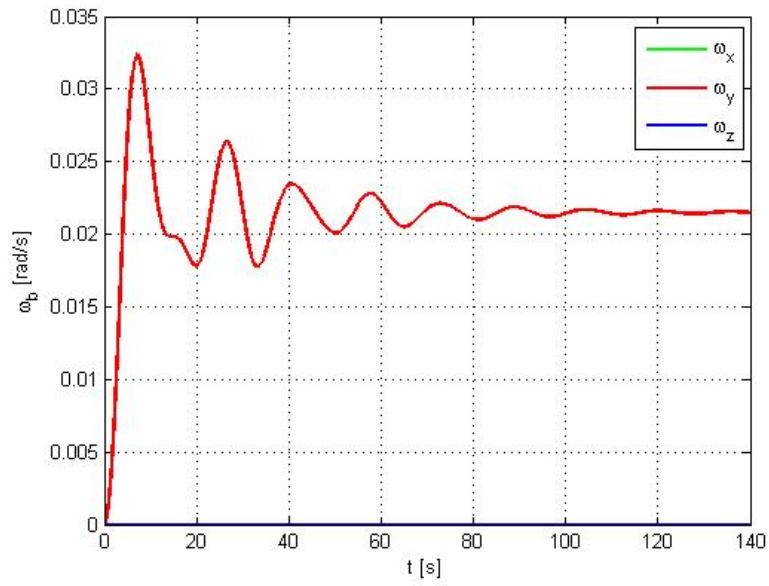
Case 1

Figure 4.24: Case 1: Angular Velocity of ESMO ($c_f = c_o = 0.1[Nms]$).
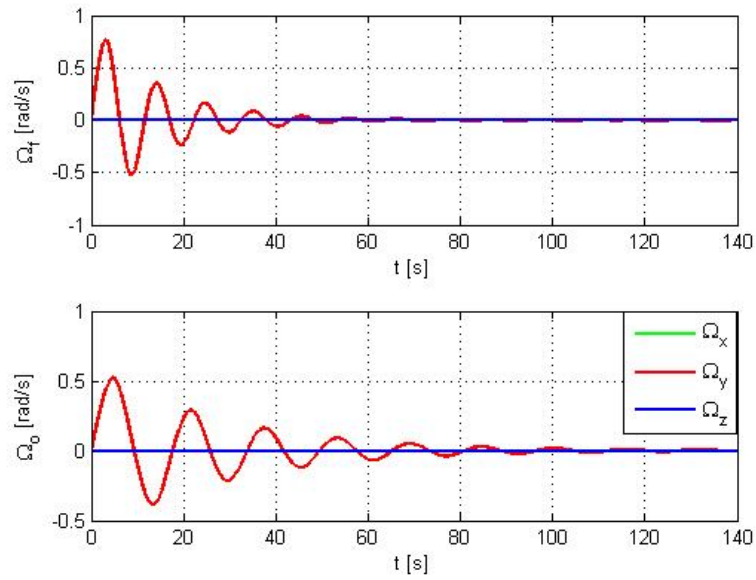
Figure 4.25: Case 1: Angular Velocity of the Fuel and Oxidizer Pendulum ($c_f = c_o = 0.1[Nms]$).
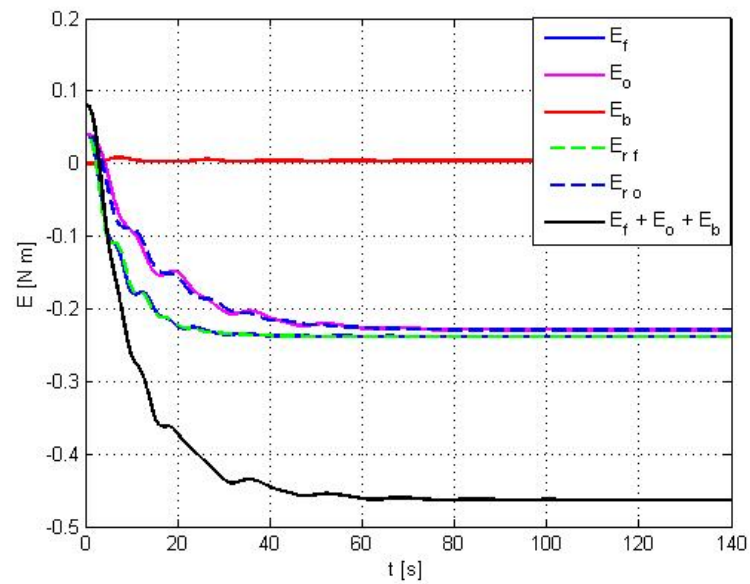

Figure 4.26: Case 1: Total Energy of the System ($c_f = c_o = 0.1[Nms]$).
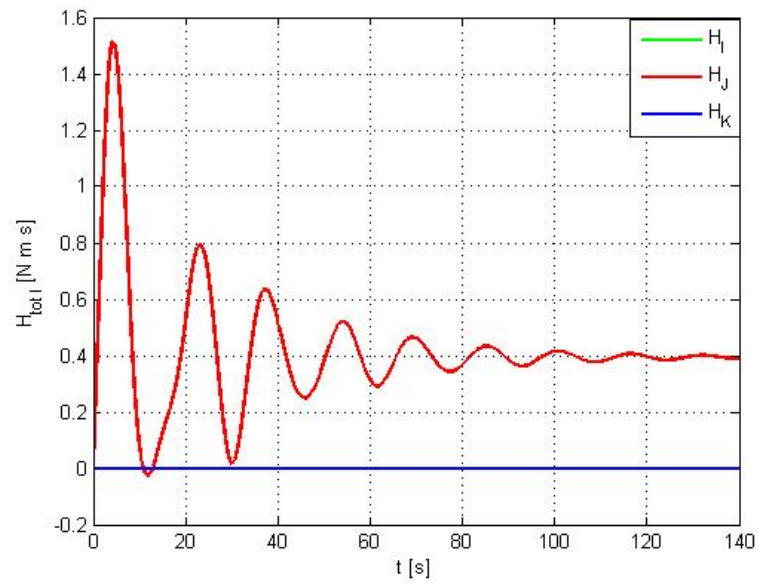
Figure 4.27: Case 1: Total Angular Momentum of the System ($c_f = c_o = 0.1[Nms]$).
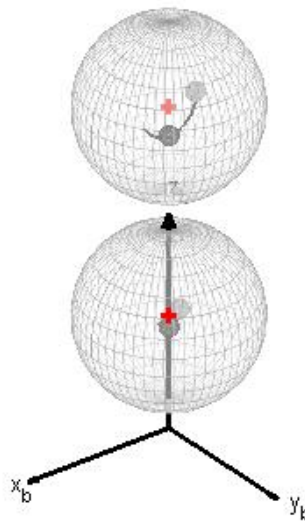

Figure 4.28: Case 1: ESMO configuration ($c_f = c_o = 0.1[Nms]$).

Case 2

Figure 4.29: Case 1: Angular Velocity of ESMO ($c_f = c_o = 3[Nms]$).

Figure 4.30: Case 1: Angular Velocity of the Fuel and Oxidizer Pendulum ($c_f = c_o = 3[Nms]$).

Figure 4.31: Case 1: Total Energy of the System ($c_f = c_o = 3[Nms]$).

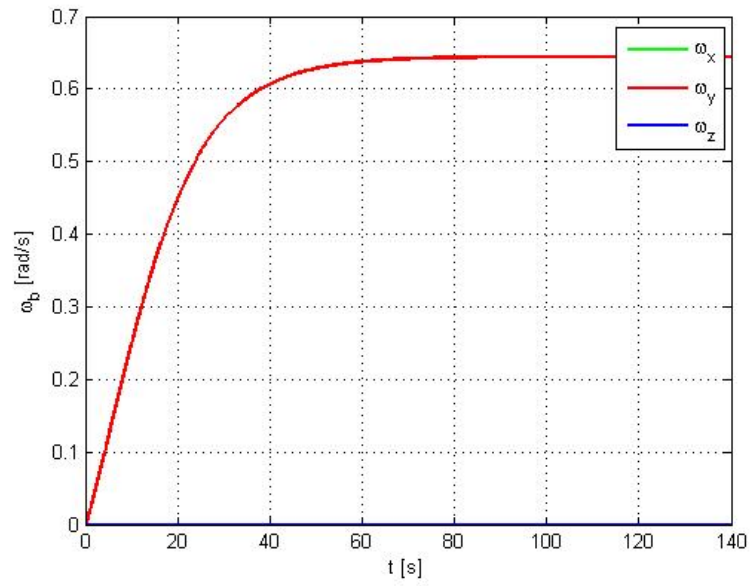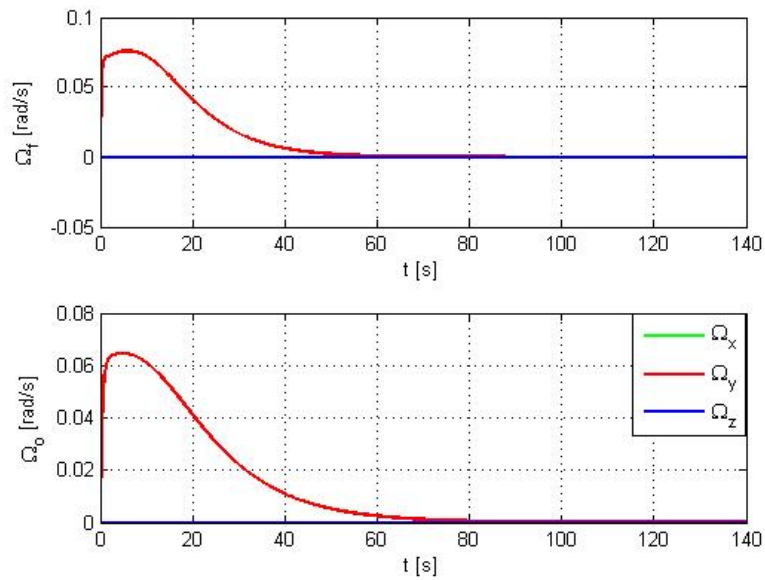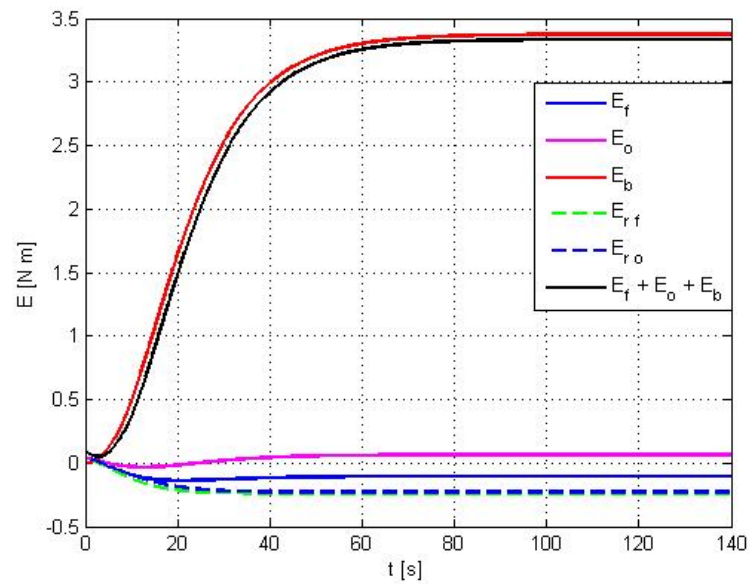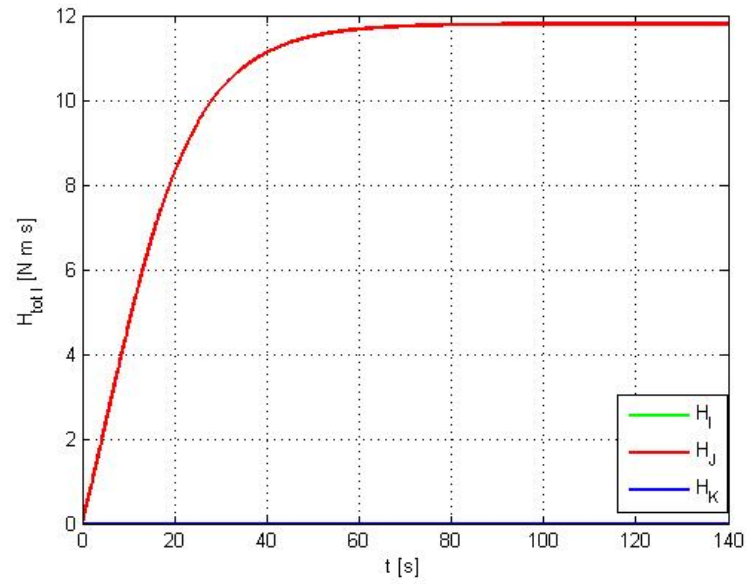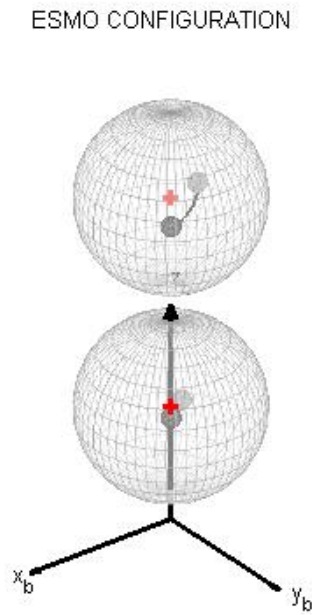Figure 4.32: Case 1: Total Angular Momentum of the System ($c_f = c_o = 3[Nms]$).

Figure 4.33: Case 1: ESMO configuration ($c_f = c_o = 3[Nms]$).

4.1.4   Propellant Consumption

In this section a solution with the consumption model Fig. (4.34), has been given. We are not considering the damper effect but anyway the energy is obviously not conserved due to the mass consumption, (see Fig. (4.35)). In Tab. (4.9) we show the thrust value $\vec{T}$ of the four main engines instead of the induced acceleration because know is time depending. In Fig. (4.37) one can notice by taking a look at the trajectory followed by the fuel and oxidizer mass center, that the length of the pendulum (the position of the mass center) is growing up due to the consumption. Finally the total angular momentum is still conserved along the z-axes Fig. (4.36) because without the damping effect the dynamics of the satellite and the fuel and oxidizer pendulums are uncoupled.

Case	$\omega_b[rad/s]$	$\Omega_f = [rad/s]$	$[rad/s]$	$c_f[Nms]$	$c_o[Nms]$
1	[0,0,0]	[0,0,0]	[0,0,0]	0	0

Table 4.8: Initial Condition.

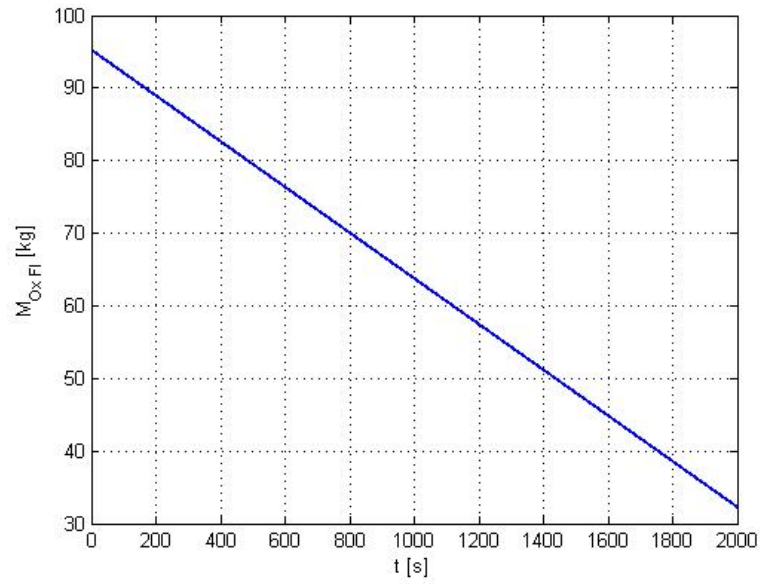| Case	$\vec{\alpha}_0[deg]$	$\vec{\alpha}_{f_0}[deg]$	$\vec{\alpha}_{o_0}[deg]$	$\vec{T}[N]$
1	[0,0,0]	[0,-10,0]	[0,-10,0]	[22,22,22,22]

Table 4.9: Kinematic and Induced Acceleration.

Figure 4.34: Propellant Mass Consumption.

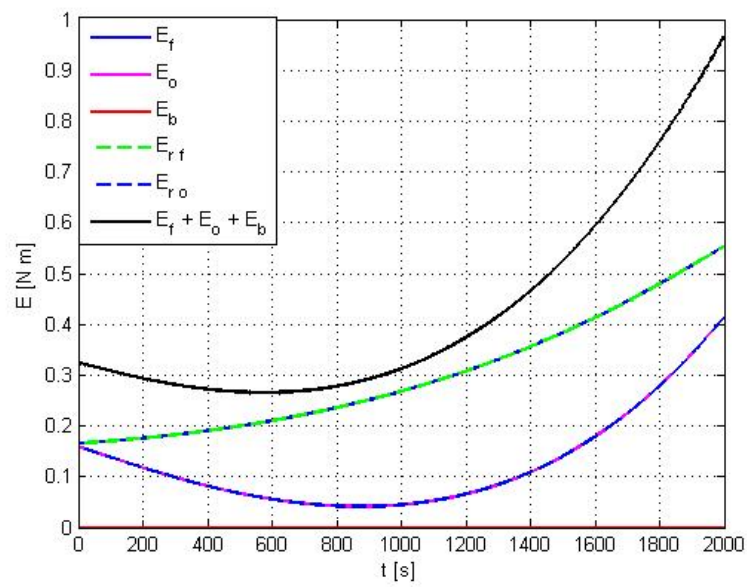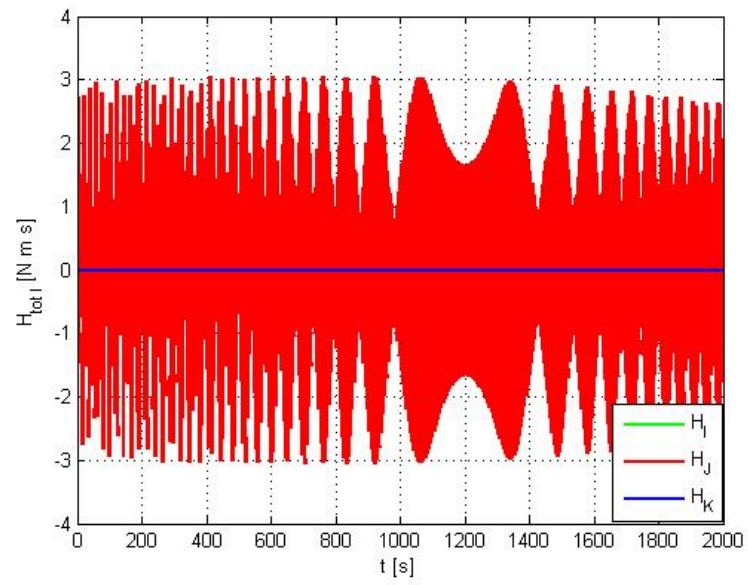Figure 4.35: Total Energy of the System.

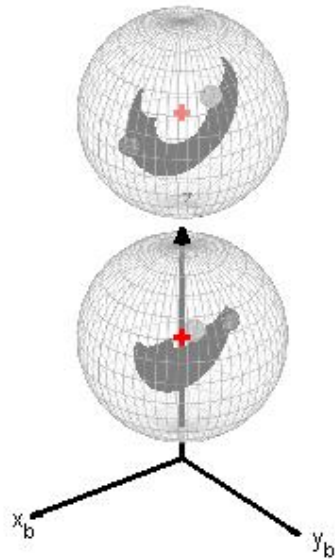Figure 4.36: Total Angular Momentum of the System.

Figure 4.37: ESMO configuration.

4.2   Mass Expulsion Torque

As we said throughout the dissertation, the thrust vector misalignment is the only disturbance within the mass expulsion torques that we have treated. In this section it has been investigated the effect of the thrust vector misalignment torques. The following results show that without the damper effect and the consumption, even if the the oxidizer and the fuel pendulum are in their stable equilibrium point, the thrust vector misalignment affect the attitude of the satellite (see Fig. (4.38)) and start the sloshing dynamics, (see Fig. (4.40 and 4.41)).

Case	$\omega_b[rad/s]$	$\Omega_f = [rad/s]$	$[rad/s]$	$c_f[Nms]$	$c_o[Nms]$
1	[0,0,0]	[0,0,0]	[0,0,0]	0	0

Table 4.10: Initial Condition

Case	$\vec{\alpha}_0[deg]$	$\vec{\alpha}_{f_0}[deg]$	$\vec{\alpha}_{o_0}[deg]$	$a_f[ms^{-2}]$	$a_o[ms^{-2}]$
1	[0,0,0]	[0,90,0]	[0,90,0]	0.1011	0.1011

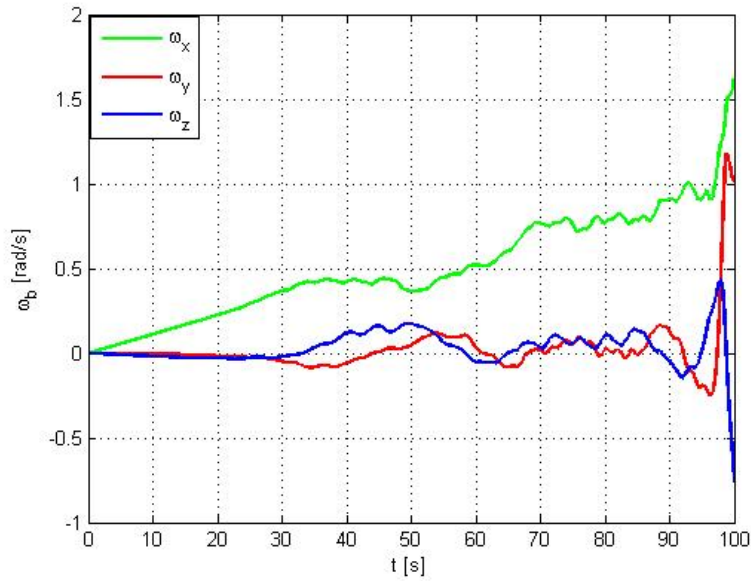Table 4.11: Kinematic and Induced Acceleration
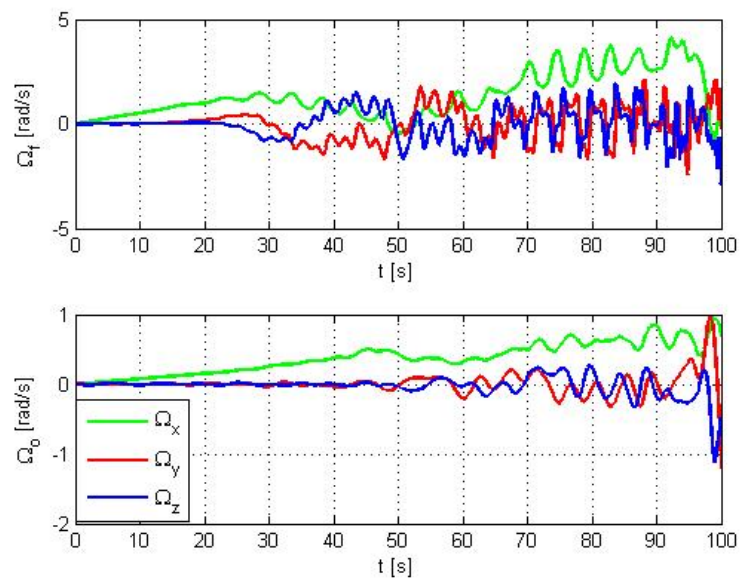

Figure 4.38: Angular Velocity of ESMO.

Figure 4.39: Relative Angular Velocity of the Fuel and Oxidizer.

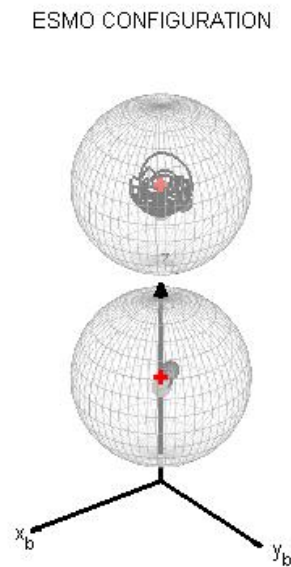ESMO CONFIGURATION

Figure 4.40: Trajectory of the Fuel and Oxidizer Center of Mass with respect to $\mathcal{F}_b$ frame.
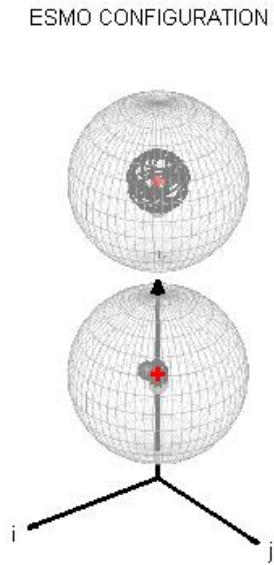
ESMO CONFIGURATION

Figure 4.41: Trajectory of the Fuel and Oxidizer Center of Mass with respect to $\mathcal{F}_i$ frame.

4.3 ESMO configuration and data

The ESMO Configuration (CONF) team has declared the mechanical properties of the satellite for both the dry and wet configuration, (see Eq. (4.3.1 and 4.3.2) and Tab. (4.13)):

$$\boldsymbol{I}_d = \begin{bmatrix} 17.53 & 0.14 & 0.61 \\ 0.14 & 16.05 & -1.04 \\ 0.61 & -1.04 & 10.73 \end{bmatrix}, \ kgm^2 \tag{4.3.1}$$

$$\boldsymbol{I}_w = \begin{bmatrix} 27.98 & 0.11 & 0.48 \\ 0.11 & 25.97 & -0.24 \\ 0.48 & -0.24 & 10.74 \end{bmatrix}, \ kgm^2 \tag{4.3.2}$$

Case	$[kg]$	$\vec{d}_{CM}[mm]$
Dry	122.35	$[0.01,-0.04,0.31]$
Wet	217.55	$[5.48,-16.72,410.28]$

Table 4.12: Mechanical Property.

The size and the configuration of both the fuel and oxidizer tanks are summarized in Tab. (4.13).

Case	Diameter $[mm]$	Position $[mm]$
Fuel Tank	484	$[0,0, 917.37]$
Oxidizer Tank	484	$[0,0,322.54]$

Table 4.13: Tanks Configuration

The fuel and oxidizer properties are, see Tab. (4.14):

ρ_{MON} $[g/cc]$	ρ_{MMH} $[g/cc]$	MON/MMH $ratio$
1.37	0.88	2.37

Table 4.14: Fuel and Oxidizer Properties.

In Tab. (4.14), MON is the oxidizer [7] and MMH is the fuel [8]. For more details in the ESMO configuration, (see Appendix (B.3)).

---

[7]MON: Mixed oxidize of nitrogen and nitric oxidize. It has been chosen by the Propulsion (PROP) team.

[8]MMH: Monomethydrazine. It has been chosen by the Propulsion (PROP) team.

4.4 ESMO trajectory overview

In this section we are going to show in brief an example of the trajectory transfer (MIAS team solution) that ESMO will follow in the early phases of the mission. This trajectory shows a multi-burned strategy by escaping the Earth, (see Fig (4.42)). In Fig. (4.43) there is sketched the same trajectory of Fig. (4.42) but on the sun viewpoint. All the solutions, that one can find throughout all the dissertation, have been computed in this trajectory transfer phase.
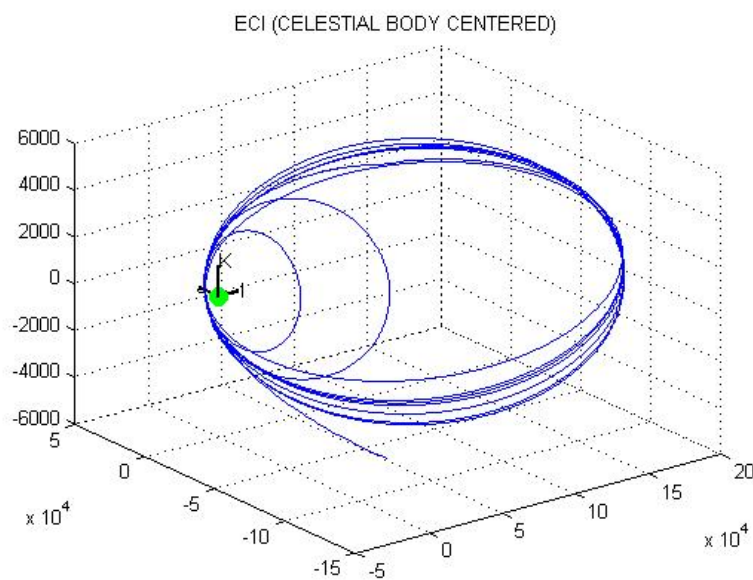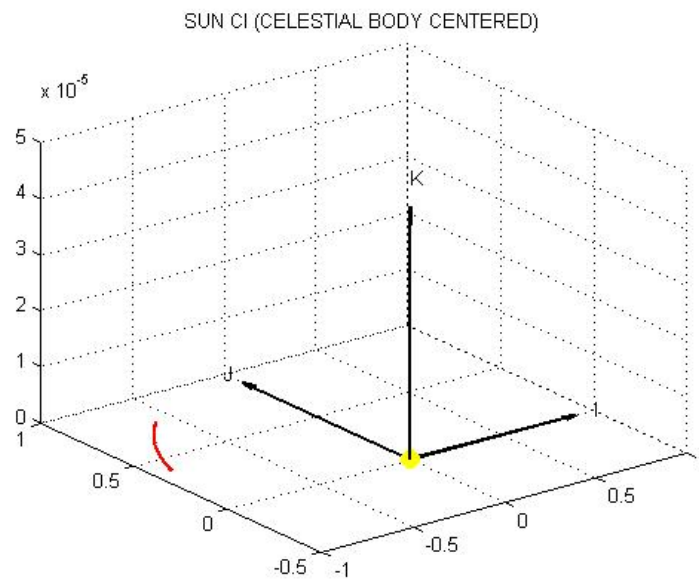

Figure 4.42: Multi-Burned Trajectory.

Figure 4.43: Sun Viewpoint Trajectory.

Conclusions

The main purpose of this thesis was to develop the mathematical formulation of the Newton and Euler equations by adding the dynamics of the non-environmental disturbances of the spacecraft. The internal disturbances, that have been investigated, are the mass expulsion torques and the propellant sloshing model. These problems have been studied from an engineering viewpoint: the mass expulsion torques have been treated with a standard procedure (fixed angle of misalignment) and the propellant sloshing dynamics have been implemented by using the equivalent mechanical model (3D spherical pendulum). Moreover the equations of motion have been evaluated in terms of propellant consumption and depending on the trajectory transfer during the time. In the first part of the thesis, the Newton and Euler equations of motions have been analyzed. Special interests has been given to the propellant sloshing model. The second part of the thesis deal with the analysis of the results. The solution of the dynamics equation is influenced by the initial conditions, the damping coefficients, the propellant consumption and the orientation in the thrust vectors. As we expect, the sloshing dynamics affect the attitude dynamics (in terms of angular velocity), this mean that the control low need to be able to supply for these disturbances. Finally we expect that resonance problems could occur, therefore the fuel and the oxidizer tanks are not equally filled so quite often the oscillations of the two pendulums are one in the opposite direction of the other.

Bibliography

[1] NASA. Spacecraft mass expulsion torques. *NASA SP-8034, Wasinghton,* 1969.

[2] Raouf A. Ibrahim. *Liquid Sloshing Dynamics.* Cambridge University Press, Cambridge, 2005.

[3] H.Q. Yang and J. Peupeot. Propellant sloshing parameter extraction from cfd analysis. *AIAA/ASME/SAE/ASEE Joint Propulsion Conference and Exhibit,* 2010.

[4] Marcel J. Sidi. *Spacecraft Dynamics and Control, A Piratical Engineering Approach.* Cambridge University Press, IAmes, Iowa, 1997.

[5] James R. Wertz. *Spacecraft Attitude Determination and Control.* Kluwer Academic Publishers, Torrance, CA, 1999.

[6] A. Gibbings, F. Zuiani, D. Novak, and M. Vasile. Optimal design of low-energy transfers to highly eccentric frozen orbits around the moon. *Glasgow University,* 2010.

[7] A. Gibbings, F. Zuiani, F. Rizzi, C. Martinez, and D. Novak. Orbit determination and control for the european student moon obiter. *Glasgow University,* 2010.

[8] E. Brandon, B. Olberts, V. Bertand-Noel, and D. Novak. Esmo phase b1 mission analysis: targeting options for lunar wsb transfers along with a multi-burn injection strategy. *Glasgow University,* 2009.

[9] W. S. Koon, M. W. Lo, J.E. Marsden, and S. D. Ross. Low energy transfer to the moon. *Pasadina, California,* 2001.

[10] M. Ceriotti, C. Colombo, N. Croisard, and T. Mclea. Preliminary mission analysis for the esmo mission, department of aerospace engineering. *Glasgow University,* 2007.

[11] E. A. Belbruno and J. O. Carrico. Calculation of weak stability boundary ballistic lunar trajectories. *AIAA/AAS Astrodynamics Specialist Conference, Denver, Colorado*, 2000.

[12] R. Walker and M. Cross. The european student moon orbiter (esmo): A lunar mission for education, outreach and science. *Celest Mech Dyn Astr, Springer*, 2009.

[13] D. Romagnoli and C. Circi. Earth-moon weak stability boundaries in the restricted three and four body problem. *Acta Astronautica*, 2000.

[14] F. Topputo, M. Vasile, and F. Bernelli-Zazzera. Interplanetary and lunar transfers using libration points. *Politecnico di Milano*, 2004.

[15] K. Chen and R. Pletcher. Simulation of three-dimensional liquid sloshing flows using a strongly implicit calculation procedure. *AIAA 91-1661, Ames, Iowa*, 1991.

[16] K. Chen, F. J. Kelecy, and Pletcher R. H. Adaptive nonlinear dynamic inversion for spacecraft attitude control with fuel sloshins. *AIAA Guidance, Navigation and Control Conference and Exhibit*, 1992.

[17] E. de Weerdt, E. J. van Kampen, D. van Gemert, Q.P. Chu, and J.A. Mulder. A numerical ans experimental study of three-dimensional liquid sloshing in a rotating spherical container. *AIAA 92-0829 , Ames, Iowa*, 2008.

[18] J. Kuang and A. Y.T. Leung. Feedback for attitude control of liquid-filled spacecraft. *Journal of Guidance, Control, and Dynamics, Manchester, England*, 2001.

[19] D. Yang and B. Yue. Study on the global chaotic dynamics and control of liquid-filled spacecraft with flexible appendage. *Acta*, 2009.

[20] K.W. London. A fully coupled multi-rigid-body fuel slosh dynamics model applied to the triana stack. *Flight Mechanics Symposium, NASA Goddard Space Flight Center*, 2001.

[21] J. Shen, A.K. Sanyal, N.A. Chaturvedi, D. Bernstein, and H. McClamroch. Dynamics and control of a 3d pendulum. *University of Michigan Ann Arbor*.

[22] F. Chaturvedi, N.Bacconi, A.K. Sanyal, N.A. Chaturvedi, D. Bernstein, and H. McClamroch. Stabilization of a 3d rigid pendulum. *University of Michigan Ann Arbor*.

[23] Y. Baozeng and X. Jiafang. Chaotic attitude maneuvers in spacecraft with a completely liquid-filled cavity. *ScienceDirect, Journal of Sound and Vibration, Elsevier, Beijing, China*.

[24] N.H. McClamroch, T. Lee, N.A. Chaturvedi, and M. Leok. Nonlinear dynamics of the 3d pendulum. *Nonlinear Science.*

[25] P.A.C. Mason and S.R. Starin. Propellant slosh analysis for the solar dynamics observatory. *Goddard Space Flight Center.*

[26] R.A. Sndfry and C.D. Hall. Steady spins and spinup dynamics of axisymmetric dual-spin satellites with dampers. *Goddard Space Flight Center*, 2004.

[27] A. K. Sen. The dynamic stability of a dual-spin satellite. *Canada*, 1977.

[28] A. K. Sen. Tools of kinematics: A crital review. *Canada*, 1978.

[29] A.J. Stofan. Comparison of prolelant sloshing parameters obtained from model and full-size centaur liquid-oxygen tanks. *NASA TM X-1286, Wasinghton*, 1966.

[30] NASA. Propellant slosh loads. *NASA SP-8009, Wasinghton*, 1968.

[31] ESMO Configuration Team. Esmo design description and justification file. *ESA*, 2011.

[32] ESMO Configuration Team. Esmo design development and verification. *ESA*, 2011.

[33] ESMO Configuration Team. Esmo subsystem requirements document. *ESA*, 2011.

[34] ESMO Configuration Team. Esmo interface control document. *ESA*, 2011.

[35] ESMO AOCS1 Team. Esmo design description and justification file. *ESA*, 2011.

[36] ESMO AOCS2 Team. Esmo design description and justification file. *ESA*, 2010.

[37] ESMO PSLF Team. Esmo design description and justification file. *ESA*, 2011.

[38] ESMO PSLF Team. Propulsion subsystem requirements. *ESA*, 2011.

[39] ESMO PSGF Team. Esmo design description and justification file. *ESA*, 2011.

[40] J. Alsayednoor. The weak stability boundary trajectory design. master thesis, Politecnico di Milano.

[41] F. Topputo. The weak stability boundary trajectory design. doctorial thesis, Glasgow University, March 2007.

[42] R. A. Sandfry. Equilibria of a gyrostat with a discrete damper. doctorial thesis, Virginia Polytechnic Institute and State University, July 2001.

[43] F.. Rizzi. Fly dynamics, orbit determination and control for esmo satellite. master thesis, Politecnico di Torino, 2009.

[44] Peter C. Hughes. *Spacecraft Attitude Dynamics.* Dover Publications, Toronto, 2004.

[45] Bong Wie. *Space Vehicle Dynamics and Control.* AIAA Education Series, Toronto, 2004.

[46] M. D. Griffin and J. R. French. *Space vehicle design.* AIAA Education Series, Blacksburg, Virginia, 2004.

Appendix A

Appendix

A.1   Fuel Rigid-Slug Dynamical Model and Results

Equations of Motion:

$$\vec{h} \triangleq \int_{\mathcal{B}} \vec{r} \times \vec{v} \; dm \tag{A.1.1}$$

This is the definition of the angular momentum for a rigid body Eq. (A.1.1). For the main body $\mathcal{B}$ [1] and the fuel slug $\mathcal{S}$ the angular momentum are:

$$\vec{h}_{sat} = \int_{\mathcal{B}} \vec{\rho}_{sat} \times \vec{v}_{sat} \; dm \tag{A.1.2}$$

Where $\vec{v}_{sat}$ and $\vec{\rho}_{sat}$ are the absolute velocity and the distance from a generic point P of the rigid body $\mathcal{B}$ [2].
The velocity is defined as:

$$\vec{v}_{sat} = \vec{v}_{\mathcal{O}} + \dot{\vec{\rho}}_{sat} + \vec{\omega} \times \vec{\rho}_{sat} \tag{A.1.3}$$

In Eq.(A.1.3), $\vec{\omega}$ is the absolute angular velocity of the body $\mathcal{B}$. For a rigid body, $\dot{\vec{\rho}}_{sat}$ is equal to zero and we can rewrite the angular momentum in the following way:

$$\vec{h}_{sat} = \int_{\mathcal{B}} \vec{\rho}_{sat} \times \vec{v}_{\mathcal{O}} \; dm + \int_{\mathcal{B}} \vec{\rho}_{sat} \times \vec{\omega} \times \vec{\rho}_{sat} \; dm \tag{A.1.4}$$

Eq. (A.1.4) can be rewritten in the form below:

$$\vec{h}_{sat} = \vec{c}_{sat} \times \vec{v}_{\mathcal{O}} + \boldsymbol{I}_{sat} \; \vec{\omega} \tag{A.1.5}$$

Where $\vec{c}_{sat}$ is the Static Momentum and $\boldsymbol{I}_{sat}$ [3] is the Angular Momentum. If the

---

[1] The main body is the satellite without the fuel mass contribution.
[2] $\vec{\rho}_{sat}$ is defined in the $\mathcal{F}_b$ frame.
[3] All the matrices are signed with a bold letter.

center of mass is coincident with the origin $\mathcal{O}$ in the body-fixed frame $\mathcal{F}_b$, the Static Momentum should be zero. Focusing our attention on the body $\mathcal{S}$ we can compute the angular momentum of the slug as:

$$\vec{h}_{slug} = \int_{\mathcal{S}} \vec{\rho}_{slug} \times \vec{v}_{slug} \ dm_{slug} \tag{A.1.6}$$

Where $\vec{v}_{slug}$ and $\vec{\rho}_{slug}$ are the absolute velocity and the distance from a generic point P of the rigid body $\mathcal{S}$ [4]. The velocity is defined as:

$$\vec{v}_{slug} = \vec{v}_{\mathcal{O}} + \dot{\vec{\rho}}_{slug} + \vec{\omega}_{slug} \times \vec{\rho}_{slug} \tag{A.1.7}$$

In Eq.(A.1.7), $\vec{\omega}_{slug}$ is the absolute angular velocity of the body $\mathcal{S}$ [5]. We will assume the slug as rigid so the inner velocity $\dot{\vec{\rho}}_{slug}$ [6] must be zero and we have:

$$\vec{h}_{slug} = \int_{\mathcal{S}} \vec{\rho}_{slug} \times \vec{v}_{\mathcal{O}} \ dm_{slug} + \int_{\mathcal{S}} \vec{\rho}_{slug} \times \vec{\omega}_{slug} \times \vec{\rho}_{slug} \ dm_{slug} \tag{A.1.8}$$

As before one can write the previous equation in the following way:

$$\vec{h}_{slug} = \vec{c}_{slug} \times \vec{v}_{\mathcal{O}} + \boldsymbol{I}_{slug} \ \vec{\omega}_{slug} \tag{A.1.9}$$

Where $\vec{c}_{slug}$ and $\boldsymbol{I}_{slug}$ are respectively the Static Momentum and the Angular Momentum of the rigid slug. After the definition of the angular momentum of both the two rigid bodies, the satellite $\mathcal{B}$ and the rigid slug $\mathcal{S}$, we can write the Euler's equation for the entire system. We start to derive the equations by defining the total Angular Momentum in the $\mathcal{F}_b$ frame.

$$\vec{h} = \boldsymbol{I}_{sat} \ \vec{\omega} + \boldsymbol{I}_{slug} \ \vec{\omega}_{slug} \tag{A.1.10}$$

The $\vec{\omega}_{slug}$ is an absolute velocity and for the decomposition of the angular velocity one can write $\vec{\omega}_{slug} = \vec{\omega} + \vec{\Omega}$ [7]. Where $\vec{\Omega}$ is the relative angular velocity of the rigid slug. The Euler's system of equation is:

$$\begin{cases} \dot{\vec{H}} = \vec{M}^{ext} \\ \dot{\vec{H}}_{slug} = \vec{M}^{ext} + \vec{M}^{int} \end{cases} \tag{A.1.11}$$

---

[4] $\vec{\rho}_{slug}$ is defined in the $\mathcal{F}_b$ frame.

[5] $\vec{\omega}_{slug}$ is defined in the $\mathcal{F}_b$ frame.

[6] $\dot{\vec{\rho}}_{slug} = \vec{0}$

[7] The decomposition of the angular velocity is written in a vectorial form. Usually we have to be careful about this expression because if we work with the components of the vector (*vectrices* as suggested in Hughes [44]) we have to keep in mind that the sum of two different vectors is allowed only if they are defined in the same reference frame. In this particular case, we can define all the vectors in the same frame in particular the $\mathcal{F}_b$ frame and this is reasonable because of the slug symmetry.

$\dot{\vec{H}}$ is the derivative of the angular momentum in the $\mathcal{F}_i$ frame and $\dot{\vec{h}}$ is the derivative of the angular momentum in the $\mathcal{F}_b$ frame where:

$$\dot{\vec{H}} = \dot{\vec{h}} + \vec{\omega} \times \vec{h} \tag{A.1.12}$$

and

$$\dot{\vec{H}}_{slug} = \dot{\vec{h}}_{slug} + \vec{\omega} \times \vec{h}_{slug} \tag{A.1.13}$$

The system above Eq. (A.1.11) can be rewritten as follow:

$$\begin{cases} \dot{\vec{h}} + \vec{\omega} \times \vec{h} = \vec{M}^{ext} \\ \dot{\vec{h}}_{slug} + \vec{\omega} \times \vec{h}_{slug} = \vec{M}^{ext} + \vec{M}^{int} \end{cases} \tag{A.1.14}$$

In particular the previous system becomes:

$$\begin{cases} \boldsymbol{I}_{sat}\, \dot{\vec{\omega}} + \boldsymbol{I}_{slug}\, \dot{\vec{\omega}}_{slug} + \vec{\omega} \times (\boldsymbol{I}_{sat}\, \vec{\omega} + \boldsymbol{I}_{slug}\, \vec{\omega}_{slug}) = \vec{M}^{ext} \\ \boldsymbol{I}_{slug}\, \dot{\vec{\omega}}_{slug} + \vec{\omega} \times \boldsymbol{I}_{slug}\, \vec{\omega}_{slug} = \vec{M}^{ext} + \vec{M}^{int} \end{cases} \tag{A.1.15}$$

Finally we will write the system above in terms of $\vec{\Omega}$. By defining $\boldsymbol{I} \triangleq \boldsymbol{I}_{slug} + \boldsymbol{I}_{sat}$ we can write:

$$\begin{cases} \boldsymbol{I}\, \dot{\vec{\omega}} + \boldsymbol{I}_{slug}\, \dot{\vec{\Omega}} + \vec{\omega} \times (\boldsymbol{I}\, \vec{\omega} + \boldsymbol{I}_{slug}\, \vec{\Omega}) = \vec{M}^{ext} \\ \boldsymbol{I}_{slug}\, \dot{\vec{\omega}} + \boldsymbol{I}_{slug}\, \dot{\vec{\Omega}} + \vec{\omega} \times (\boldsymbol{I}_{slug}\, \vec{\omega} + \boldsymbol{I}_{slug}\, \vec{\Omega}) = \vec{M}^{ext} + \vec{M}^{int} \end{cases} \tag{A.1.16}$$

Concerning the right part of the system, we define the external and internal torques. In this particular case $\vec{M}^{int}$ [8] is the damping effect due to the viscous layer that covers the rigid slug. We studied the free-body dynamics to demonstrate that without external torques the angular momentum is conserved in the $\mathcal{F}_i$ and without the damping effects the energy is conserved. In the results below a comparison is made between the dynamics written for the two and one rigid body models. We analyze the free-dynamics in a principal axes $\mathcal{F}_b$ [9] by solving the eigenvalue problem. As we said before, the other dynamical quantity of interest is the kinetic energy:

$$\begin{aligned} T &= \frac{1}{2} \int_{\mathcal{B}} (\vec{v}_{\mathcal{O}} + \vec{\omega} \times \vec{\rho}_{sat}) \cdot (\vec{v}_{\mathcal{O}} + \vec{\omega} \times \vec{\rho}_{sat}) dm + \\ &\quad + \frac{1}{2} \int_{\mathcal{S}} (\vec{v}_{\mathcal{O}} + \vec{\omega}_{slug} \times \vec{\rho}_{slug}) \cdot (\vec{v}_{\mathcal{O}} + \vec{\omega}_{slug} \times \vec{\rho}_{slug}) dm_{slug} \end{aligned} \tag{A.1.17}$$

---

[8] $\boldsymbol{C}_{slug}\, \vec{\Omega}$
[9] Where $I_{xx} < I_{yy} < I_{zz}$

$$
T \;=\; \frac{1}{2}\, m\, \vec{v}_{\mathcal{O}} \cdot \vec{v}_{\mathcal{O}} - \vec{v}_{\mathcal{O}} \cdot \vec{c}_{sat} \times \vec{\omega} - \vec{v}_{\mathcal{O}} \cdot \vec{c}_{slug} \times \vec{\omega}_{slug} +
$$
$$
+ \frac{1}{2}\, \vec{\omega} \cdot \boldsymbol{I}_{sat}\, \vec{\omega} + \frac{1}{2}\, \vec{\omega}_{slug} \cdot \boldsymbol{I}_{slug}\, \vec{\omega}_{slug} \tag{A.1.18}
$$

In the following figures the initial angular velocity of the satellite has a principal component in the direction of the axes of minimum inertia and a small perturbation in the other two directions. As we said before, the damping effect shows that in case of dissipation the axes of minimum inertia is no longer a stable equilibrium point. In all the simulations the relative angular velocity of the rigid slug is settled to zero. As we can notice, the angular velocity of the satellite Fig. (A.1), the angular momentum in the $\mathcal{F}_i$ Fig. (A.3) and its module Fig. (A.4) and the kinetic energy Fig. (A.5) are all conserved quantities. A comparison with the dynamics of the satellite without the slug (one rigid-body dynamics) was made and it was verified that without the damper effect the two dynamics are the same. In this case the axes of minimum inertia is a stable equilibrium point as it is shown in Fig. (A.6) and Fig. (A.7).
The inertia dry matrix of ESMO is:

$$
\boldsymbol{I}_{sat} = \begin{bmatrix} 17.53 & 0.14 & 0.61 \\ 0.14 & 16.05 & -1.04 \\ 0.61 & -1.04 & 10.74 \end{bmatrix} \tag{A.1.19}
$$

The inertia matrix in the principal axes is:

$$
\boldsymbol{I}_{sat} = \begin{bmatrix} 10.488 & 0 & 0 \\ 0 & 16.246 & 0 \\ 0 & 0 & 17.586 \end{bmatrix} \tag{A.1.20}
$$

Inertia of the slug is:

$$
\boldsymbol{I}_{slug} = \begin{bmatrix} J_p & 0 & 0 \\ 0 & J_p & 0 \\ 0 & 0 & J_p \end{bmatrix} \tag{A.1.21}
$$

Where for a sphere the inertia is $J_p = \frac{1}{2}\, m_{slug}\, r_{slug}^2$. The diameter of the tank is 484 $[mm]$ and the diameter of the slug is supposed to be 400 $[mm]$.

Case 1: slug dynamics without damper
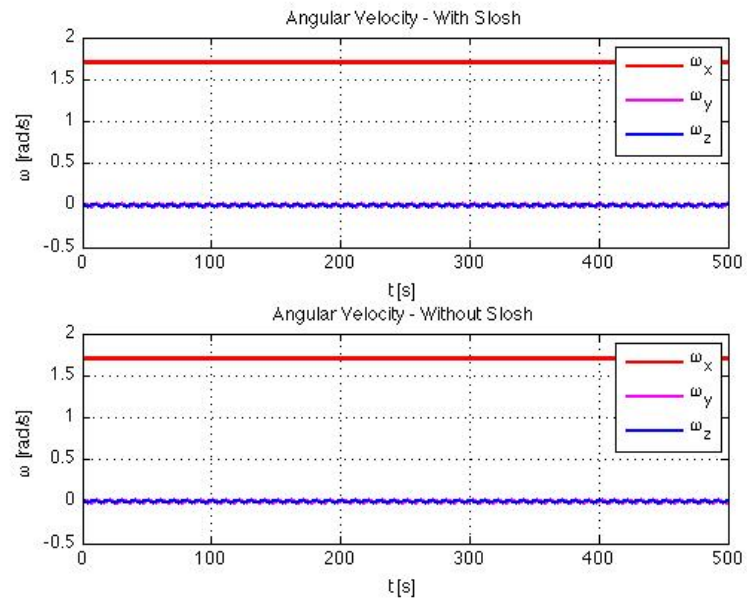
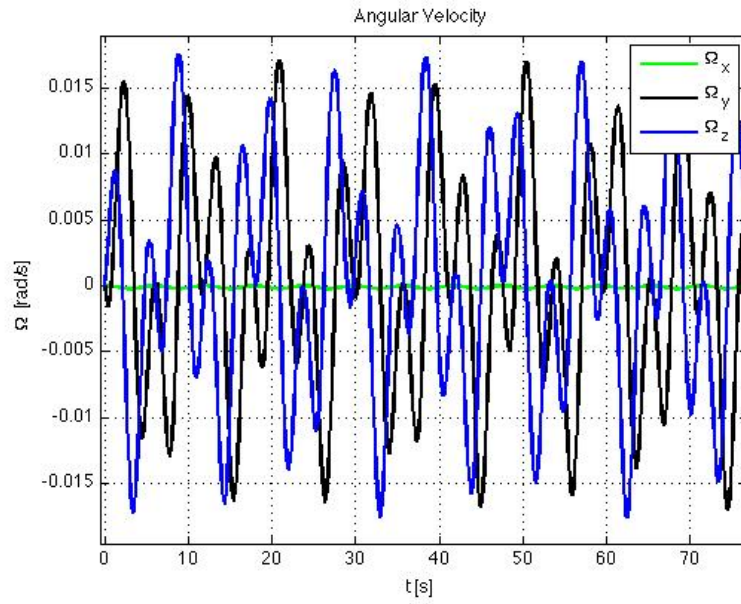Figure A.1: Satellite Angular velocity: $\vec{\omega}_0 = [1.7, 0.01, 0.01][rad/s]$ and $c_{slug} = 0[Nms]$.

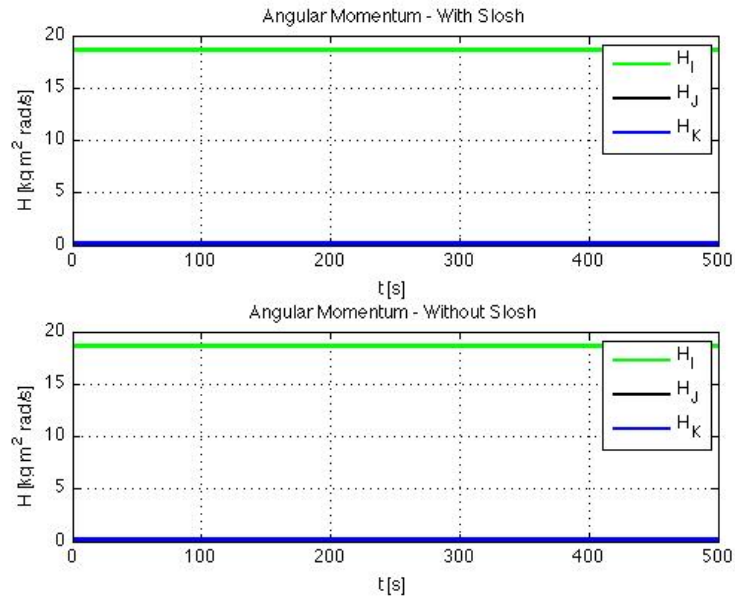Figure A.2:   Slug Relative Angular velocity: $\vec{\omega}_0 = [1.7, 0.01, 0.01][rad/s]$ and $c_{slug} = 0[Nms]$.

Figure A.3:   Total Angular Momentum in the $\mathcal{F}_i$ frame: $\vec{\omega}_0 = [1.7, 0.01, 0.01][rad/s]$ and $c_{slug} = 0[Nms]$.
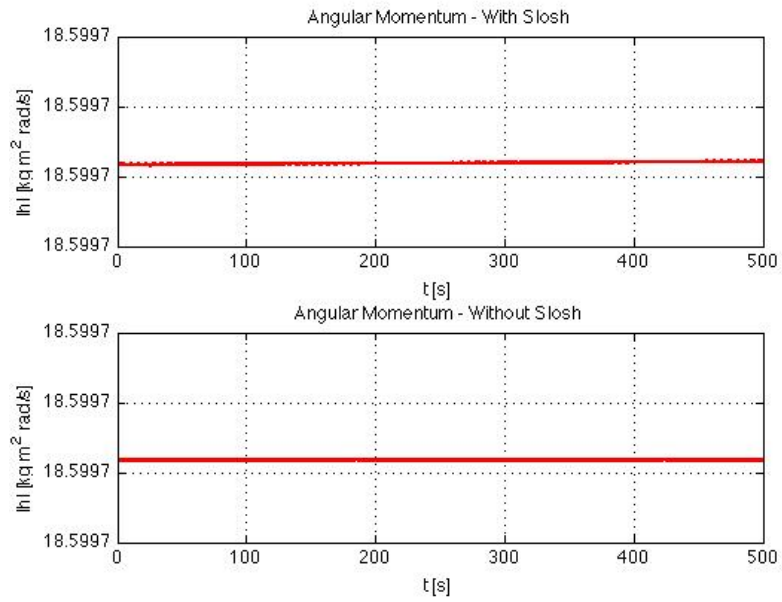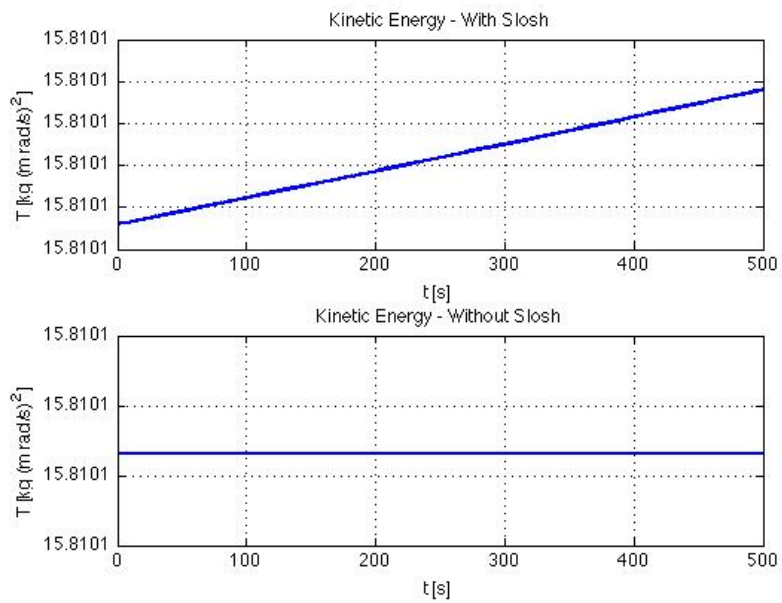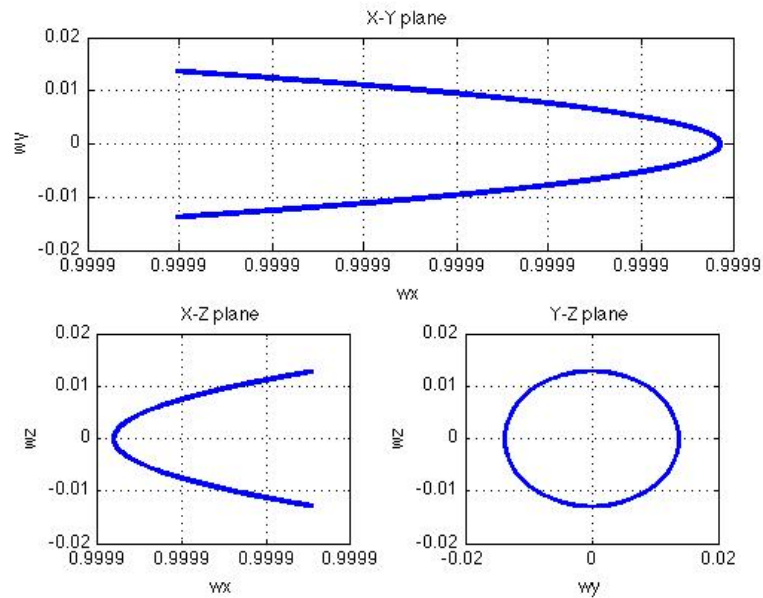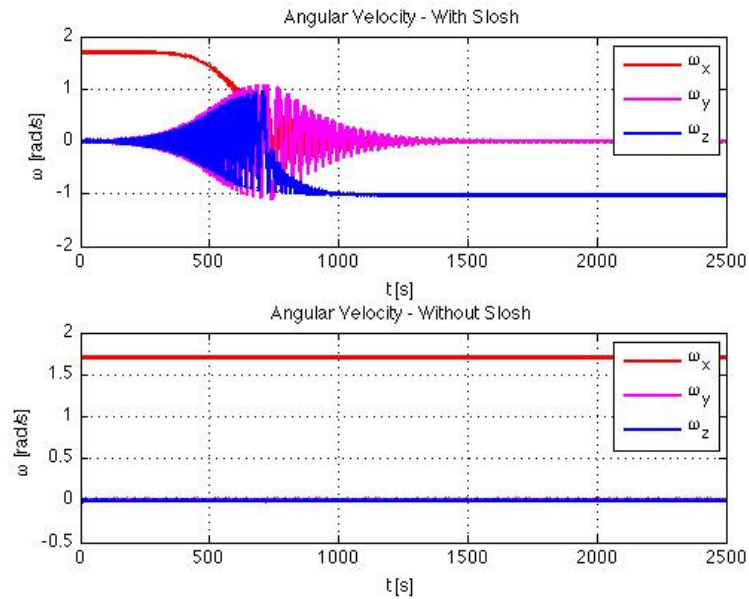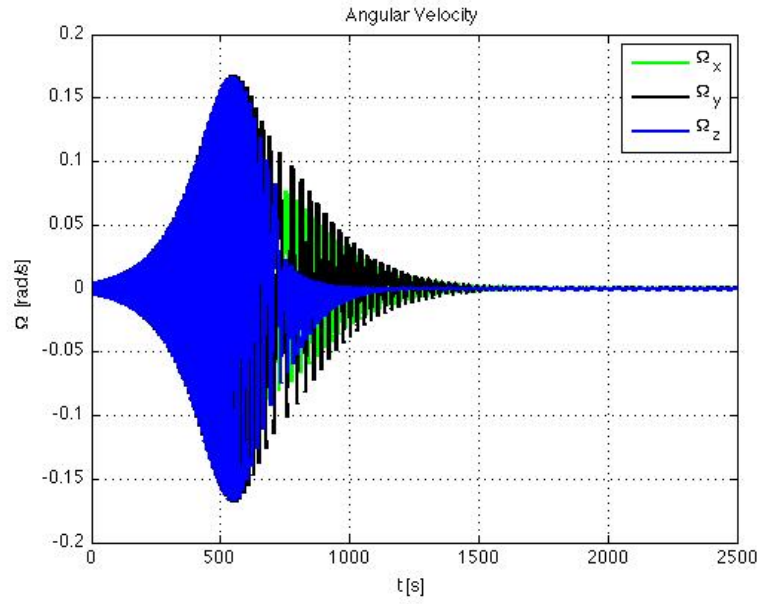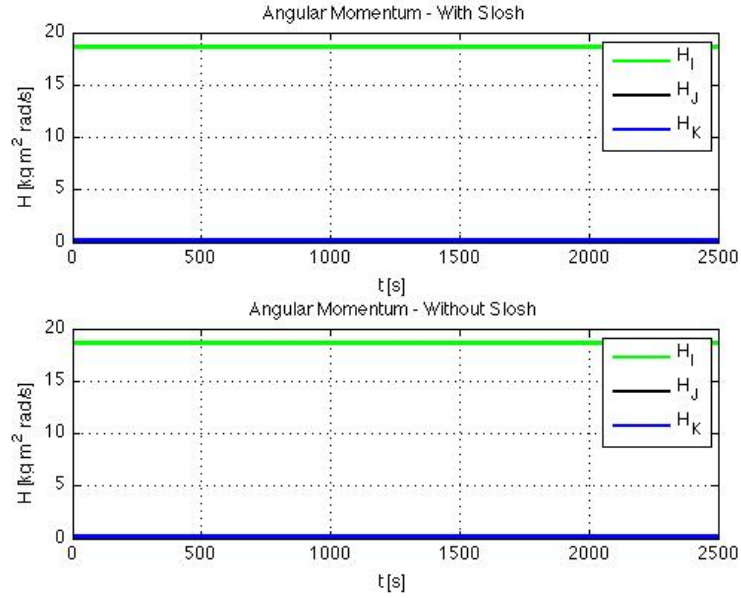
Figure A.4: Absolute Angular Momentum: $\vec{\omega}_0 = [1.7, 0.01, 0.01][rad/s]$ and $c_{slug} = 0[Nms]$.

Figure A.5: Kinetic Energy: $\vec{\omega}_0 = [1.7, 0.01, 0.01][rad/s]$ and $c_{slug} = 0[Nms]$.
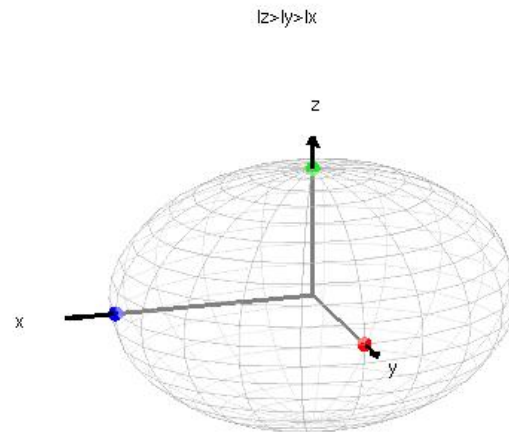
Figure A.6: Angular Momentum Ellipsoid, 3D View: $\vec{\omega}_0 = [1.7, 0.01, 0.01][rad/s]$ and $c_{slug} = 0[Nms]$.

Figure A.7:   Angular Momentum Ellipsoid: $\vec{\omega}_0 = [1.7, 0.01, 0.01][rad/s]$ and $c_{slug} = 0[Nms]$.

Case 2: slug dynamics with damper

With the same initial condition as the test before and a damping coefficient of 0.7 [N m s] we obtain the following results. In this case the kinetic energy Fig. (A.12) is not conserved but the angular momentum Fig. (A.10) and its module Fig. (A.11) is conserved. The axes of minimum inertia is now an unstable equilibrium point and with this particular initial condition the final angular velocity is along the axes of maximum inertia (see Fig. (A.13) , Fig. (A.14) and Fig. (A.8)). The damper reduces the angular velocity of the rigid slug to zero Fig. (A.9). As one can notice in Fig. (A.8) at the end of simulation the angular velocity is directed along the negative z-axes. The orientation of the spacecraft is unpredictable, it can end up with either a positive or negative spin about the major axis.

Figure A.8: Satellite Angular velocity: $\vec{\omega}_0 = [1.7, 0.01, 0.01][rad/s]$ and $c_{slug} = 0.7[Nms]$.

Figure A.9: Slug Relative Angular velocity: $\vec{\omega}_0 = [1.7, 0.01, 0.01][rad/s]$ and $c_{slug} = 0.7[Nms]$.

Figure A.10: Total Angular Momentum in the $\mathcal{F}_i$ frame: $\vec{\omega}_0 = [1.7, 0.01, 0.01][rad/s]$ and $c_{slug} = 0.7[Nms]$.
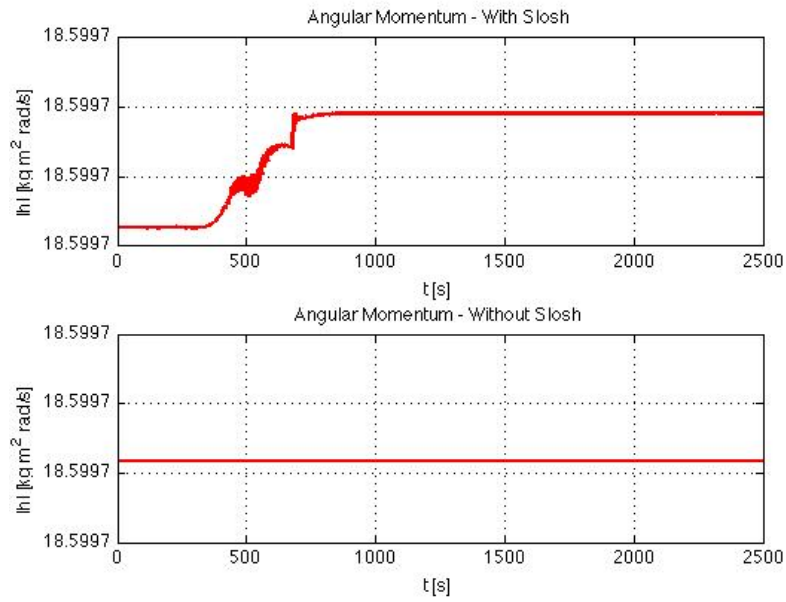
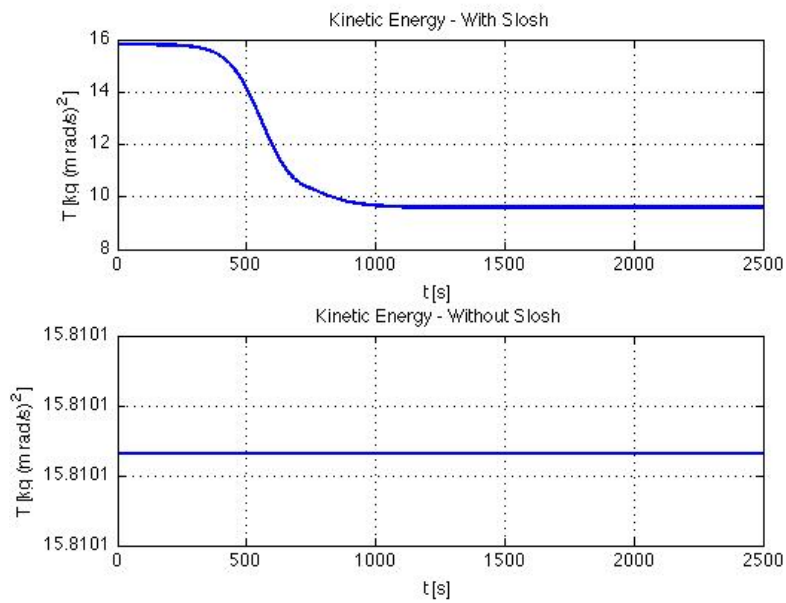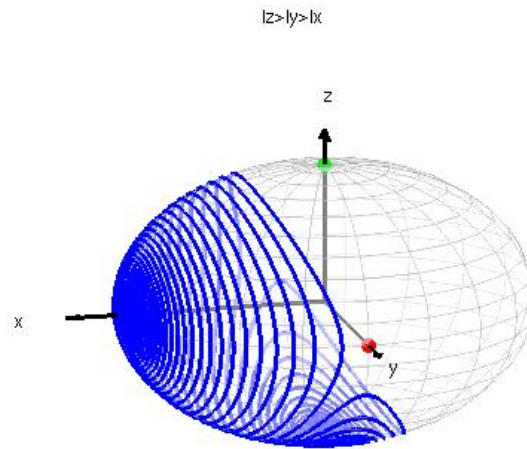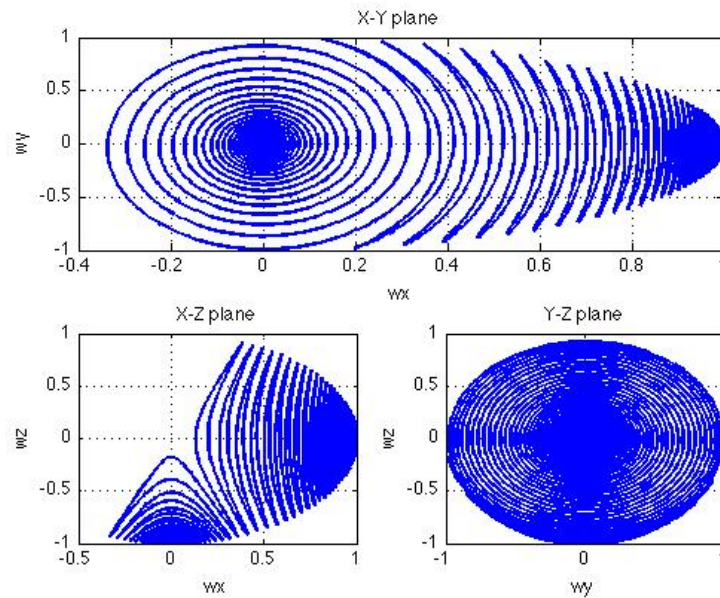Figure A.11: Absolute Angular Momentum: $\vec{\omega}_0 = [1.7, 0.01, 0.01][rad/s]$ and $c_{slug} = 0.7[Nms]$.

Figure A.12: Kinetic Energy: $\vec{\omega}_0 = [1.7, 0.01, 0.01][rad/s]$ and $c_{slug} = 0.7[Nms]$.

Figure A.13: Angular Momentum Ellipsoid, 3D View: $\vec{\omega}_0 = [1.7, 0.01, 0.01][rad/s]$ and $c_{slug} = 0.7[Nms]$.

Figure A.14: Angular Momentum Ellipsoid: $\vec{\omega}_0 = [1.7, 0.01, 0.01][rad/s]$ and $c_{slug} = 0.7[Nms]$.

In the following table we summarized the prevues cases analyzed:

Case	$\vec{\omega}_0[rad/s]$	$\vec{\omega}_{end}[rad/s]$	$c_{fl}[Nms]$
1	[1.7,0.01,0.01]	[1.7,0.01,0.01]	0
2	[1.7,0.01,0.01]	[0,0,-1.031]	0.7

Table A.1: Slug Model: initial spin condition.

Appendix B

Appendix

B.1 Approximate Closed-Form Solution for the Kinematic Quaternions

The closed-form solution to the kinematic quaternion Eq. (B.1.1) is:

$$\boldsymbol{q}(t_{n+1}) = e^{\frac{1}{2}\boldsymbol{\mathcal{Q}}_n T}\boldsymbol{q}(t_n) \tag{B.1.1}$$

Where T is the sampling interval $(t_{n+1} - t_n)$, $\boldsymbol{\mathcal{Q}}_n$ is evaluated at time t_n, $\boldsymbol{q}(t_n)$ is the attitude quaternions at time t_n and $\boldsymbol{q}(t_{n+1})$ is the propagated attitude quaternions at time t_{n+1}. The Eq. (B.1.1) can be rewritten in a more convenient form for numerical computation as:

$$\boldsymbol{q}(t_{n+1}) = \left[\cos\left(\frac{|\vec{\omega}|T}{2}\right)\mathbf{1} + \frac{1}{|\vec{\omega}|}\sin\left(\frac{|\vec{\omega}|T}{2}\right)\boldsymbol{\mathcal{Q}}_n \right]\boldsymbol{q}(t_n) \tag{B.1.2}$$

In figure (B.1 and B.2), one can see that with a generic angular velocity, the numerical solution in term of quaternions follow the approximate one.
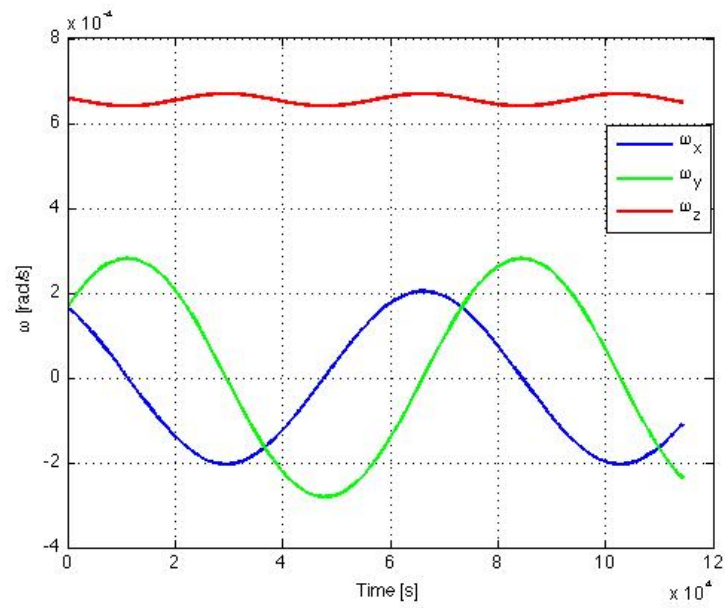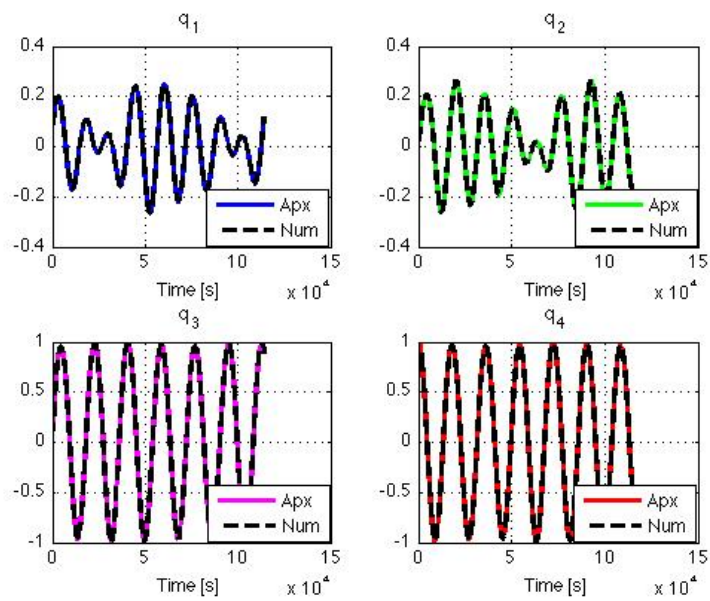
Figure B.1: Angular Velocity.

Figure B.2: Kinematic Quaternions.

B.2 Two-Rigid Body Dynamics: Generalization of the Fuel-Slug Model

In the Appendix (B.2) we analyze the two-rigid body or the *quasi*-rigid body dynamics. The main body corresponds to ESMO and the second body describes the 3D fuel-rigid spherical pendulum. We verify the equation in special case, where the solution is well known. As it is well known every term in the vectorial equation must be expressed in the same frame. For analyses that employ many reference frames we need to became very careful, understanding of which vector has been expressed in which frame.The equations have been derived by describing the dynamics of body $\mathcal{B}$ and $\mathcal{P}$ with respect to the inertial frame $\mathcal{F}_i$. The vector $\vec{R}_{\mathcal{O}}$ is the distance from the origin $\mathcal{O}$, belonging to both body-fixed $\mathcal{B}$ and pendulum-fixed $\mathcal{P}_f$ frames, to the origin $\mathcal{O}_i$ of the $\mathcal{F}_i$ frame. We are not going to redefine every terms of the equations that we will encounter in this Appendix, (see Chapter 2). The linear momentum of body $\mathcal{B}$ and body $\mathcal{P}_f$ are therefore:

$$\vec{p_b} = \int_{\mathcal{B}} \vec{v}_{\mathcal{O}} + \vec{\omega} \times \vec{\rho} \; dm_b = m_b \vec{v}_{\mathcal{O}} + \vec{\omega} \times \vec{c_b} \tag{B.2.3}$$

$$\vec{p_f} = \int_{\mathcal{P}_f} \vec{v}_{\mathcal{O}} + \vec{\omega}_f \times \vec{\rho}_f \; dm_f = m_f \vec{v}_{\mathcal{O}} + \vec{\omega}_f \times \vec{c_f} \tag{B.2.4}$$

The total linear momentum of the system is as follow:

$$\vec{p} = \vec{p_b} + \boldsymbol{C}_{fb}^{T} \; \vec{p_f} \tag{B.2.5}$$

Where the $\vec{p_f}$ components are defined in the $\mathcal{F}_{p_f}$ frame and so we need to express it in the $\mathcal{F}_b$ frame. The absolute angular momentum about $\mathcal{O}$ are calculated in the following way:

$$\vec{h_b} = \int_{\mathcal{B}} \vec{\rho} \times (\vec{v}_{\mathcal{O}} + \vec{\omega} \times \vec{\rho}) \; dm_b = \vec{c_b} \times \vec{v}_{\mathcal{O}} + \boldsymbol{I}_d \; \vec{\omega} \tag{B.2.6}$$

$$\vec{h_f} = \int_{\mathcal{P}_f} \vec{\rho}_f \times (\vec{v}_{\mathcal{O}} + \vec{\omega}_f \times \vec{\rho}_f) \; dm_f = \vec{c_f} \times \vec{v}_{\mathcal{O}} + \boldsymbol{I}_f \; \vec{\omega}_f \tag{B.2.7}$$

The total angular momentum of the system is:

$$\vec{h} = \vec{h}_b + \boldsymbol{C}_{fb}^T \, \vec{h}_f \tag{B.2.8}$$

Notice that $\vec{c}_b$, $\boldsymbol{I}_d$, $\vec{c}_f$, and $\boldsymbol{I}_f$ are the first momentum and the inertia matrix of both the body $\mathcal{B}$ and the body $\mathcal{P}_f$. They are defined in the $\mathcal{F}_b$ frame and in the $\mathcal{F}_{p_f}$, this means that they are constants in their frame. Where, as before, we expressed the $\vec{h}_f$ in the $\mathcal{F}_b$ frame. The Euler's equations of the entire system are:

$$\dot{\vec{H}} = \dot{\vec{h}} + \vec{\omega} \times \vec{h} \tag{B.2.9}$$

Using the Eq. (B.2.8) in the Eq. (B.2.9), we can also write:

$$\dot{\vec{H}} = \dot{\vec{h}}_b + \vec{\omega} \times \vec{h}_b + \boldsymbol{C}_{fb}^T \, \dot{\vec{h}}_f + \dot{\boldsymbol{C}}_{fb}^T \, \vec{h}_f + \vec{\omega} \times \boldsymbol{C}_{fb}^T \, \vec{h}_f \tag{B.2.10}$$

and the pendulum dynamics is described by the following equation:

$$\dot{\vec{H}}_f = \dot{\vec{h}}_f + \vec{\omega}_f \times \vec{h}_f + \boldsymbol{D}_f \, \vec{\Omega}_f \tag{B.2.11}$$

Where $\vec{\Omega}_f$ is the relative angular velocity from the body $\mathcal{B}$ to the body $\mathcal{P}_f$ and it is defined in the $\mathcal{F}_b$ frame. The absolute angular velocity of the pendulum $\vec{\omega}_f$ is equal to $\boldsymbol{C}_{fb} \, \vec{\omega} + \vec{\Omega}_f$. In the Eq. (B.2.10) and Eq. (B.2.11) $\vec{h}_b$ is equal to $\boldsymbol{I}_d \, \vec{\omega}$ and $\vec{h}_f$ is equal to $\boldsymbol{I}_f \, \vec{\omega}_f$. As in the case of the dynamic of a 3D Spherical Pendulum, the $\boldsymbol{I}_f$[1] is computed in the $\mathcal{F}_{p_f}$ frame. The system of equations are:

$$\begin{cases} \dot{\vec{h}}_b + \vec{\omega} \times \vec{h}_b + \boldsymbol{C}_{fb}^T \, \dot{\vec{h}}_f + \dot{\boldsymbol{C}}_{fb}^T \, \vec{h}_f + \vec{\omega} \times \boldsymbol{C}_{fb}^T \, \vec{h}_f = \vec{M}^{ext} + \boldsymbol{C}_{fb}^T \, \vec{M}_f \\ \dot{\vec{h}}_f + \vec{\omega}_f \times \vec{h}_f + \boldsymbol{D}_f \, \vec{\Omega} = \vec{M}_f \end{cases} \tag{B.2.12}$$

In the Eq. (B.2.12) the $\vec{M}_f$ is the torque due to the induced acceleration and it is defined in the $\mathcal{F}_{p_f}$ frame. The direction of the length of the pendulum $\vec{l}_f$ is constant in the $\mathcal{F}_{p_f}$ frame and the direction of the induced acceleration $\vec{a}_f$ is constant in the $\mathcal{F}_b$ frame. The length of the pendulum defined in the $\mathcal{F}_{p_f}$ frame is:

$$\vec{l}_f = \begin{Bmatrix} l_f \\ 0 \\ 0 \end{Bmatrix} \tag{B.2.13}$$

---

[1]It is a diagonal matrix where $I_{zz} = I_{yy} = J_f$ and $I_{xx} = J_f + m_f \, l_f^2$ where $J_f = 2/5 \, m_f \, l_f^2$.

The gravity vector defined in the $\mathcal{F}_b$ frame is:

$$\vec{a}_f = \left\{ \begin{array}{c} 0 \\ 0 \\ -a_f \end{array} \right\} \tag{B.2.14}$$

The torque due to the induced acceleration is defined in the $\mathcal{F}_{p_f}$ frame, therefore it can be written as $\vec{M}_f = m_f \, \vec{l}_f \times \boldsymbol{C}_{fb}^T \, \vec{a}_f$. The kinetic energy of the system is written as follow:

$$\begin{aligned} T &= \frac{1}{2} \int_{\mathcal{B}} (\vec{v}_\mathcal{O} + \vec{\omega} \times \vec{\rho}_b) \cdot (\vec{v}_\mathcal{O} + \vec{\omega} \times \vec{\rho}_b) dm_b + \\ &+ \frac{1}{2} \int_{\mathcal{P}_f} (\vec{v}_\mathcal{O} + \vec{\omega}_f \times \vec{\rho}_f) \cdot (\vec{v}_\mathcal{O} + \vec{\omega}_f \times \vec{\rho}_f) dm_f \end{aligned} \tag{B.2.15}$$

$$\begin{aligned} T &= \frac{1}{2} m \, \vec{v}_\mathcal{O} \cdot \vec{v}_\mathcal{O} - \vec{v}_\mathcal{O} \cdot \vec{c}_b \times \vec{\omega} - \vec{v}_\mathcal{O} \cdot \vec{c}_f \times \vec{\omega}_f + \\ &+ \frac{1}{2} \vec{\omega} \cdot \boldsymbol{I}_d \, \vec{\omega} + \frac{1}{2} \vec{\omega}_f \cdot \boldsymbol{I}_f \, \vec{\omega}_f \end{aligned} \tag{B.2.16}$$

In the Eq. (B.2.16) m is the sum of the dry mass of the satellite m_b and the fuel mass m_f. The potential energy is $U = m_f \, \vec{l}_f \cdot \boldsymbol{C}_{fb}^T \, \vec{a}_f$ and the total energy is $E = T - U$. In order to test the equation before, we can simplify the system by setting the $\vec{v}_\mathcal{O}$ equal to zero. In that way we studied only the rotational motion of the two-bodies dynamics. In Tab (B.1), is summarized the test case that we have investigated.

Case	$\vec{\alpha}_0[deg]$	$\vec{\omega}_0[rad/s]$	$\vec{\alpha}_{f_0}[deg]$	$\vec{\Omega}_0[rad/s]$	$c_f[Nms]$	$a_f[ms^{-2}]$
1	[0,0,0]	[0,0,0]	[0,-10,0]	[0,0,0]	0	0.1011
2	[0,0,0]	[0,0,0]	[0,-10,0]	[0,0,0]	0.1	0.1011

Table B.1: Initial Condition: two-bodies dynamics.

In this table $\vec{\alpha}_0$ is the vector of the Euler's angles from the $\mathcal{F}_i$ to the $\mathcal{F}_b$ frame:

$$\vec{\alpha}_0 = \left\{ \begin{array}{c} \alpha \\ \beta \\ \rho \end{array} \right\} \tag{B.2.17}$$

Where α is the azimuth and β is the declination of the ESMO's thrust vector direction. The vector α_{f_0} is the vector of the Euler's angles from the $\mathcal{F}_b$ to the $\mathcal{F}_{p_f}$ frame:

$$\vec{\alpha}_{f_0} = \left\{ \begin{array}{c} \theta \\ \phi \\ \delta \end{array} \right\} \tag{B.2.18}$$

Case 1: pendulum dynamics without damper

The equations of the two bodies are coupled by the damper effect so as one can notice in this case the dynamics of the pendulum does not influence the initial condition of the satellite dynamics Fig. (B.3) and the relative and the absolute angular momentum of the pendulum have the same value (see Fig. (B.4) and Fig. (B.5)). The angular momentum is conserved along the induced acceleration direction Fig. (B.7) and the norm vector of the total angular momentum is not a constant Fig. (B.6). Usually the angular momentum is constant when the free-body dynamics is investigated. In this particular case the induced acceleration is direct along the z-axes, so the angular momentum can not be conservative along the other two axes direction as one can see in the following results. The total energy of the system is influenced by only the pendulum dynamics Fig. (B.10) and it is a constant during the motion as in the 3D Pendulum Dynamics.
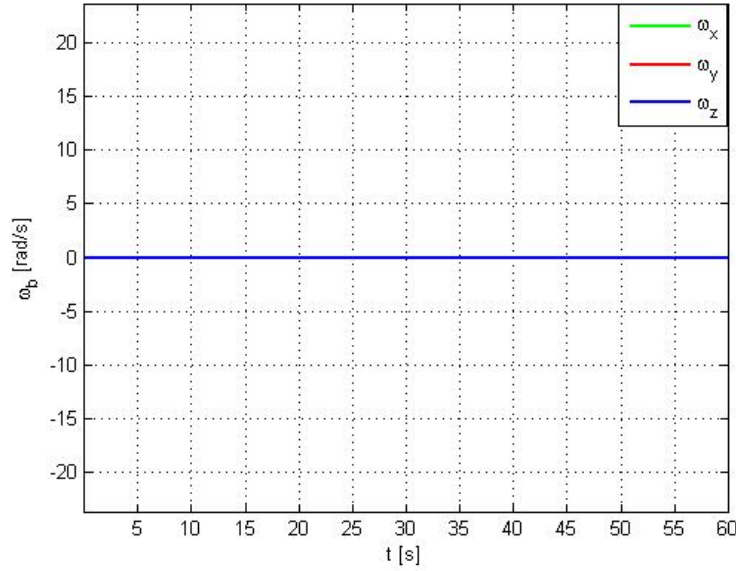
Figure B.3: Absolute Angular Velocity of the Satellite in the $\mathcal{F}_b$ frame: $\vec{\omega}_0 = [0, 0, 0]$ and $\vec{\Omega}_0 = [0, 0, 0]$ rad/s and $c_f = 0$ [N m s].
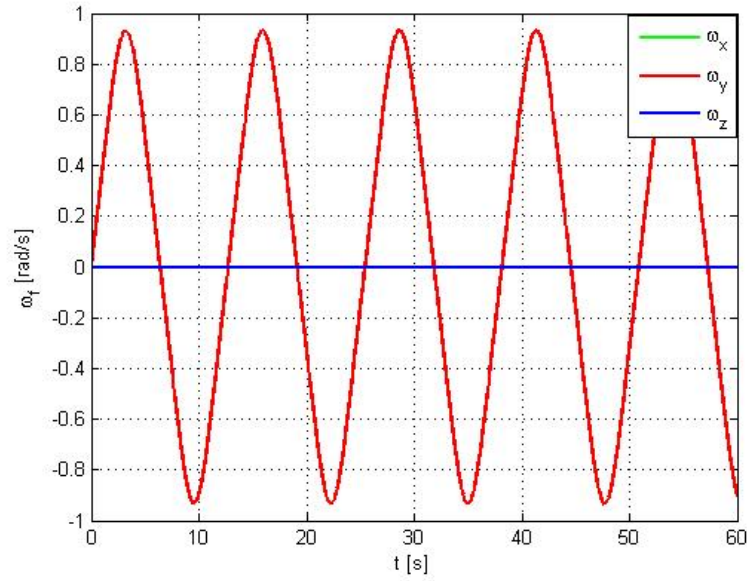
Figure B.4: Absolute Angular Velocity of the Pendulum in the $\mathcal{F}_{p_f}$ frame: $\vec{\omega}_0 = [0,0,0]$ and $\vec{\Omega}_0 = [0,0,0]$ rad/s and $c_f = 0$ [N m s].
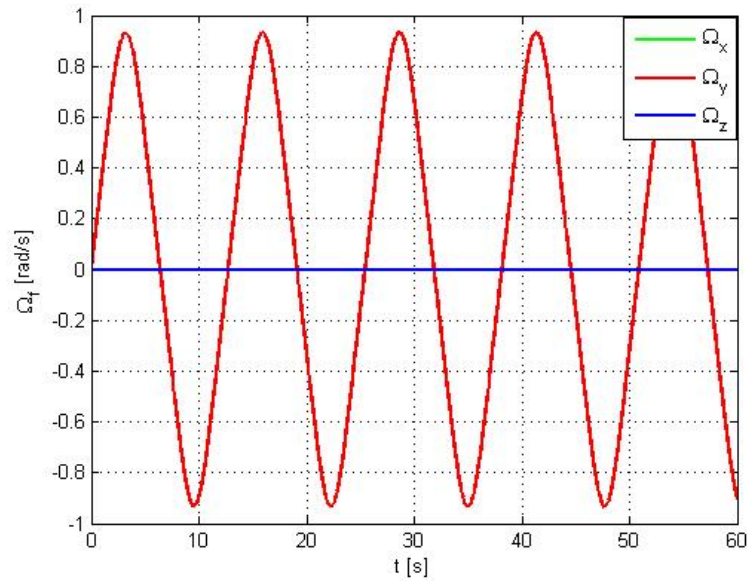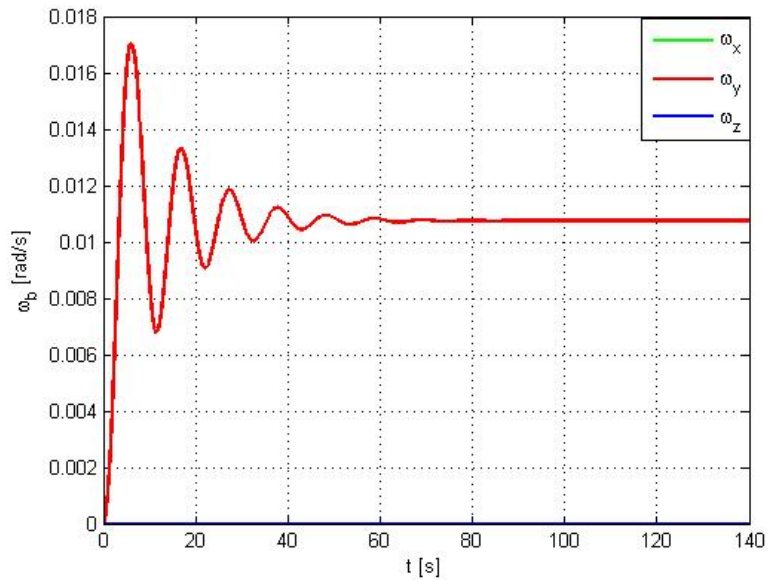

Figure B.5: Relative Angular Velocity of the Pendulum in the $\mathcal{F}_{p_f}$ frame: $\vec{\omega}_0 = [0,0,0]$ and $\vec{\Omega}_0 = [0,0,0]$ rad/s and $c_{Fl} = 0$ [N m s].
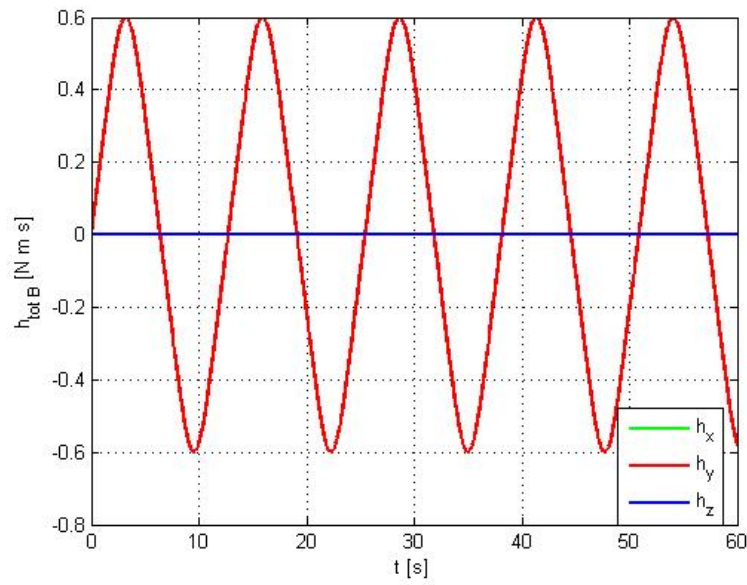
Figure B.6:   Absolute Total Angular Momentum: $\vec{\omega}_0 = [0, 0, 0]$ and $\vec{\Omega}_0 = [0, 0, 0]$ rad/s and $c_f = 0$ [N m s].
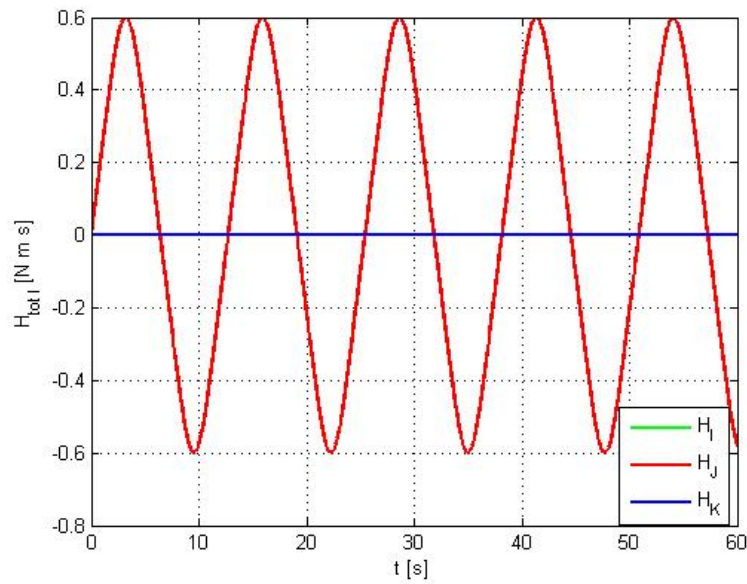
Figure B.7:   Total Angular Momentum in the $\mathcal{F}_i$: $\vec{\omega}_0 = [0, 0, 0]$ and $\vec{\Omega}_0 = [0, 0, 0]$ rad/s and $c_f = 0$ [N m s].
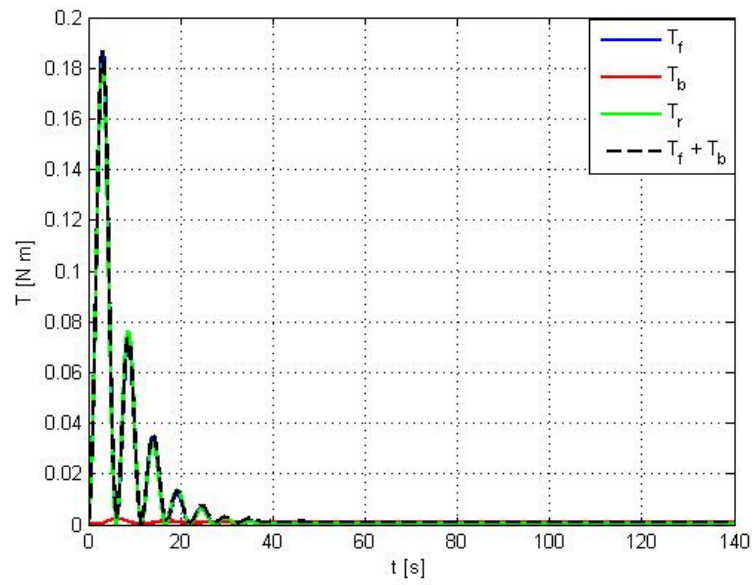
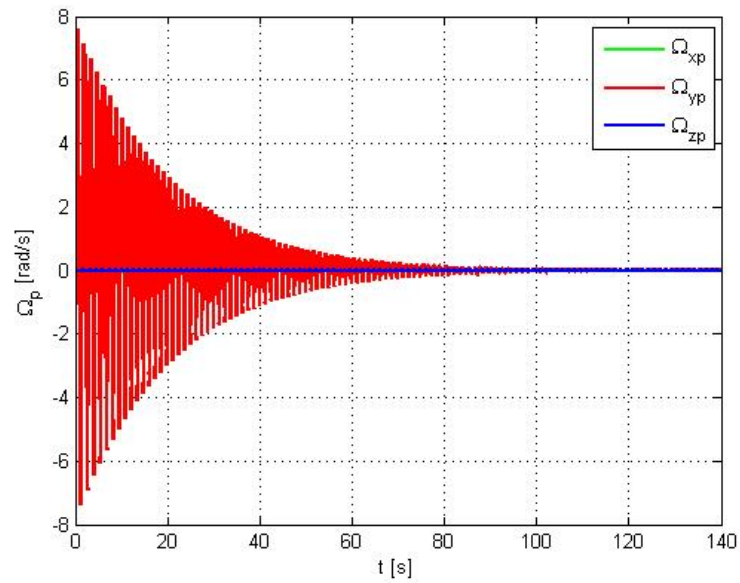Figure B.8:   Kinetic Energy: $\vec{\omega}_0 = [0, 0, 0]$ and $\vec{\Omega}_0 = [0, 0, 0]$ rad/s and $c_f = 0$ [N m s].
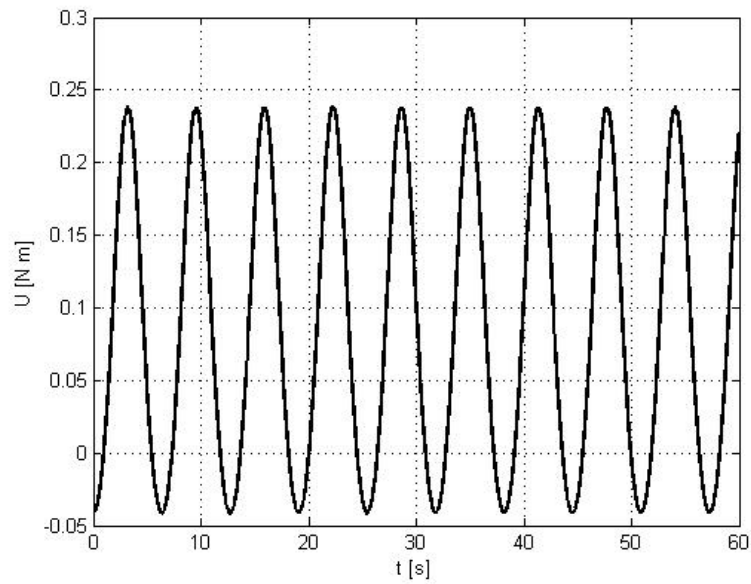
Figure B.9:   Potential Energy: $\vec{\omega}_0 = [0, 0, 0]$ and $\vec{\Omega}_0 = [0, 0, 0]$ rad/s and $c_f = 0$ [N m s].
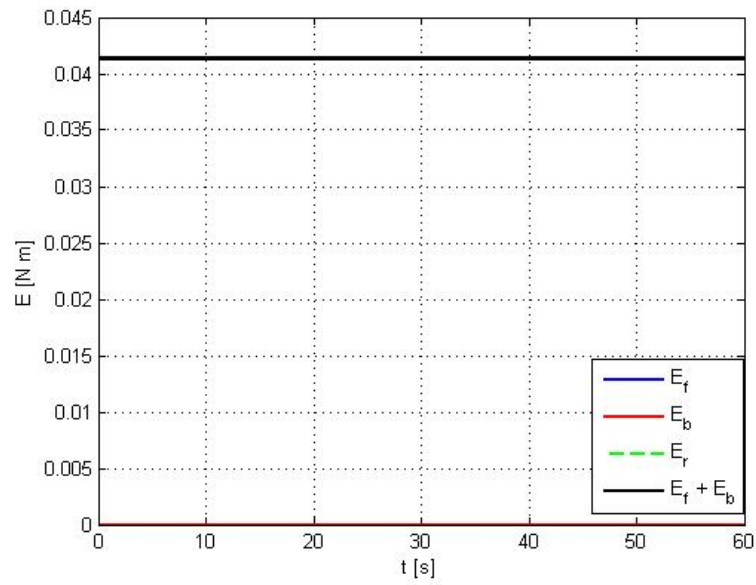
Figure B.10: Total Energy: $\vec{\omega}_0 = [0, 0, 0]$ and $\vec{\Omega}_0 = [0, 0, 0]$ rad/s and $c_f = 0$ [N m s].
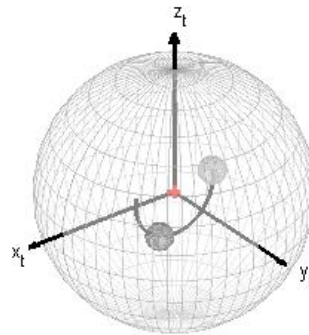
Figure B.11: Tank, 3D view: $\vec{\omega}_0 = [0, 0, 0]$ and $\vec{\Omega}_0 = [0, 0, 0]$ rad/s and $c_f = 0$ [N m s].

In Fig. (B.11) one can see the trajectory followed by the fuel center of mass.

Case 2: pendulum dynamics with damper

By introducing the damping effect, we can notice that the total energy Fig. (B.19) is not still conserved like in the case of the 3D Pendulum Dynamics and at the end the relative angular velocity of the pendulum Fig. (B.14) end up to a zero value. In this simulation one can notice that the interaction of the pendulum mass with the tank changes the initial angular velocity of the satellite. Indeed the satellite end up with a positive angular velocity of 0.0109 rad/s and the spin velocity is along the y-axes. Fig. (B.12).

Figure B.12:   Absolute Angular Velocity of the Satellite in the $\mathcal{F}_b$ frame: $\vec{\omega}_0 = [0, 0, 0]$ and $\vec{\Omega}_0 = [0, 0, 0]$ rad/s and $c_f = 0.1$ [N m s].
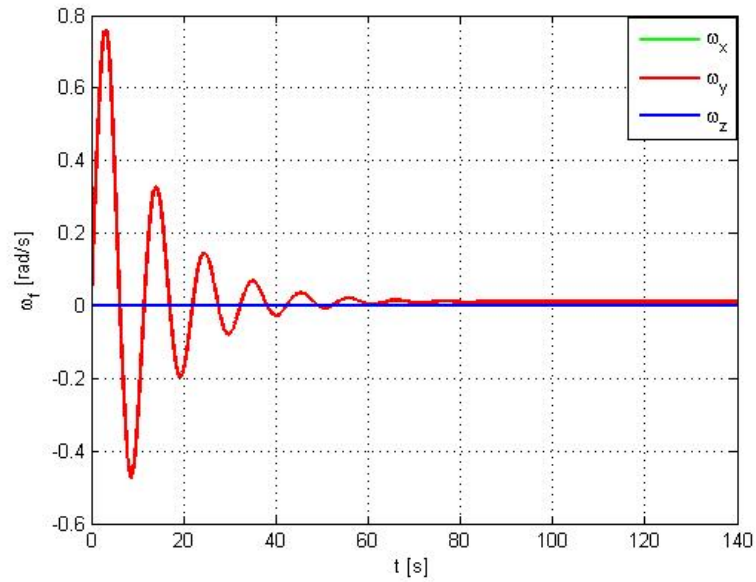
Figure B.13: Absolute Angular Velocity of the Pendulum in the $\mathcal{F}_{p_f}$ frame: $\vec{\omega}_0 = [0, 0, 0]$ and $\vec{\Omega}_0 = [0, 0, 0]$ rad/s and $c_f = 0.1$ [N m s].
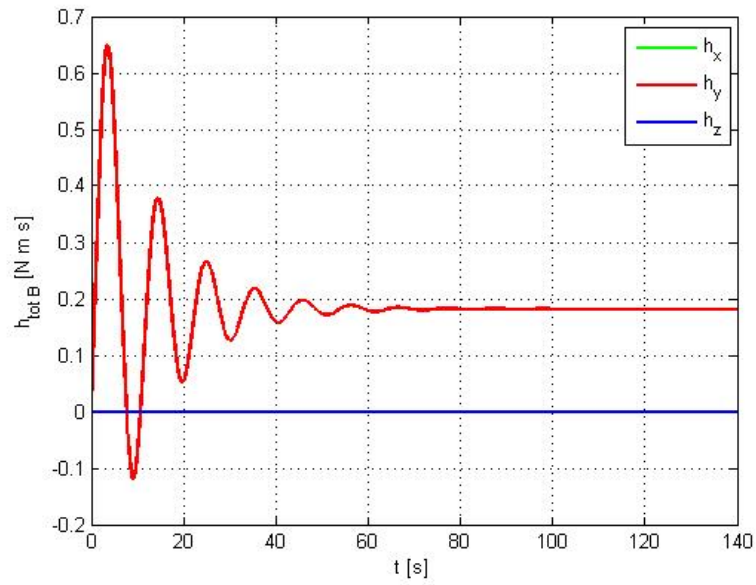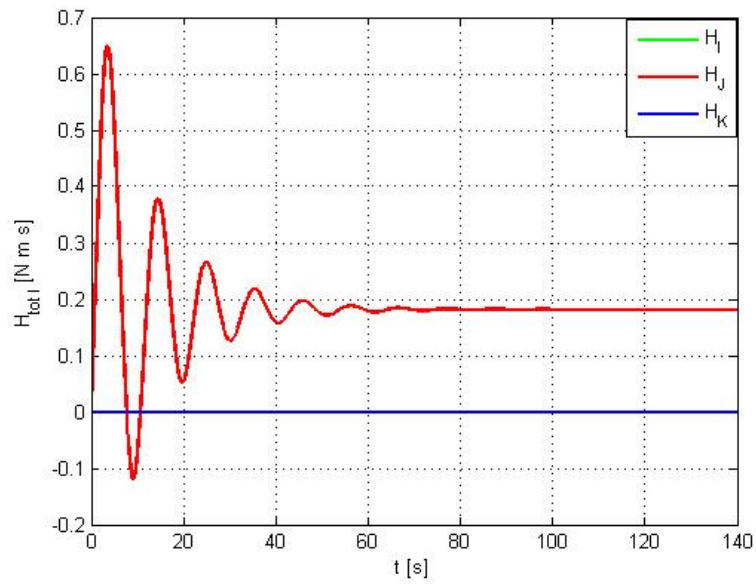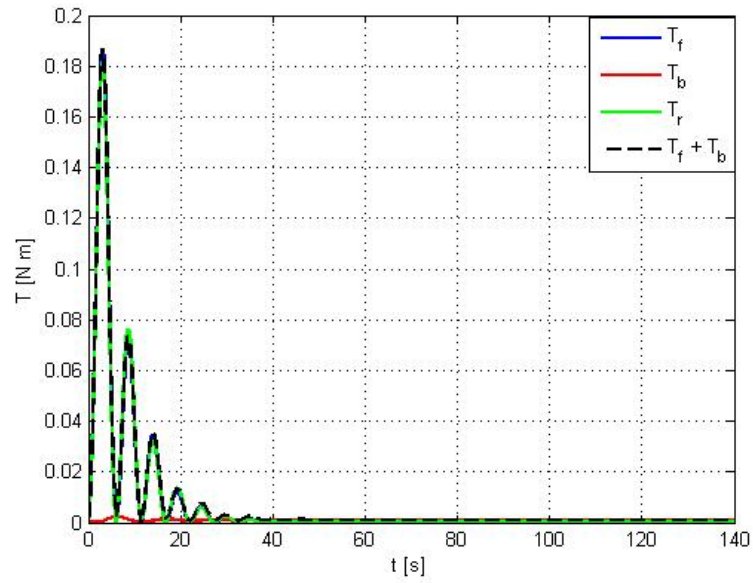

Figure B.14: Relative Angular Velocity of the Pendulum in the $\mathcal{F}_{p_f}$ frame: $\vec{\omega}_0 = [0, 0, 0]$ and $\vec{\Omega}_0 = [0, 0, 0]$ rad/s and $c_f = 0.1$ [N m s].

Figure B.15: Absolute Total Angular Momentum: $\vec{\omega}_0 = [0, 0, 0]$ and $\vec{\Omega}_0 = [0, 0, 0]$ rad/s and $c_f = 0.1$ [N m s].

Figure B.16: Total Angular Momentum in the $\mathcal{F}_i$: $\vec{\omega}_0 = [0, 0, 0]$ and $\vec{\Omega}_0 = [0, 0, 0]$ rad/s and $c_f = 0.1$ [N m s].

Figure B.17: Kinetic Energy: $\vec{\omega}_0 = [0, 0, 0]$ and $\vec{\Omega}_0 = [0, 0, 0]$ rad/s and $c_f = 0.1$ [N m s].
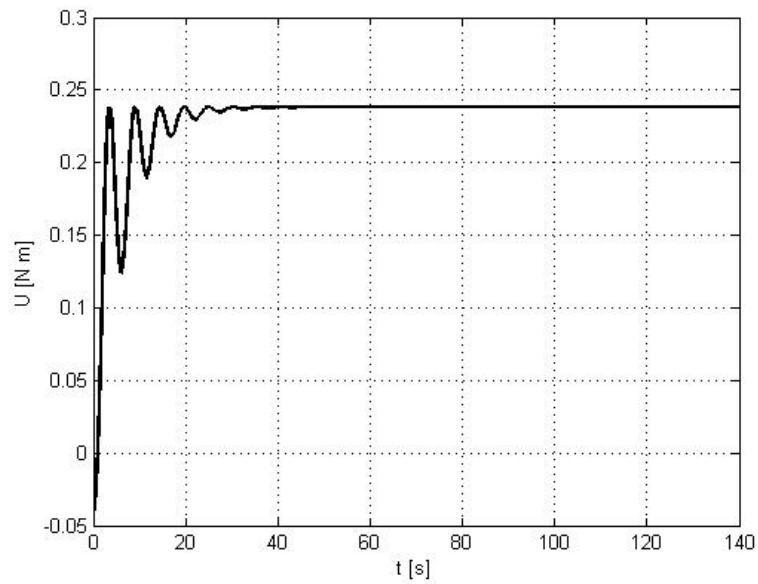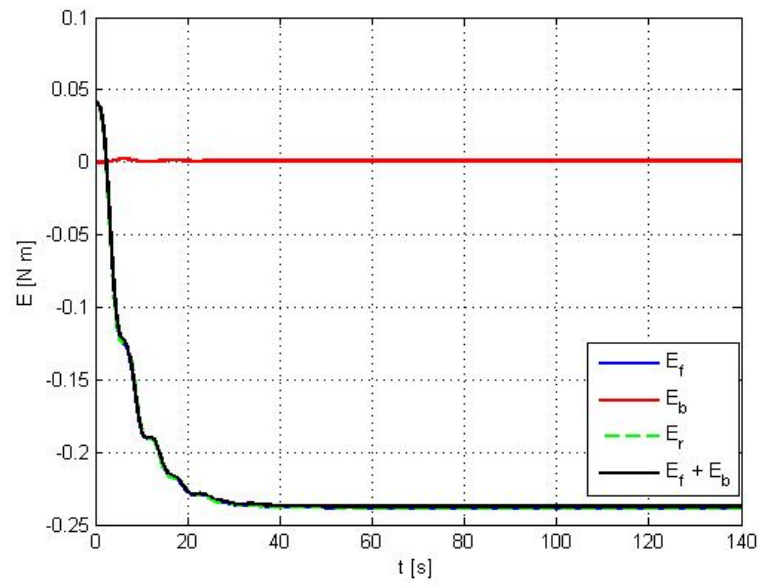

Figure B.18: Potential Energy: $\vec{\omega}_0 = [0, 0, 0]$ and $\vec{\Omega}_0 = [0, 0, 0]$ rad/s and $c_f = 0.1$ [N m s].

Figure B.19: Total Energy: $\vec{\omega}_0 = [0, 0, 0]$ and $\vec{\Omega}_0 = [0, 0, 0]$ rad/s and $c_f = 0.1$ [N m s].
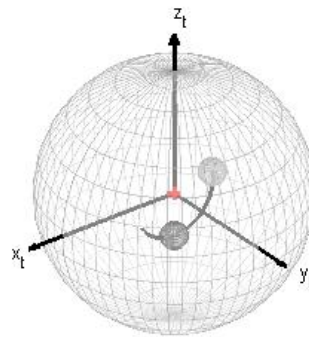

Figure B.20: Tank, 3D view: $\vec{\omega}_0 = [0, 0, 0]$ and $\vec{\Omega}_0 = [0, 0, 0]$ rad/s and $c_f = 0.1$ [N m s].

As for the case 1, in Fig. (B.20) one can see the trajectory followed by the fuel center of mass.
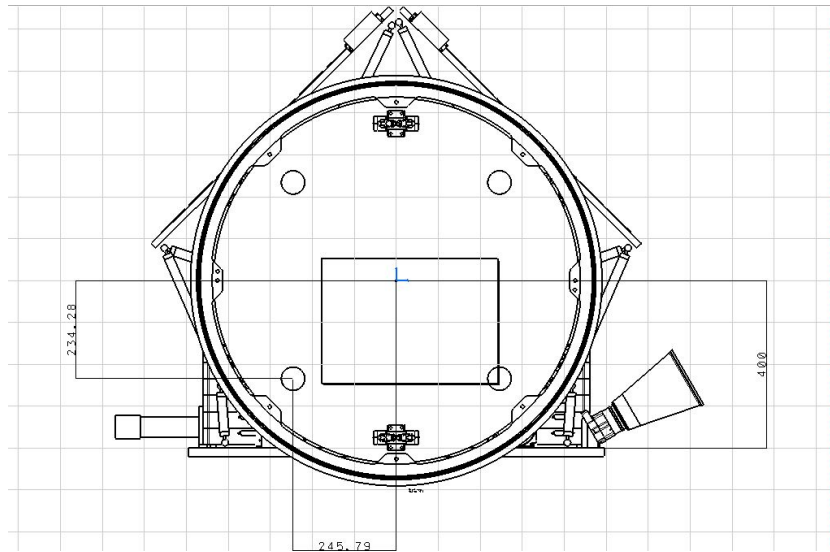
B.3   ESMO drawing

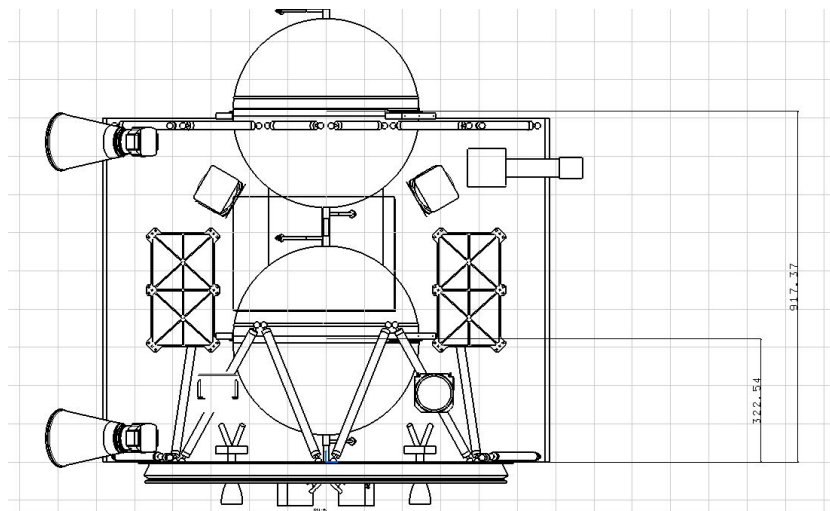Figure B.21:   ESMO Drawing 1: CONF team concession.

Figure B.22:   ESMO Drawing 2: CONF team concession.

B.3.1   Damper Coefficient Effect

| Case	$\omega_b[rad/s]$	$\Omega_f = [rad/s]$	$[rad/s]$	$c_f[Nms]$	$c_o[Nms]$
1	[0,0,0]	[0,0, 0]	[0,0, 0]	30	30

Table B.2: Initial Condition.

Case	$\vec{\alpha}_0[deg]$	$\vec{\alpha}_{f_0}[deg]$	$\vec{\alpha}_{o_0}[deg]$	$a_f[ms^{-2}]$
1	[0,0,0]	[0,-10, 0]	[0,-10, 0]	0.1011 [ms^{-1}]

Table B.3: Kinematic and Induced Acceleration.

In this section, the third case of the Chapter 4 (4.1.3) has been showed. In the Case 3, the damping coefficient is ten times higher then the Case 2 and the two solutions seams quite similar but in the third case the final energy of the satellite is higher. This mean that if the damping coefficient growing up, also the energy of the satellite and its final spin velocity will grow up, see Fig. (B.23, B.24, B.25, B.26 and B.27).
Case 3
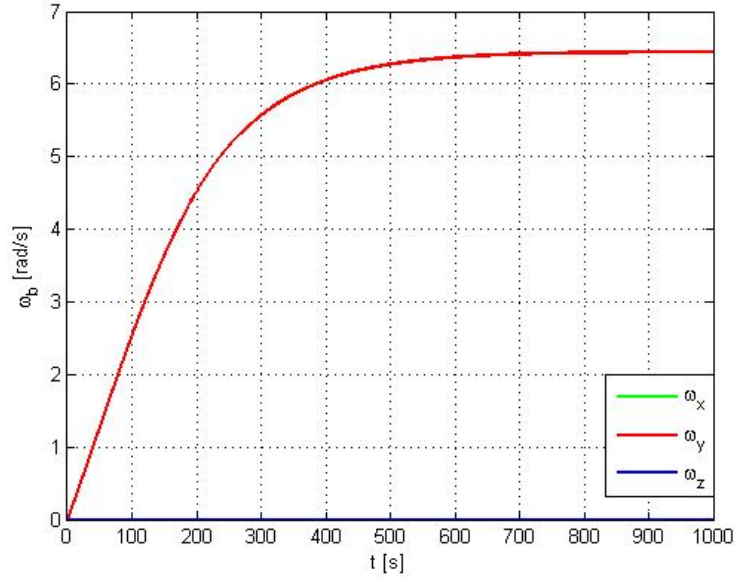
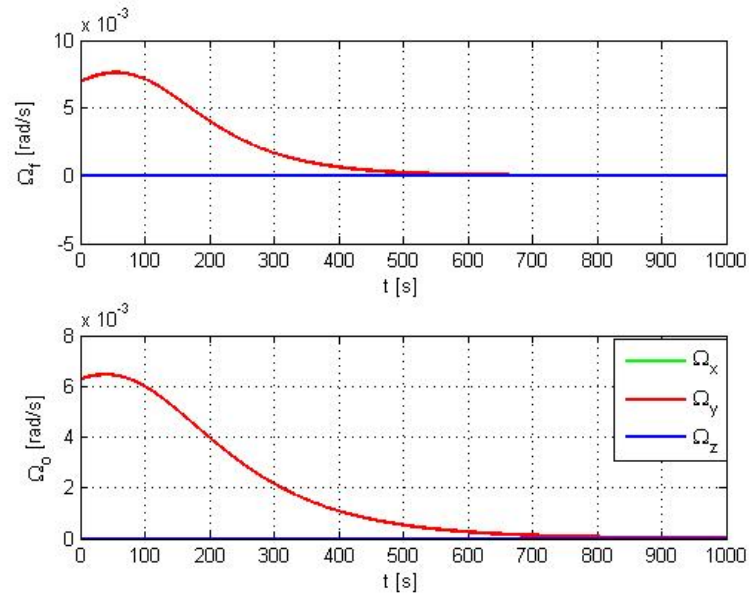Figure B.23: Case 1: Angular Velocity of ESMO ($c_f = c_o = 30[Nms]$).

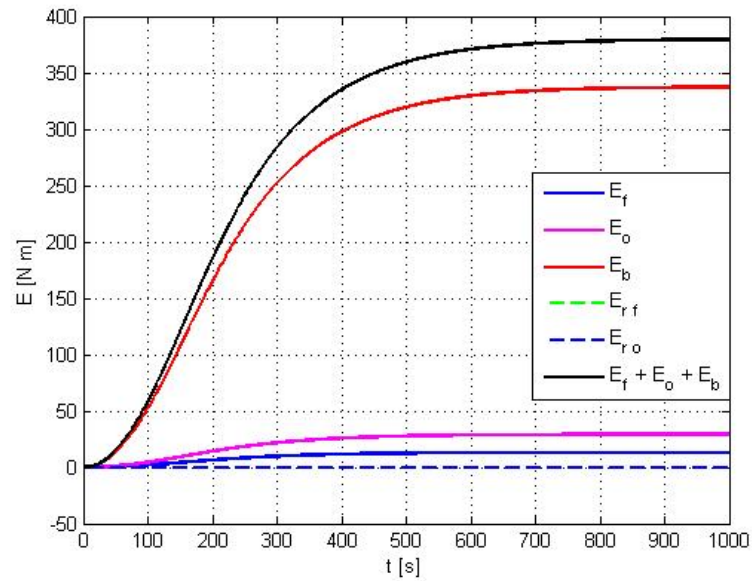Figure B.24: Case 1: Angular Velocity of the Fuel and Oxidizer Pendulum ($c_f = c_o = 30[Nms]$).

Figure B.25: Case 1: Total Energy of the System ($c_f = c_o = 30[Nms]$).
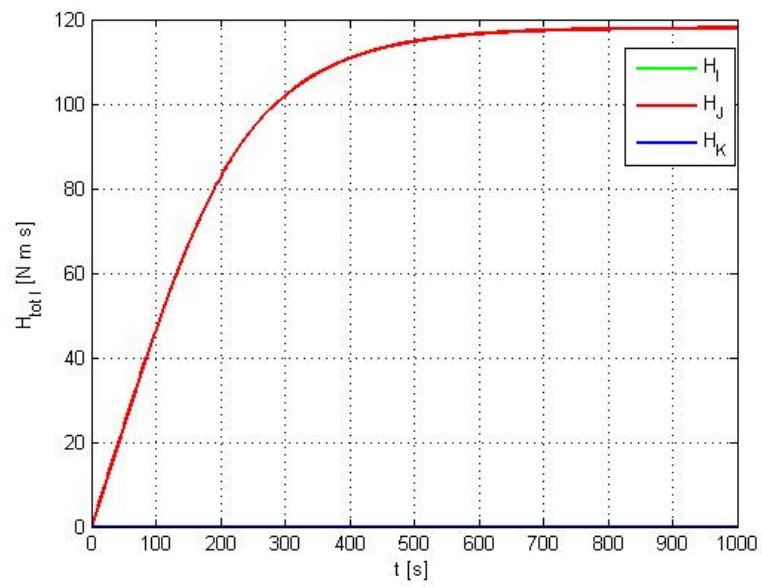
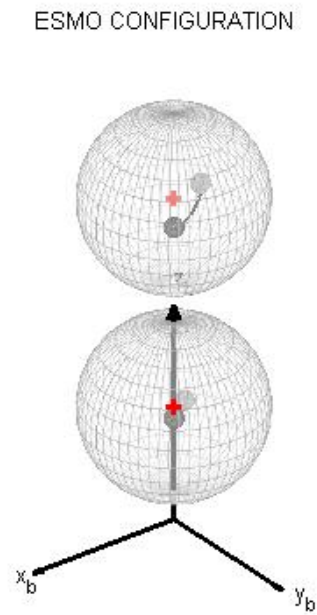Figure B.26: Case 1: Total Angular Momentum of the System ($c_f = c_o = 30[Nms]$).

Figure B.27: Case 1: ESMO configuration ($c_f = c_o = 30[Nms]$).

Appendix C

Appendix

C.1   ESMO: Data and Characteristics

Size[cm]	120 x 110 x 100
Weight [kg]	265 (inc. 93 kg propellant)
Power System	2 body-mounted gallium arsenide solar panels (70 W)
Telemetry, tracking and Control	2 star trackers, 4 sun sensors 2 star trackers, 4 sun sensors
Attitude Determination and Control	3-axis stabilized: 2 inertial measurements units, 4 reaction wheels, 4 cold gas thrusters
Communications	S-band (both uplink and downlink), Low gain antennas for omni-directional coverage
Propulsion	4 x 22 N bipropellant thrusters, I_{sp} = 285 s, TotalΔ V = 1150 m/s
Structure	Aluminum honeycomb central thrust tube with load bearing struts for launch adapter mating
Thermal Control	Passive: MLI and surface coatings; active: local heaters for eclipse (e.g. propellant tanks)
Ground Segment	Malindi (10 m dish), Weilheim (15/30 m) and ESAC (15 m), Perth and Kourou (early GTO phase) for additional coverage

Table C.1: ESMO Overview.